MOLECULAR DYNAMICS STUDIES OF THE STRUCTURAL, THERMO-MECHANICAL AND FINITE SIZE ELASTIC PROPERTIES OF HEXAGONAL BORON NITRIDE

Thesis

submitted in partial fulfillment of the requirements for the degree of

DOCTOR OF PHILOSOPHY

by

SIBY THOMAS

DEPARTMENT OF PHYSICS
NATIONAL INSTITUTE OF TECHNOLOGY KARNATAKA (NITK),
SURATHKAL, MANGALORE - 575 025
JULY, 2017

DECLARATION

By the Ph.D Research Scholar

I hereby *declare* that the Research Thesis entitled **"MOLECULAR DYNAMICS STUDIES OF THE STRUCTURAL, THERMO-MECHANICAL AND FINITE SIZE ELASTIC PROPERTIES OF HEXAGONAL BORON NITRIDE"**, which is being submitted to the ***National Institute of Technology Karnataka, Surathkal*** in partial fulfillment of the requirements for the award of the Degree of ***Doctor of Philosophy*** in ***Physics*** is a *bonafide report of the research work carried out by me*. The material contained in this thesis has not been submitted to any University or Institution for the award of any degree.

Siby Thomas
Register No.: 112027 PH11F09
Department of Physics
National Institute of Technology Karnataka
Surathkal.

Place: NITK - Surathkal

Date: 26 July, 2017

CERTIFICATE

This is to *certify* that the Research Thesis entitled **"MOLECULAR DYNAMICS STUDIES OF THE STRUCTURAL, THERMO-MECHANICAL AND FINITE SIZE ELASTIC PROPERTIES OF HEXAGONAL BORON NITRIDE"**, submitted by **Siby Thomas** (Register Number: 112027 PH11F09) as the record of the research work carried out by him, is *accepted* as the *Research Thesis submission* in partial fulfillment of the requirements for the award of degree of ***Doctor of Philosophy***.

Dr. Ajith K M
Research Guide
Assistant Professor
Department of Physics
NITK Surathkal - 575025

Chairman - DRPC
(Signature with Date and Seal)

This Thesis is dedicated to Prof. M. C. Valsakumar and Dr. Ajith K. M., whose enthusiasm and knowledge inspired me as a student !

ACKNOWLEDGEMENT

This research work could not have been possible without the support, help, and encouragement from many people. First of all, I am indebted to my supervisor, Dr. Ajith K M for his guidance, patience, motivation and constant support. His philosophy towards the work and life has always been an endless energy to me. I am very fortunate to have him as my mentor, teacher and a role model, whom I have never seen without a smiling face. It is my privilege to be the student of such a compassionate human being. I also would like to express my gratitude to his beloved wife Mrs. Padmaja U K and son AdiSankaran (Appu), for the love and care they have shown towards me. Many thanks, my beloved sir.

I have been fortunate enough to get into contact with Prof. M. C. Valsakumar, our beloved Valsa sir. He is a teacher extraordinaire, a kind of inspiring personality, has always been there to lead, to teach and to motivate. His enthusiasm, immense help, and graceful presence is the backbone of this work. Valsa sir has always tried to impart his great knowledge to the students and I owe him every ounce of knowledge that I learned through this work. On this occasion, I express my heartfelt gratitude towards Valsa Sir. I also owe my deep gratitude towards Mrs. Leela Valsakumar, his wife, for her support and encouragement. I am greatly indebted to her for the caring and happy domesticity, endless love, and support.

I owe my gratitude to Dr. G. Harikrishnan, Associate professor, Dept. of Physics, Govt. College Madappally, Vatakara, Kerala. He was always there to encourage, teach, help and motivate me like an elder brother. He extended his great help and advice which filled me with hope during my hard times of research. I am indebted to Dr. Chandhini G., Department of MACS, NITK Surathkal for her moral support, practical suggestions and devoted sisterly affection which helped me to tide over many hard times and which will always be cherished. Dr. T. K. Shajahan, Department of Physics, NITK Surathkal has always inspired me with his timely advice, pleasant and straight forward comments about my research, which have been a real boost of motivation.

I would like to thank my Research Progress Assessment Committee members, Dr. Rajendra Udupa, Professor, The Department of Metallurgical and Materials Engineering, and Dr. Darshak R. Trivedi, Assistant Professor, Department of Chemistry for their constructive and timely suggestions and constant support, which always provided me extra energy to do my work within the time frame. I remember with gratitude the international travel support received from TEQIP-II of NITK, to present our research work during the British Carbon Group's Conference on Carbon Nanoscience and Nanotechnology at Trinity College, Dublin, Ireland in 2016.

I am grateful to all the faculty members of the Physics Department of NITK Surathkal, Prof. G. K. Shivakumar, Prof. G. Umesh, Prof. Kasturi. V. Bangera, Prof. N. K. Udayashankar, Prof. H. D. Shashikala, Dr. M. N. Satyanarayan, Dr. H. S. Nagaraja, Dr. Partha P. Das, Dr. Deepak Vaid, Dr. Kartick Tarafder and Dr. Kishore Sridharan for the constant support, motivation and help they provided during my research life. I am also indebted to the non-teaching staff of the Department, Mrs. Saritha Shetty, Mr. Dhanraj, Mrs. Mohini, Mrs. Ashalatha, Ms. Usha, Mr. Chandranath, Mr. Sheshappa Nayak, Mrs. Veena, Mr. Pradeep, Mr. Harshith, Mr. Karthik and Mrs. Suma for their endless support for my day-to-day activities in the department. I would also like to thank all the staff of the Institute and Hostel office for their cooperation and support during my research life.

I thank Dr. Sharat Chandra and Mr. Anees P, the scientists at the Computational Materials Science group of the Materials Physics Division, IGCAR, Kalpakkam, for their valuable guidance and help during all stages of my research work. I thank Mr. Manan Dholakia, Mrs. Gurpreet Kaur, Mr. P. Jegadeesan, Mr. B. Radhakrishna and all the scientists at the materials Physics Division of IGCAR who have been very helpful during the initial stages marked by uncertainty, inhibitions, and inexperience in this field. I would like to acknowledge the computational resources at the IUAC, New Delhi, in addition to our own resources at NITK.

I am indebted to Dr. N. Sathish, Senior scientist at the CSIR-Advanced Materials and Processes Research Institute for his innovative ideas and motivation for my work. I am grateful to Dr. Madhu K of UC College, Aluva for his encouragement and support throughout my research career. I would like to mark my deep gratitude to Dr. Padmesh Anjukandi, Assistant Professor of Chemistry, Indian Institute of Technology Palakkad, for his unceasing motivation and encouragement. I thank Dr. Beneesh P. B. and Dr. Deepu Vijayasenan of the NITK family for their inspiring and motivating approach which has positively influenced my life and career. I remember all my teachers and mentors with gratitude, who have always inspired me and shed light on my personal path as well as academic life. I thank all the teachers of Rajah's Higher Secondary School Nileshwar, Govt. Higher Secondary School Chayoth, Nehru Arts and Science College Kanhangad and St. Stephen's college Uzhavoor, Kerala, in particular Chandramathi Teacher, Mr. Dinesh Kumar, Prof. Lally Cyriac, Dr. K. M. Udayanandan, Prof. R K Sathish, Prof. P. V. Siddharthan, Dr. K. V. Murali, Ms. Marykkutty, Mr. Pradeep Kumar, Mr. Prakash T V, Dr. Bobby Jose, Mr. Hariprasad and Mrs. Mini.

I am fortunate to have a lot of friends and well wishers in my life. First and foremost, I express my profound gratitude to Mr. Sreejesh M, who has always been there to motivate me since 2004, to push me through the hard times and the only reason for my entry to NITK as a research student. I thank Mr. Nimith K M and Dr. Manoj Kumar N, for their endless help, support and camaraderie which will ever be cherished. I am indebted to my Computational Physics Lab (CPL) colleagues of NITK, Mrs. Manju M S, Mr. Kartheek Hegde, Mr. Naveena Kumara for their positive energy during my research life.

I would like to heartily thank Ms. Manju Mahipalan and Ms. Revathy B S, my incredibly nice friends for all their support and for providing comments and valuable suggestions for my thesis in spite of their busy academic schedule. My sincere thanks to my beloved friends, Mr. Ahmed Rizwan C L, Mr. Safir T K, Ms. Rajani K V, Mr. Sterin N S, Mr. Ahamed Khasim, Mr. Shreyas, Mrs. Amrutha S V who treated me like a brother and made my life at NITK Surathkal an ever memorable one. I thank all the research scholars and M. Sc students of the Department of Physics for their kindness towards me. I also thank all my friends in and around NITK, Mr. Bibhudatta Dash, Dr. K. K. Nagaraj, Dr. Arun P. Parameswaran, Dr. Ansal V, Mr. Arun Augustin, Dr. Dickson D. Babu, Dr. Gibin George, Dr. Goutham Sarang, Mr. Sreebhash, Mr. Vishnu M Nair, Mr. Jithin M A, Mr. Sangeeth, Mr. Yadhunath, Mr. Liju Elias, Mr. Sibin K P, Mr. Vimal Edachery, Mrs. Melby Chacko, Mr. Abhinav, Dr. Vijeesh, Mr. Ramana Reddy, Ms. Bindu K, Mrs. Pranitha Shankar, Mr. Rino Cheriyan, Mr. Mahendra K, Mr. Achyutha, Mr. Brijesh, Mr. Dhanush Shanbhag, Mrs. Sruthi, Ms. Nayana Devaraj, Mr. Ramesh Reddy, Dr. Venkateswara Rao G, Dr. Santhosh Kumar and Mr. Abid Rahman are few among them, who have extended their love, support, motivation and care during my academic and research time. I wish to thank the all the members of the NITK community who have helped me over these years. I thank all my schoolmates, degree and post-graduate friends for their ever cherishing friendship and support. I also thank my friends from other institutions, Mrs. Dilna Azhikodan, Mrs. Priyanka K P, Mr. P A Praveen, Ms. Jyoti Krishna, Ms. Shikha Kumari and Ms. Haripriya K for their help, constant encouragement and love towards me. Thank you all for your help and affection which will always be cherished.

I remember with gratitude, the support and goodwill extended to me by my family friends, especially Tomy M. Lasar, Balakrishnan Nair, Rajeevan K, Prasannan P K, Jose Kalangalil, Shyam M V, Sachin P S, Binoy Hareendran and Muhammed Rafi. I am also deeply indebted to my young friends, Mr. Nikhil Dev, Mr. Ubais, Mr. Vishnu M. Shivaraman, Mr. Rajesh and Mr. Ratheesh who showered their love, care, help, and kindness to my parents during my brother's and my absence at home. I thank my all other friends and relatives for being there as a source of motivation and encouragement.

The successful completion of this work was only because of my parents and brother, Mr. V. K. Thomas, Mrs. Lucy Thomas and Mr. Samson Thomas, who are my greatest strength and weakness. I owe my love and gratitude to them, for their unconditional love, trust in me and whole-hearted support during every stage of my life and Ph.D. candidature. The immense encouragement and inspiration I received from my parents and brother for this pursuit were splendid.

Finally, I remember with gratefulness all the people and well-wishers for the help, support and blessings for my research work who I may have unknowingly not mentioned. Many thanks to all who have made this happen.

Siby Thomas

ABSTRACT

This thesis investigates the structural, thermo-mechanical and finite size elastic properties of hexagonal boron nitride (h-BN) using classical molecular dynamics simulations. At high temperatures, specific heat shows considerable increase beyond the Dulong-Petit limit which is interpreted as a signature of strong anharmonicity present in h-BN. Analysis of the height fluctuations shows that the bending rigidity and variance of height fluctuations are strongly temperature dependent and this is explained using the continuum theory of membranes. The observed Young's modulus and Poisson ratio of h-BN is increase with system size in accordance with a power law, and are found to be anisotropic for finite sheets whereas they are isotropic for infinite sheets and they also satisfy Born's criterion for mechanical stability. Using the formula derived from Foppl-von Karman plate theory, variation of bending rigidity with system size is determined from the measured value of thin shell thickness. As the system size increases, the zero Kelvin Young's modulus also increases, which leads to an increase in the longitudinal and shear wave velocities. The strain fluctuation method is employed to investigate the temperature dependent elastic constants of h-BN. It has been noticed that the size of the h-BN sheet increases the thermal rippling, which not only decreases the thermal expansion coefficient and the elastic moduli, but also leads to a large deviation from the isotropic elasticity. The effect of changing the cut-off distance in the empirical potential on the stress-strain relation and the temperature dependent Young's modulus of pristine and defective hexagonal boron nitride is also studied. The observed mechanical strength of h-BN is significantly affected by the vacancy and Stone-Wales type defects. The defect analysis shows that presence of vacancy type defects leads to a higher Young's modulus, in the studied range with different percentage of defect concentration, in comparison with Stone-Wales defect. The estimation of various thermo-mechanical and elastic properties of h-BN has underlined their importance in many applications.

Keywords: Hexagonal boron nitride; Molecular dynamics; Ripples; Defects; Bending rigidity; Finite size effect; Elastic constants; Strain-fluctuations; Anisotropy; Sound velocities.

Contents

List of Figures v

List of Tables xiii

Nomenclature xvii

1 Introduction **1**

1.1 Hexagonal Boron Nitride 4

1.1.1 Structural Characteristics 6

1.1.2 Thermal Characteristics 7

1.1.3 Mechanical and Elastic Characteristics 8

1.1.4 Defect-Associated Characteristics 9

1.2 Scope and Objectives of the Present Research Work 9

1.2.1 Scope 9

1.2.2 Objectives 11

1.3 Organization of the Thesis 11

2 Details of Atomistic Simulation **15**

2.1 Classical Molecular Dynamics 16

2.2 LAMMPS 23

2.3 The Empirical Interatomic Potential 24

2.3.1 Tersoff Potential 25

3 Temperature Dependent Structural and Thermal Properties **29**

3.1 Introduction 29

3.2 Methodology 30
3.3 Results and discussions 31
  3.3.1 Structural Properties 31
  3.3.2 Radial distribution function 35
  3.3.3 Specific heat at constant volume 36
  3.3.4 Linear thermal expansion coefficient 38
  3.3.5 Defects in h-BN 41
  3.3.6 Thermally excited ripples 44
  3.3.7 Bending rigidity and scaling property 46
3.4 Conclusions 54

4 Directional Anisotropy, Finite Size Effect and Elastic Properties 55
4.1 Introduction 55
4.2 Molecular dynamics modelling 56
4.3 Results and discussions 59
  4.3.1 Elastic Constants 59
  4.3.2 Acoustic wave velocity using elastic constants 67
  4.3.3 Thin shell thickness and bending stiffness 71
4.4 Conclusions 74

5 Effect of Ripples on the Finite Temperature Elastic Properties using Strain-fluctuation Method 75
5.1 Introduction 76
5.2 Methodology 77
5.3 Results and discussions 81
  5.3.1 Thermal rippling behavior of h-BN 81
  5.3.2 Temperature dependence of lattice parameter and thermal expansion coefficient 83
  5.3.3 Elastic constants 85
  5.3.4 Sound velocities 91
5.4 Conclusions 92

6 Effect of temperature and defects on the mechanical properties 95
6.1 Introduction 96
6.2 Methodology 96
6.3 Results and discussions 97
6.3.1 Effect of original cut-off parameter on the mechanical behaviour 97
6.3.2 Influence of optimized cut-off parameter on the anisotropic mechanical behavior 100
6.3.3 Stiffness of pristine h-BN 102
6.3.4 Young's Modulus of defective h-BN 104
6.3.5 Deformation dynamics 108
6.3.6 Structural integrity analysis 108
6.4 Conclusions 111

7 Summary and Future Work 113
7.1 Summary 113
7.2 Future prospects 115

Appendices 117

A LAMMPS Features 119

B LAMMPS Input File 123

C Theory of Two dimensional Crystalline Membrane 125

Bibliography 131

List of publications 144

Curriculum Vitae 147

List of Figures

1.1 The lattice structure of h-BN with lattice constants a=b=2.505 Å, c=15 Å and γ=120°. The honey-comb lattice of h-BN consists of boron atoms (blue) and nitrogen atoms (red) and are located at the vertices of the hexagon. The unit cell of the configuration is represented using the black rhombus. 6

2.1 Schematic of potential cutoff under periodic boundary conditions in two dimensions 19

2.2 The Flow chart of an MD trajectory simulation 22

3.1 The two triangular sublattices (the B- and N-lattice) creating the honeycomb structure, and the defining vectors in h-BN. 32

3.2 Temperature dependence of lattice parameter a (marked in the left y-axis) and B-N interatomic distance in the xy-plane R_{xy} (marked in the right y-axis) of h-BN sheet with 12800 atoms calculated at different temperatures with zero external pressure. 34

3.3 Figure (a), (b) and (c) shows the Radial distribution function of B-N, B-B and N-N pairs in h-BN sheet at various temperatures. The value of RDF at any r decreases as the temperature increases due to thermal broadening. 36

3.4 (a) Variation of the total energy (per atom) of the monolayer h-BN sheet as a function of temperature. (b) The variation on specific heat capacity at constant volume with temperature of h-BN sheet at a time step of 0.1 fs using NVT simulation. We have chosen 20000 atoms for the simulation. 38

3.5 The nonlinear dependence of total energy with temperature. The $U(T)$ vs T data is fitted to a quartic polynomial with the fractional residual less than 10^{-6}. 39

3.6 Variation of linear thermal expansion coefficient of h-BN sheet. h-BN shows negative thermal expansion at low temperatures due to presence of low frequency bending modes in its phonon spectrum. The results obtained from the present study are in qualitative agreement with the overall trend suggested by the results obtained from experimental and QHA based investigations. 40

3.7 Formation of the vacancy and Stone-Wales defect in the h-BN sheet. A SW defect is formed when a pair of atoms is rotated by 90 degrees to form two pentagons and two heptagons. 42

3.8 Variation of cohesive energy with defect concentration in h-BN sheet. As the percentage of defect concentration increases, energy per atom also increases (equivalently, cohesive energy decreases). 43

3.9 Monolayer h-BN sheet at 0 K (top) and the flat surface becomes corrugated due to thermally excited ripples at 300 K (bottom) under periodic boundary condition. 45

3.10 Variation in $\langle h^2 \rangle$ with time step for different temperatures in h-BN sheet. When the simulation is carried out for long time, the value of $\langle h^2 \rangle$ stabilizes to a constant level. The black line corresponds to a temperature of 100 K and the cyan line is for 2400 K. The rest of the lines correspond to temperature in between 100 and 2400 K. 47

3.11 The variation in mean square displacement as a function of concentration of SW and vacancy defects at 300 K for h-BN sheet with 20000 atoms. 48

3.12 (a) Height-height correlation function $H(q)/N$ of pristine and defective h-BN sheet with 20000 atoms at different temperatures. Both Stone-Wales and vacancy type defects are considered. The solid line corresponds to power law fit q^{β} for small values of q, namely 0.1 to 1 Å^{-1}. The exponent is found to be dependent on temperature. Its value differs from the value of 4 that is expected from the harmonic theory of membranes. (b) System size dependence of the correlation function is shown with cells containing up to 80000 atoms. The continuum theory breaks down and deviations from power-law behaviour occur if the value of $q \geq 1.0$ Å^{-1}, which is close to the Bragg peak position at $q = 4\pi/\sqrt(3)a$ = 2.8948 Å^{-1}. 50

3.13 (a) Bending rigidity (κ) of pristine and defective h-BN sheet as a function of temperature, (b) variation of scaling exponent with temperature for pristine and defective h-BN sheets and (c) the variation of height-height correlation function with temperature for pristine and defective h-BN sheets. The bending rigidity calculated using the continuum formula increases monotonically with temperature in pristine h-BN sheet and the bending rigidity starts decreasing above 2000 K in defective h-BN sheet. 51

3.14 Room temperature (a) variation in $\langle h^2 \rangle$ against L=$\sqrt{L_x L_y}$ of pristine and defective sheets, (b) system size dependence of bending rigidity and (c) variation of the scaling exponent β with system size. 53

4.1 Bond length and bond angles of an infinite (a) unstrained pristine BN sheet. Considerable change in the bond length and bond angle has been observed after applying a deformation to the (b) armchair and (c) zigzag direction. The white arrow in fig (b) and (c) represents the direction of deformation in armchair and zigzag chirality. 58

4.2 Variation of Young's modulus with inverse system size. As the system size become higher, the value of Young's modulus tends to a saturated value in both armchair and zigzag directions. 64

4.3 The variation of Poisson's ratio with inverse system size in armchair and zigzag chirality. 64

4.4 The energy-strain response graph for the calculation of elastic constants of h-BN. The total energy is plotted as a function of various specific strains necessary for calculating the elastic constants. (a) Calculations on a sheet with 10000 atoms subject to periodic boundary condition show that C_{11} = C_{22}. (b) A finite system consisting of 400 atoms with periodic boundary condition and a vacuum space of 20 Å, shows significant difference in the computed elastic constants. (c) and (d) When the system size increases from 25,600 to 90,000 atoms, respectively, behaviour of the finite system tends to that of an infinite system. 66

4.5 Dependence of the elastic constants C_{11} on the inverse system size. We fitted the values of C_{11} in each system size to the equation $C(N) = A - B/N^{\nu}$ and plotted the results as a function of $1/N$, where N is the number of atoms in the simulation cell. The value of the scaling exponent ν obtained from the fit is 0.4. The blue line represents the value of the respective elastic constant extrapolated to infinite system size limit. . 68

4.6 Dependence of the elastic constants C_{12} on the inverse system size is shown in figure. We fitted the values of C_{12} in each system size to the equation $C(N) = A - B/N^{\nu}$ and plotted the results as a function of $1/N$, where N is the number of atoms in the simulation cell. 69

4.7 As the system size increases, the Young's modulus of h-BN system increases, leading to an increase in longitudinal and shear wave velocities. 70

4.8 As the Young's modulus and Poisson's ratio increases, the bending rigidity also increases to a saturated value of 0.56 eV. 72

4.9 The calculated bending rigidity and its scaling with inverse system size. The blue line represents the value of the respective bending rigidity extrapolated to infinite system size limit. 73

5.1 Dependence of the elastic constants C_{11} and C_{12} on the inverse system size ($1/N$) at 300 K is shown in (a) and (b) respectively. Here, we fitted the values of C_{11} and C_{12} in each system size using a polynomial function, where N is the number of atoms in the simulation cell. Variation of Young's modulus with inverse system size at 300 K is shown in (c). As the system size become higher, the value of Young's modulus decrease consistently with the variation of elastic constants due to the thermally excited ripples. 84

5.2 (a) Variation of in-plane lattice parameter (a_{int}) of h-BN with temperature; (b) The linear thermal expansion coefficient (LTEC) as a function of temperature. 85

5.3 Variation in (a) simulation cell size and (b) angle gamma of h-BN as a function of MD timestep at different temperatures. 87

5.4 Temperature dependent elastic constants of h-BN calculated using strain-fluctuation method. Independent elastic constants (a) C_{11} and (b) C_{12} are calculated using the values of instantaneous strain. 88

5.5 Temperature dependent (a) Young's modulus and (b) Poisson's ratio are calculated from the computed values of elastic constants. 89

5.6 Variation of computed (a) bulk and (b) shear modulus using strain-fluctuation method for h-BN as a function of temperature. 90

5.7 Variation of calculated (a) longitudinal and (b) shear wave velocities of h-BN using strain-fluctuation method with temperature. 92

6.1 Variation of engineering stress due to the bond stretch with bond strain of armchair and zigzag deformation direction of h-BN sheet using the original Tersoff potential cut-off parameter of 1.95 Å. 98

6.2 The variation in potential energy of pristine h-BN at room temperature with different potential cut-off parameter for armchair and zigzag configurations. It has been observed that the potential energy shows a sudden decrease of slope beyond a strain value of 0.3. Using the original and lower cut-off parameters, we observed a sudden rise in engineering stress corresponding to a small amount of engineering strain. This can be understood from the fact that the force is zero for all the particles whose nearest neighbour distance exceeds the upper cut-off distance S_{ij} in the expression for the potential. Since the potential energy of these atoms is zero, instead of a negative value if the interaction was calculated with a larger cut-off, the average potential energy increases. The nonzero kinetic energy of these particles manifests as an outward pressure which leads to increase in stress and leads to a run-away situation. . 99

6.3 The variation in stress-strain relationship of h-BN at room temperature with different potential cut-off function for armchair and zigzag configurations. Due to this sharp rise in stress value using the original (1.95 Å) and below original (< 1.95 Å) cut-off parameter, h-BN shows an unphysical as well as fictitious fracture behavior. This is due to the failure of the smoothing function in the empirical potential and at the stage of deformation, the force on all these particles become zero as $f_c(r)$ becomes zero, and hence the potential as well as the force becomes zero, by definition of the cut-off. 100

6.4 Variation in engineering stress corresponds to the applied strain of armchair and zigzag configurations at various temperatures of pristine h-BN using the optimized cut-off parameter (2.25 Å) of the potential. 101

6.5 Variation of Young's Modulus with temperature of pristine h-BN along the armchair and zigzag configurations using the optimized cut-off parameter (2.25 Å) of the potential. 103

6.6 Temperature dependence on the elastic energy of pristine h-BN along the armchair and zigzag orientations using the optimized cut-off parameter. The variation in stored elastic energy with increase of temperature has been noticed and the strain rate for the simulation is kept constant at 10^9 s^{-1}. 105

6.7 The variation in engineering stress corresponds to the applied strain of armchair and zigzag configurations of defective h-BN at 300 K using the optimized cut-off parameter (2.25 Å) of the potential. 106

6.8 The variation of Young's modulus with vacancy and Stone-Wales defect concentration along the armchair and zigzag configurations of h-BN at 300 K using the optimized cut-off parameter. The decrease in Young's modulus shows a linear behavior with increase in defect concentration. . 107

6.9 Snapshots of the fracturing dynamics of pristine h-BN sheet at 300 K. The snapshot of the deformation during the initial relaxation at 200 ps is shown in (a) and the deformation mechanisms at 400 ps is shown in (b). The oval shape shows the deformed areas in the sheet. 109

6.10 The radial distribution functions of pristine and defective h-BN under tensile tests at a temperature of 300 K. The binsize is taken as Δr = 0.005. The RDFs of pristine h-BN at the equilibrium state is in comparison to the case of Vacancy and SW defect of (a) armchair and (b) zigzag configuration. When the sample is elongated along x direction, it should contract in the y-direction. For pristine h-BN in the armchair termination, the bond length increases to 1.55 Å in the x direction and decreases to 1.41 Å in the y direction both starting from the original value of 1.45 Å. For pristine h-BN in the zigzag termination, the bond length increases to 1.54 Å in the x direction and decreases to 1.44 Å in the y direction both starting from the original value of 1.45 Å. Thus h-BN in zigzag configuration is more resilient to deformation than the one in armchair counterpart. 110

List of Tables

2.1 Tersoff-type inter atomic potential parameters optimized for hexagonal boron nitride. 28

3.1 Comparison of lattice parameter of Monolayer h-BN Sheet reported during various calculations. 33
3.2 Formation energy of various defects in h-BN calculated for 0 K. N_V is the number of vacancies required for creating the defect. 42
3.3 Bending rigidity κ and scaling exponent β at different temperatures for pristine and defective h-BN sheet. 53

4.1 Calculated elastic properties of the infinite h-BN and comparison with the experimental and other theoretical calculations. Young's modulus (Y) [in GPa] and Poisson's ratio (ν) are tabulated. 67

6.1 The system size (rectangular sheet) dependence of Young's modulus (YM) of h-BN at 300 K. The variation in Young's modulus with system are negligible as shown in the table. 102
6.2 Calculated Young's modulus (Y) of pristine h-BN using the engineering stress-strain relation in comparison to the earlier experimental, theoretical and computational analysis. The interatomic potential parameter (IPP) used for the method of calculation has also given. 104

Nomenclature

κ	Bending rigidity
ρ_m	Two dimensional mass density
$^\circ$	Degree
$^\circ$ C	Degree Celsius
C_p	Specific heat at constant pressure
C_v	Specific heat at constant volume
r_c	Cut-off function of the potential
v_p	Longitudinal wave velocity
v_s	Shear wave velocity
2D	Two dimensional
Å	Angstrom
B	Boron
BC_3	Boron carbide
BNNT	Boron nitride nanotube
BOP	Bond order potential
C	Carbon

C_{ij}	Elastic constants
c-BN	Cubic boron nitride
CNT	Carbon nanotube
DFT	Density functional theory
e.g.	Example
etc.	et cetera
eV	Electron volt
FvK	Foppl-von Karman
FWHM	Full width at half maximum
GGA	Generalized gradient approximation
H(q)	Height-height correlation function
h-BN	Hexagonal boron nitride
i.e.	That is
K	Kelvin
k_B	Boltzman constant
LAMMPS	Large-scale Atomic/Molecular Massively Parallel Simulator
LDA	Locan density approximation
LTEC	Linear thermal expansion coefficient
MC	Monte Carlo
MD	Molecular dynamics
MEMS	Micro-Electro-Mechanical Systems

MoS_2	Molybdenum disulfide
MSD	Mean square displacement
N	Nitrogen
NEMS	Nano electro mechanical systems
NPT	Isothermal-isobaric ensemble
NVE	Microcanonical ensemble
NVT	Isochoric-isothermal ensemble
QHA	Quasi harmonic approximation
RDF	Radial distribution function
SiO_2	Silicon dioxide
SW	Stillinger-Weber
SW-Defect	Stone-Wales defect
TEC	Thermal expansion coefficient
$U(\mathbf{r}_{ij})$	Potential energy
$\mathbf{F}_{ij}$	Force

Chapter 1

Introduction

This chapter provides a brief introduction to the computational materials science and the two dimensional (2D) material hexagonal boron nitride. The advantages and applications of hexagonal boron nitride along with the detailed literature survey are also presented. In addition to that, scope and objectives of the present research work and the structure of the thesis are detailed in this section.

The man-made world we see today is a brilliant example of how mankind has progressed from cave-dwelling existence to a completely modern, socially oriented lifestyle. In this process of advancing, mankind has used all kinds of materials available to bring into life his creativity and imagination. Humans have been using materials for at least 10,000 years of the recorded history. From earlier tools which were found in the pre-historic era to the modern high-tech gadgets, the role of materials has been inevitable in the journey. Some materials have even defined the culture which humans have today and some are so tied with our progression towards advancement. Many of the significant developments in the human history including the growth of architecture, the transition to a machine dominated industry from an agrarian economy can be attributed to the use of and advancement in the materials. Materials even named the ages of human civilization: the Stone Age, the Bronze Age, and the Iron Age. The study of materials, their characteristics and properties is called Material Science. The progress in this field has enabled humans to employ materials as a crucial element in almost all walks of life. Innovations in materials is an expanding process and involves either the discovery of a completely new material or, more commonly, the modification and replacement of a material by increasing functionality or reducing cost. Many research areas immensely benefit when basic science and engineering join hands. A notable advantage is the ability to control material structures at molecular, nano, meso and macro scales. Another headway in the field is the synthesis and production of new materials.

The human brain, although extremely gifted, has certain limitations. This has paved way for the invention of computers with which simulation models were made so as to handle things which are too complex for human brains (Landau and Binder 2005). Basically, simulation and modelling involves creating a digital prototype or physical performance so as to understand its working in the real world. Thus simulation provides a theoretical basis for understanding experimental measurements. Scientific problems which are complex can be studied in a detailed and comprehensive manner using experiments and simulations which in turn generate deeper insights on the phenomenon. Computer simulation methods are extremely powerful and greatly helpful when it comes to solving problems in different but related fields of statistical mechanics, material science, physical chemistry, biophysics, etc. For many fields, these methods could be the only logical way to dive into the problems. Let us consider Statistical Physics. The well developed theoretical description of complex systems in the field and sophisticated experimental techniques for microscopic information naturally calls for deploying simulation methods to study the specific aspects of these systems in great detail.

Simulations require particular information parameters, which come either from hypothetical contemplations or from exploratory information. Simulations are frequently utilized both to illuminate hypothetical models, past specific approximations and to give an insight to experimentalists for further examinations. In the case of big experimental facilities, it is frequently required to demonstrate the potential result of an experiment by computer simulations. Simulation can bridge the gap between hypothesis and examination and it helps theorists and experimentalists go past their intrinsic confinements. The power of computers has now achieved its most extreme level at which we can comprehend the complex numerical conditions and quantum mechanical computations for vast frameworks. Progress in the synthesis of materials has empowered ever more extensive research exercises in science and engineering devoted totally to two dimensional (2D) materials and their applications. This is due to the combination of their expected structural perfection, small size, low density, high stiffness, high strength and excellent electronic properties (Tang and Zhou 2013).

Materials science turned out to be more mainstream in the late nineteenth century and the contributions of the acclaimed American theoretical researcher Josiah Willard Gibbs is also noticable. Gibb's contributions in thermodynamics is helped to identify the various physical and chemical properties of materials. This includes relating thermodynamic laws to the atomic structure, electronic properties, phase transitions, and so forth., of materials through experiments and additionally theoretical methodologies. So as to simulate the macroscopic engineering designs, results from simulations at the intermediate length scale naturally feed the program and help to predict the properties of materials (Frenkel and Smit 2001). The main aims of the computational materials science are extensively the following (Lee 2011):

- To determine the stable and metastable structures of materials.
- To obtain insight into the physical basis of observed materials behavior (electric, magnetic, optic, thermal, rheological, tribological and mechanical properties).
- To be able to incorporate micro structural details of practical materials with defects and inhomogeneities.
- To predict a materials response under extreme conditions (like high pressure, temperature, magnetic field, nuclear radiation, shock, etc.).
- To provide guidelines for the design of a material with desired properties.
- To provide guidelines for optimization of materials processes.

1.1 Hexagonal Boron Nitride

A two dimensional (2D) material is the one in which the atomic organization and bond length along two dimensions are similar and much stronger than along a third dimension. Study of two-dimensional materials has become a vibrant field in condensed matter physics. Two dimensional molecular sheets have received a lot of attention in recent years because of their excellent properties and applications. Two dimensional atomic layers derived from bulk layered materials are very interesting from both scientific and engineering point of view. The interest in two dimensional materials has been intensified by the discovery of graphene, the honeycomb lattice having hexagonal atomic arrangement of carbon atoms (Novoselov et al. 2005, Geim and Novoselov 2007).

A recent field of research activity in materials science has been on graphene-analogous low dimensional materials (including 2D nano sheets, nanotubes and 1D nano ribbons) and their features and potential applications extracted using both experimental and computational methods. Examples of low dimensional materials analogous to graphene include hexagonal boron nitride (h-BN) (Jin et al. 2009), silicene (Takeda and Shiraishi 1994, Vogt et al. 2012, Kara et al. 2012), borene (Lau and Pandey 2008, Liu et al. 2013a), phosphorene (Liu et al. 2014), BC_3 (Kouvetakis et al. 1986, Popov and Boldyrev 2012), BC_5, BC_7, MoS_2(Radisavljevic et al. 2011) and h-$MoSe_2$. This thesis focuses on the analysis of various structural and thermo-mechanical properties of a promising two dimensional material, hexagonal boron nitride.

Monolayer hexagonal boron nitride (h-BN) (Zeng et al. 2010) is the lightest of group III-V compounds of alternate boron and nitrogen atoms and has high optical phonon modes and large electrical band gap of 5-6 eV (Golberg et al. 2010). Hexagonal boron nitride is tightly packed into a two dimensional honeycomb crystal lattice with sp^2 hybridization and is a versatile material having a number of potential applications (Eichler and Lesniak 2008). The novel properties of hexagonal boron nitride sheet include high dielectric breakdown strength, high volume resistivity and good chemical inertness (Lipp et al. 1989). These properties make it a good choice for many industrial applications. Hexagonal boron nitride is a promising dielectric material (Song et al. 2010) similar to graphite, but it is an insulator exhibiting ionic character with a wide band gap and can be used in hybrid graphene devices (Kinaci et al. 2012). It is stable up to 1500°C in air and does not react with most chemicals. It can be used as a part of high temperature oxidation resistant coatings and also the next generation electronic devices. Graphene layers coated with a few h-BN layers are used in high temperature graphene devices (Liu et al. 2013b). Since hexagonal boron nitride coatings can withstand ultra high temperature, it is used as a protective material against high temperature oxidation damage in aerospace applications. Boron nitride sheet is a planar isomorph of graphite (Jain et al. 2013) and lattice constant of h-BN is 2.504 Å and that of graphene is 2.456 Å. It has high optical phonon energy ($\sim$ 2 times that of SiO_2), high chemical inertness, high thermal conductivity, thus it is an excellent substrate for graphene (Xue et al. 2011, Dean et al. 2010).

Monolayer hexagonal boron nitride is also known as 'white graphene', because it is iso-electronic with carbon. Hexagonal boron nitride consists of alternate boron and nitrogen hexagonal structure having $(BN)_3$ rings. Hexagonal boron nitride can be used as a substrate for high quality graphene electronics, because it provides more superior characteristics than that of the usual SiO_2 substrate. Earlier studies have reported that h-BN does not react with steel and iron, making it a promising material for the coating of heavy-duty tools. It can also be used for manufacture of protecting cages and molds (Rubio et al. 1994). It has been reported that boron nitride nano sheets and its derivatives are expected to have better mechanical and electronic properties over layered carbon counter parts (Verma et al. 2007). The excellent mechanical stability and thermal conductivity of boron nitride derivatives make this a promising material for the construction of nano devices (Dean et al. 2010).

Hexagonal boron nitride is one of the ultimate thin membranes having high Young's modulus and tensile strength, but, less than that of graphene. The combination of these mechanical properties makes it a suitable candidate for biological membranes and stretchable electronic applications (Wu et al. 2013). Because of the high chemical and thermal stability of hexagonal boron nitride and its derivatives such as boron nitride nanotubes (BNNTs) and BN-heterostructures are extensively used as a part of high temperature devices and also in gas seals of oxygen sensors, crucibles for molten glasses and melts, parts of high temperature furnaces, etc. The first isolation and experimental study of thin sheets of h-BN has been reported by Pacilé et al. in which their crystallinity and continuity over several microns are established (Pacile et al. 2008).

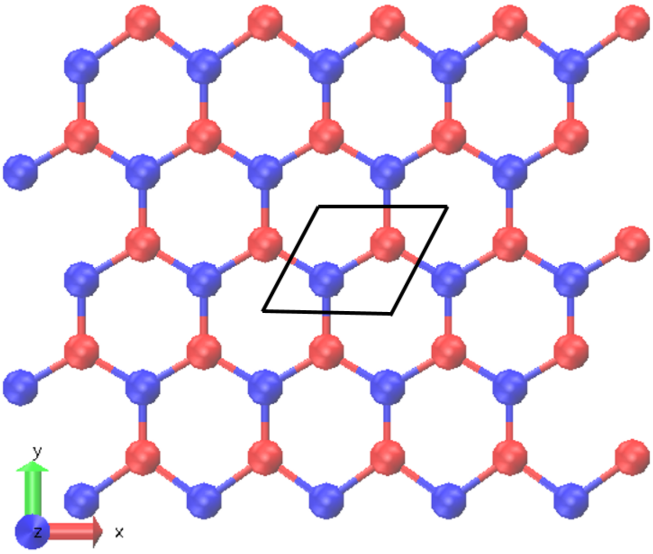

Figure 1.1: The lattice structure of h-BN with lattice constants a=b=2.505 Å, c=15 Å and γ=120°. The honey-comb lattice of h-BN consists of boron atoms (blue) and nitrogen atoms (red) and are located at the vertices of the hexagon. The unit cell of the configuration is represented using the black rhombus.

1.1.1 Structural Characteristics

Albe et al., has presented the *ab initio* density functional theory (DFT)- local-density approximation (LDA) and empirical simulation methods to calculate the properties of different BN structures (Albe et al. 1997). An empirical interatomic potential is also introduced and is parameterised by means of *ab initio* method. The classical molecular dynamics (MD) simulation for h-BN is also then studied using this empirical potential. Matsunaga et al., have developed Tersoff potential parameters to investigate the properties of cubic boron nitride systems by MD simulation (Matsunaga et al. 2000). Even though boron nitride normally has a hexagonal structure, cubic BN (c-BN) with zinc blende structure is also produced at high pressure and high temperature. It has been mentioned that the accuracy and validity of MD studies strongly depend on the interatomic potential used to describe the energy surface between particles. Experimentally observed lattice parameter of h-BN at room temperature is a=2.504 Å with an average B-N interatomic distance of 1.44 Å (Paszkowicz et al. 2002).

Molecular Statics simulations using a modified Albe, Moller and Heining interatomic potential gives the equilibrium lattice parameter as a=2.532 Å (Albe et al. 1997) with an average B-N interatomic distance as 1.46 Å. Slotman et al., have investigated the structural properties of single layer h-BN in comparison to graphene using classical MD simulations and reported that the non-monotonic behaviour of the lattice parameter with temperature (Slotman and Fasolino 2012). Figure 1.1 shows the honey-comb lattice of h-BN used in the present work with boron and nitrogen atoms situated in the two sub-lattices.

1.1.2 Thermal Characteristics

By using the first principles quantum mechanical approach, Hamdi et al., have investigated the thermodynamic properties such as thermal equation of state (free energy, P-V equation of state), in-plane and out-of-plane thermal expansion coefficient, the bulk modulus and the heat capacity, etc (Hamdi and Meskini 2010). Kaloni et al., have studied the ground state properties of h-BN by employing the pseudo potential plane wave method in DFT. They have performed LDA calculation using a (6×6×4) K-point mesh and concluded that h-BN is a large bandgap (3.4 - 4.5 eV) insulator (Kaloni and Mukherjee 2011). The thermal conductivity of BNC nanostructures has been calculated using the equilibrium MD by Kinaci et al (Kinaci et al. 2012). They have developed a new interatomic empirical potential to study the many-body interactions in the 2D layered materials mainly in graphene/hBN hybrid nano structures. They have parameterised a Tersoff type interaction potential for B-C-N systems with the help of *ab initio* energetics of the B-C and N-C bonds . The thermal transport properties of these BN nanostructures are systematically studied using equilibrium molecular dynamics with a Tersoff-type empirical interatomic potential which is re-parameterised to represent experimental structure and phonon dispersion of two-dimensional hexagonal BN (Sevik et al. 2011).

Using classical molecular dynamics simulations, Slotman et al., have investigated the various thermal properties of h-BN (Slotman and Fasolino 2012). By following the work by Fasolino et al (Fasolino et al. 2007), Singh et al., have investigated the thermo-mechanical properties of single layer of h-BN using atomistic simulation method and by analysing the mean square height fluctuations and bending rigidity they have found that the h-BN sheet is a less stiff material as compared to graphene (Singh et al. 2013). The bending rigidity is very small at room temperature as compared with graphene and it increases with increase in temperature. Using a parameterised Tersoff bond order potential, Singh et al., have estimated the room temperature linear thermal expansion coefficient (LTEC), heat capacity, etc., of h-BN.

Using first principle based quasi harmonic approximation (QHA), Sevik (2014) studied the LTEC of 2D-honey comb structures and found that the LTEC of graphene and h-BN are more negative than that of their multilayerd counter parts graphite and white graphite (Sevik 2014). The obtained room temperature LTECs of graphene is $-3.0\times10^{-6}\mathrm{K}^{-1}$ and that of h-BN is $-6.5\times10^{-6}\mathrm{K}^{-1}$. Using classical molecular dynamics simulation, Anees et al., have reported the room temperature LTEC of h-BN is $-5.32\times10^{-6}\mathrm{K}^{-1}$ and using a combination of lattice dynamics and molecular dynamics, the phonon-phonon coupling in graphene and h-BN have also been analysed (Anees et al. 2015, 2016) and reported that they exhibit strong anharmonicities. In h-BN, the strong anharmonic coupling between the stretching and bending modes suppress the long wavelength fluctuations present in it, which stabilizes its flat geometry.

1.1.3 Mechanical and Elastic Characteristics

In general, the mechanical robustness of materials plays a prominent role for the manufacturing of nano-devices and also in nano-electronics. The effect of temperature and strain rate on the mechanical properties of h-BN have been investigated by Han et al., and they have observed that the Young's modulus considerably decreases with increase of temperature (Han et al. 2013). Using the framework of molecular dynamics and finite element analysis the uniaxial tensile properties of pristine and defective h-BN have been investigated and it is found that the uniaxial tensile stress-strain curves of defective and pristine h-BN sheets are almost identical up to fracture points (Le and Nguyen 2014). Using classical molecular dynamics simulation, the tensile response of boron nitride nanosheets have been investigated by Mortazavi et al., and concluded that the tensile properties are greatly influenced by the armchair and zigzag direction of the nanosheet (Mortazavi and Rémond 2012). Recently, Kumar et al., have investigated the need for an optimized cut-off function of the empirical interatomic potential for a reliable tensile calculation of boron nitride nanosheets (Kumar et al. 2016).

1.1.4 Defect-Associated Characteristics

The detailed computational study of materials incorporating defects provides a realistic picture prior to experimental analysis. The study of different types of defects including Stone-Wales defects, single vacancy and divacancy defects, grain boundaries and tetrahedron defects using nudged-elastic-band (NEB) method would help to predict the properties realistically. The usual defects observed in the h-BN layer are point vacancy and Stone-Wales (Stone and Wales 1986). Various research groups have investigated the impact of defects on the properties of BN nanosheet. By means of molecular dynamics simulations, Slotman et al., have investigated the energetics of defects in h-BN (Slotman and Fasolino 2012). Activation energies and reaction paths for diffusion and nucleation of mono and divacancy defects in hexagonal boron nitride layers are theoretically investigated using the nudged elastic band method combined with density-functional-based techniques (Zobelli et al. 2007). Qi-lin et al., have investigated the defect induced fracture behavior of h-BN sheet using molecular dynamics simulation (Qi-lin et al. 2015) and Ding et al., were studied the mechanical properties and failure behaviors of the interface of hybrid graphene/h-BN sheet using density functional theory (Ding et al. 2016).

1.2 Scope and Objectives of the Present Research Work

1.2.1 Scope

The review of the literature on h-BN reveals that the atomistic simulations using classical molecular dynamics is a powerful tool to investigate the various properties of layered structures. In MD, the accuracy of the predicted properties strongly depends on the accuracy of the potential used in the simulation. In the present study we try to explore the various physical properties of monolayer h-BN that have not been studied in detail so far using a newly developed tuned Tersoff potential especially for the studies of hybrid graphene/h-BN nano structures in which the interactions between boron, carbon and nitrogen atoms are considered (Kinaci et al. 2012).

The present work focuses on the study of temperature dependent structural, thermo-mechanical and finite size elastic properties of free standing monolayer hexagonal boron nitride. According to the well-known Mermin-Wagner theorem (Mermin and Wagner 1966), the stability of any two dimensional crystal is explained on the basis of the the presence of out-of-plane fluctuations present in the surface of the material called 'ripples'. The remarkable finding by Fasolino et al., that even at very low temperatures, the 2D graphene crystal remains intact and exhibits the thermally excited out-of-plane excursions called as 'ripples'has motivated us. This has been explained on the basis of the anharmonic coupling between the bending and stretching modes present in graphene (Fasolino et al. 2007). Understanding the behavior of ripples is important because they affect most of the physical properties of 2D materials like h-BN. In h-BN and most of the other 2D materials and membranes, the out-of-plane fluctuations with ripples have been reported and which arise naturally from the coupling between in-plane stretching and out-of-plane bending modes (Xu and Buehler 2010). In our work, we have attempted to investigate this phenomenon (ripples) in the case of h-BN.

In the present work, we have investigated the temperature dependence of lattice parameter, radial distribution function, specific heat at constant volume, linear thermal expansion coefficient, correlation function of the thermally excited ripples and formation of defects. The influence of defects on the bending rigidity is also analyzed. The finite size effect on the anisotropic elastic properties of a finite and infinite 2D sheet of h-BN at zero Kelvin have been analyzed using the energy method. The variation of bending rigidity with system size is also validated using the equation derived from the Foppl-von Karman approach. The effect of ripples on the temperature dependent elastic constants are investigated for the first time using strain fluctuation method. We also extracted the sound velocities using the derived elastic constants. We have also attempted to investigate the effect of temperature and defects on mechanical properties of pristine and defective h-BN by varying the cut-off function of the empirical interatomic potential.

1.2.2 Objectives

The major objective of this thesis is the "Molecular dynamics studies of the structural, thermo-mechanical and finite size elastic properties of hexagonal boron nitride". This work specifically focuses on:

- Study of temperature dependent structural integrity analysis, thermal properties and the bending rigidity of pristine and defective hexagonal boron nitride nanosheets.
- Study of the directional anisotropy, finite size effect and elastic properties of hexagonal boron nitride at zero Kelvin using energy method.
- Investigation of the effect of ripples on the temperature dependent elastic constant of 2D h-BN using the strain-fluctuation method.
- Analysis of the effect of temperature and defects on mechanical properties of pristine and defective h-BN by varying the cut-off function of the empirical interatomic potential.

1.3 Organization of the Thesis

The rest of thesis is organized as follows:

Chapter 2 presents a brief introduction of the computational methodology relevant for the analysis of various properties explained in this thesis. In particular classical molecular dynamics simulation is discussed.

In **Chapter 3**, we present our results on the temperature dependence of lattice parameter, radial distribution function, specific heat at constant volume, linear thermal expansion coefficient, height-height correlation function of the thermally excited ripples on pristine as well as defective h-BN sheet, etc. The Specific heat shows considerable increase beyond the Dulong-Petit limit at high temperatures, which is interpreted as a signature of strong anharmonicity present in h-BN. Analysis of the height fluctuations, $\langle h^2 \rangle$, shows that the bending rigidity and variance of height fluctuations are strongly temperature dependent and this is explained using the continuum theory of membranes.

In **chapter 4**, we present a systematic study of the finite size effect on the anisotropic elastic properties of h-BN for various system sizes. The Young's modulus and Poisson ratio are found to be anisotropic for finite sheets whereas they are isotropic for the infinite sheet. Both of them increase with system size in accordance with a power law. From the computed values of elastic constants, it is noticed that both finite and infinite sheets satisfy Born's criteria for mechanical stability. We have also presented that, due to the the strong in-plane sp^2 bonds and the small mass of boron and nitrogen atoms, h-BN possesses high longitudinal and shear velocities. The variation of bending rigidity with system size is also validated using the equation derived from the Foppl-von Karman approach.

Chapter 5 explains the effect of ripples on the calculation of temperature dependent elastic constants of monolayer h-BN for the first time using strain fluctuation method. We observed that the out-of-plane intrinsic ripples responsible for strong anharmonic behavior of h-BN leads to large deviation from the isotropic elasticity. Because of the strong thermal rippling in large systems, the h-BN sheet may have a negative thermal expansion coefficient at relatively low temperatures, with a transition to positive thermal expansion at high temperatures and this also soften the elastic constants. The calculations show that h-BN sheet satisfy Born's criterion for mechanical stability. As the temperature increases, the Young's modulus of h-BN decreases, which leads to the decrease of longitudinal and shear wave velocities.

In **chapter 6**, the effect of changing the cut-off distance in the empirical potential on the stress-strain relation and also the temperature dependent Young's modulus of pristine and defective hexagonal boron nitride has been reported. As the temperature increases, the computed Young's modulus shows a significant decrease along both the armchair and zigzag directions. The computed Young's modulus shows a trend in keeping with the structural anisotropy of h-BN. The variation of Young's modulus with system size is elucidated. The observed mechanical strength of h-BN is significantly affected by the vacancy and Stone-Wales type defects. The defect analysis shows that presence of vacancy type defects leads to a higher Young's modulus, in the studied range with different percentage of defect concentration, in comparison with Stone-Wales defect.

Chapter 7 summarizes the findings of the present research work by highlighting the important results of the thesis along with conclusions. This chapter also comprises scope for further research work in the area of 2D materials such as graphene and MoS_2.

Chapter 2

Details of Atomistic Simulation

This chapter presents a brief introduction of the computational methodology which are relevant for the calculations in this thesis. In particular, classical molecular dynamics simulations and its most important features are detailed in this section.

The best existing approaches to describing atomic interactions in condensed phases are based on quantum-mechanical descriptions of bonding. Unfortunately, first-principles quantum-mechanical descriptions are computationally expensive and, hence, their application is usually limited to situations where the number of unique atoms is a few hundred or (much) less (Mendelev et al. 2003). One of the ways of performing effective computational simulation with millions of atoms, is by considering the trajectory of the constituent atoms of the systems as classical point particles which interact and evolve under an effective interatomic potential. In general, the empirical interatomic potentials (e.g. Lennard-Jones, Morse, etc.) and the semi-empirical potentials (e.g. bond order potentials by Tersoff, reactive empirical bond order (REBO), embedded atom model (EAM) and Brenner) do not treat the quantum nature of electrons explicitly and hence allowing enormously faster calculations than quantum mechanical methods. These empirical interatomic potentials are derived by coupling the experimental data and quantum-mechanical analysis.

In the present thesis, we have employed the classical molecular-dynamics (MD) simulations for the study of h-BN using the Tersoff potential. A brief explanation of the molecular dynamics method is also presented, which will be useful to understand and interpret the results of the following chapters. The more detailed theory of MD simulation can be found in the standard text books (Allen and Tildesley 1989, Frenkel and Smit 2001, Tuckerman 2010, Rapoport 1995).

2.1 Classical Molecular Dynamics

The basic idea of molecular dynamics (MD) simulations is to calculate how a system of particles evolves in time. MD is a computational approach capable both of sampling an equilibrium distribution and producing true dynamical observables, which also employs the method of classical mechanics for the movements of atoms. As the name indicates, though MD has initially simulated a handful of molecules, later it has been extended to liquids, solids, and materials in parallel with the growth in computer power (Tuckerman 2010). The first Molecular Dynamics simulation which was applied to atoms interacting via a continuous potential was performed by A. Rahman in 1964 (Rahman 1964). Molecular Dynamics is a deterministic way to simulate the movement of atoms i.e., state of the system at any future time can be predicted from its current state. The simulation is divided into a number of time steps, usually in the order of Femto seconds (10^{-15} Seconds). Newton's equation of motion is successively solved in each time step, where the forces between all the atoms are calculated and then integrated to obtain new positions and velocities. This is iterated till the end of the simulation. During the time steps material properties can be calculated from the positions, velocities and forces. Molecular Dynamics can solve two-body, three-body and N-body problem numerically.

Before moving into the details of force calculation, it should be mentioned that two approximations underly the use of the classical equation of motion. The first of the two main approximations in MD is the Born-Oppenheimer (Born and Huang 1966) approximation in which the electrons follow the motion of the nucleus instantaneously. Moreover, the ground state is the only allowed electronic state. Consequently, for each atom of a certain element, the same potential function applies. The second approximation includes the description of atoms as point particles that follow classical Newtonian dynamics. Practically, MD is the only option for big systems of more than thousands of atoms for calculating the processes such as melting, deforming, sintering, crack-propagation, etc., in materials (Lee 2011).

In Molecular Dynamics we use Newton's law to move atoms. It is already a well known fact that the quantum effects become significant only when the particle wavelength, λ, is comparable with the interatomic distance (1 - 3 Å). Otherwise, the use of Newton's equations of motion is well justified. The validity of the classical approximation in atomistic simulation is based on the de Broglie thermal wavelength (λ) and is defined as $\lambda = \frac{h}{\sqrt{2\pi m k_B T}}$, where m is the atomic mass and T the temperature, k_B and h represent the Boltzmann constant and the Planck's constant, respectively. The classical approximation is justified if $\lambda << a$, where a is the mean nearest neighbour separation. For example, if we consider the case of diamond at 1000 °C, the thermal de Broglie wavelength λ of carbon atoms equal $1.41 \times 10^{-11} m$ (Ercolessi 1997), such that $\frac{a}{\lambda} = 11.0$. The classical treatment of carbon structures at temperatures as high as 1000 ° C is thus justified. For most elements and at higher temperatures, therefore, atomic dynamics can be predicted using Newton's equations of motion. The most important features of molecular dynamics simulations are explained in detail in coming sections:

i Initialization

It is an essential practice to assign the initial positions and velocities of all the particles in the system at the beginning of the molecular dynamics simulation. To attain a faster convergence as well as reliable results a good initial guess of positions and velocities is required. The initial positions of atoms could be anywhere but are normally specified according to the known lattice positions. Indeed, setting up an initial condition depending on the complexity of the system can be a nontrivial problem. This preparation is important to minimize meaningless data and to have reliable results. Alternatively, one can begin with random initial coordinates, restricting only the distance between particles so as to avoid strong repulsive forces initially. Once initial coordinates are specified, remaining is to set the initial velocities. This is generally done by *sampling* the velocities of atoms. The initial velocities of all the atoms could be zero, but are normally chosen randomly from a Maxwell-Boltzmann or Gaussian distribution at a given temperature.

From the theorem of equipartition of energy we can use the following relation to obtain the average kinetic energy per degree of freedom as,

$$\langle \frac{1}{2} m v_\alpha^2 \rangle = \frac{1}{2} k_B T \tag{2.1}$$

Then the instantaneous temperature at time t can be given as,

$$T(t) = \sum_{i=1}^{N} \frac{m_i v_i^2(t)}{k_B N_f}, \tag{2.2}$$

where N_f is the number of degrees of freedom.

ii **Force Calculation**

Molecular Dynamics integrates Newton's equations of motion for collections of atoms, molecules, or macroscopic particles that interact via short or long-range forces with a variety of initial and/or boundary conditions. In molecular dynamics simulations, the most time consuming part is the computation of forces generated by the potentials acting on atoms as $\frac{-dU}{dr}$ (Cai et al. 2012). Normally, a potential tail off at long distances and becomes negligible. This allows us to disregard the force calculation where the interatomic distances are beyond a certain cutoff distance, r$_{cut}$ and at this point, the force is made to go smoothly to zero. The r$_{cut}$ must be smaller than half of the primary box size as shown in the smaller circle in figure 2.1 (Lee 2011). To find the atomic trajectories, one needs to solve the following equations, the equations governing the particle coordinates. For an N-particle system with potential energy U, the equations are:

$$m_i \frac{d^2 \mathbf{r_i}}{dt^2} = \sum_{j=1(\neq i)}^{N} \mathbf{F}_{ij} = -\frac{\partial U(\mathbf{r}_{ij})}{\partial \mathbf{r}_{ij}}, for \;\; i = 1,2,3,....,N, \tag{2.3}$$

where m_i and r_i is the mass and position vector for each particle i, and t is the time. Even though this equation may look deceptively simple, it is as complicated as the famous N-body problem that one generally cannot solve exactly when N is > 2.

This equation is a system of coupled second-order, nonlinear ordinary differential equations and can be solved numerically, and this is carried out in MD simulation.

The **Conjugate gradient** minimization algorithm is an iterative method used for the structural relaxation and also to find the local minimum of the potential energy function, that can be of many variables. In the present case, the potential energy of the sample has to be minimized, with a number 3*N* of variables, where *N* is the number of atoms in the system.

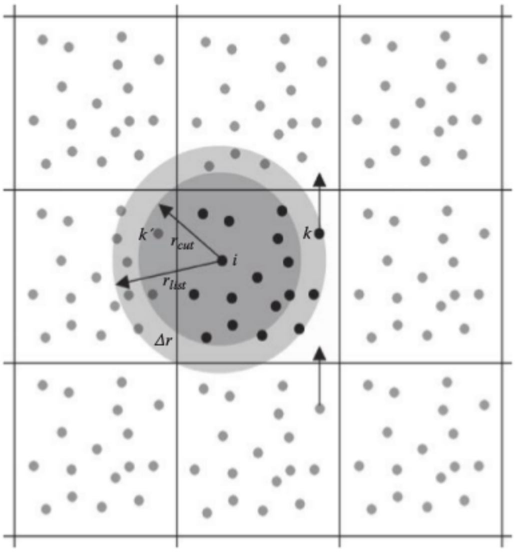

Figure 2.1: Schematic of potential cutoff under periodic boundary conditions in two dimensions

iii Numerical Integrator

The atomic trajectories of a set of *N* interacting atoms can be generated by the numerical integration of Newton's equation of motion (equation 2.3) with certain initial and boundary conditions. In molecular dynamics, the most commonly used time integration algorithm is probably the so-called Verlet algorithm (Verlet 1967). In general, an integrator should be accurate (approximate the true trajectory), stable (conserve energy) and robust (should not be sensitive to the time step scale). In the present thesis the simple and most used **velocity Verlet** integrator is discussed.

For a small time step Δt, one forward step and one backward step in time can be expressed as two third-order Taylor expansions of the coordinate of a particle :

$$\mathbf{r}(t+\Delta t) = \mathbf{r}(t) + \mathbf{v}(t)\Delta t + \frac{1}{2}\mathbf{a}(t)\Delta t^2 + \frac{1}{6}\mathbf{b}(t)\Delta t^3 + O(\Delta t^4) \tag{2.4}$$

$$\mathbf{r}(t-\Delta t) = \mathbf{r}(t) - \mathbf{v}(t)\Delta t + \frac{1}{2}\mathbf{a}(t)\Delta t^2 - \frac{1}{6}\mathbf{b}(t)\Delta t^3 + O(\Delta t^4) \tag{2.5}$$

where, $\mathbf{r}(t)$ is the position vector of the particle at time t, $\mathbf{v}(t)$ is the velocity, $\mathbf{a}(t)$ is the acceleration, $\mathbf{b}(t)$ is the third derivative of $\mathbf{r}$ with respect to t and $O(\Delta t^4)$ represents the higher order terms. After adding the above two expressions (equations 2.4 and 2.5),

$$\mathbf{r}(t+\Delta t) = 2\mathbf{r}(t) - \mathbf{r}(t-\Delta t) + \mathbf{a}(t)\Delta t^2 + O(\Delta t^4) \tag{2.6}$$

This is the basic form of the Verlet algorithm. Since we are integrating Newton's equations, $\mathbf{a}(t)$ is just the force divided by the mass, and the force is in turn a function of the positions $\mathbf{r}(t)$ and

$$\mathbf{a}(t) = -\frac{1}{m}\nabla V\left(\mathbf{r}(t)\right) \tag{2.7}$$

In this way, the new positions are calculated with an error of order Δt^4. We can derive the velocity also from above Eqs. (2.4) and (2.5) using the central difference scheme:

$$\mathbf{r}(t+\Delta t) - \mathbf{r}(t-\Delta t) = 2\mathbf{v}(t)\Delta t + O(\Delta t^3) \tag{2.8}$$

or

$$\mathbf{v}(t) = \frac{\mathbf{r}(t+\Delta t) - \mathbf{r}(t-\Delta t)}{2\Delta t} + O(\Delta t^3). \tag{2.9}$$

These velocities are used to calculate the kinetic energy and therefore, instantaneous temperature. In each time step, the current temperature and potential energy are calculated. One can easily notice that the truncation error of the algorithm while evolving the system by Δt is of the order of Δt^4, even if third derivatives do not appear explicitly. At the same time, this Velocity Verlet algorithm is simple to implement, accurate and stable, explaining its large popularity among molecular dynamics simulators. The efficiency of an MD simulation, therefore depends on performing the force calculation as simplified as possible without compromising the physical description (simulation fidelity). Since the force is calculated by taking the gradient of the potential U, the specification of U essentially determines the compromise between physical fidelity and computational efficiency (Frenkel and Smit 2001). A typical flowchart for an MD code is shown in figure 2.2.

iv **Ensembles**

According to statistical physics, physical quantities are represented by an average over configurations, which refers to a collection of systems that share common macroscopic properties. An *ensemble* is a collection of systems described by the same set of microscopic interactions and sharing a common set of macroscopic properties (e.g. the same total energy, volume, and number of moles, etc). Averages performed over an ensemble yield the thermodynamic quantities of a system as well as other equilibrium and dynamic properties. Using the framework of statistical physics, various physical quantities are calculated by an average over configurations distributed according to a certain statistical ensemble. In a simulation box of an MD run, each atom moves and behaves differently, and a new microstate of the system is generated in every timestep. After a proper simulation and equilibration, however, it becomes an ensemble that is a collection of all possible configurations and yet has the same macroscopic or thermodynamic properties.

The ensemble in which the number of particles N, volume V and the total energy E are constant is known as the microcanonical (NVE) ensemble, equivalent to the conventional MD simulation over ensemble averages. This ensemble is most often used in equilibrium MD since it represents normal real systems at its best. However, most of the experiments are carried out at a specific temperature.

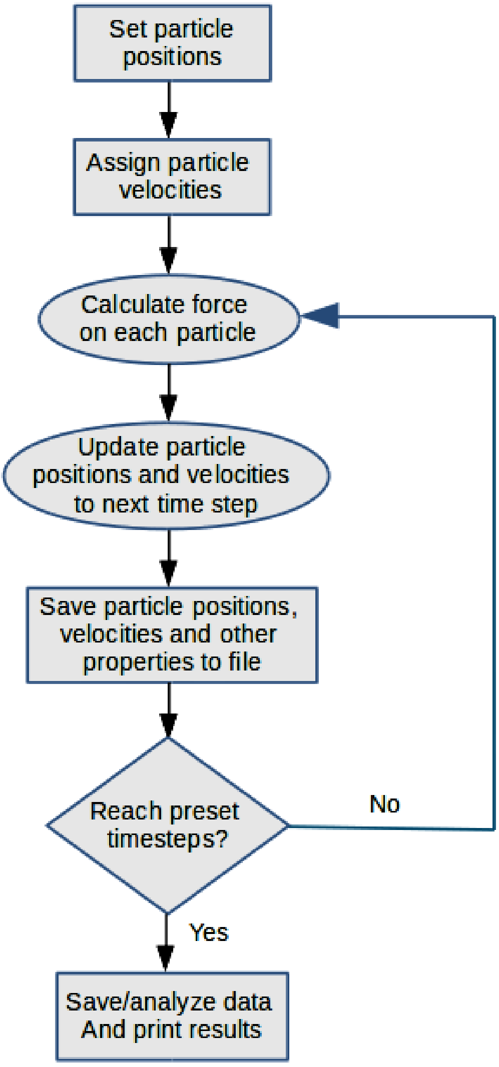
Set particle positions
Assign particle velocities
Calculate force on each particle
Update particle positions and velocities to next time step
Save particle positions, velocities and other properties to file
Reach preset timesteps?
No
Yes
Save/analyze data And print results

Figure 2.2: The Flow chart of an MD trajectory simulation

Therefore, to have canonical ensemble (NVT-isochoric-isothermal) by MD simulation and obtain the corresponding thermodynamic properties, one needs to add a thermostat interacting with the system by coupling the system to a heat bath (thermostat methods), which gives a more realistic picture prior to experimental analysis (Hoover 1985). It is also often desirable to sample from an isothermal-isobaric ensemble to be relevant with experimental studies under constant pressures. To maintain constant pressure, the use of barostat is often adopted, and the volume of the system is allowed to change. Typically, the simulation box length is coupled to the pressure piston that has its own degree of freedom.

Molecular Statics simulations are performed at zero Kelvin temperature and the finite temperature Molecular Dynamics Simulations were carried out using the NVT and NPT ensemble. For the temperature and pressure control in the simulations, the Nosé-Hoover thermostat and barostat were employed, which ensure the average temperature and pressure of the system to be a desired constant.

2.2 LAMMPS

For the present thesis work, classical Molecular Dynamics simulations have been performed using a free and open-source software package LAMMPS (Large scale Atomic/Molecular Massively Parallel Simulator) developed by Sandia National Laboratories (Plimpton et al. 2007). We have also used the in-house codes written in MATLAB and FORTRAN for the modelling of pristine and defective h-BN sheet as well as post processing the data. LAMMPS can model atomic, polymeric, biological, metallic, granular and coarse-grained systems using a variety of force fields and boundary conditions from a few particles to million or billions.

Different statistical ensembles are incorporated in LAMMPS and has been used to derive the required physical quantities. One need to perform canonical (NVT) and isobaric-isothermal (NPT) calculations using the Nosé-Hoover chain equations and need to set the *'fix nvt'* or *'fix npt'* command and able to set values for the initial (T_i) and final (T_f) temperature, as well as the temperature and pressure damping factor τ_t and τ_p respectively. The temperature (T_{damp}) and pressure damping (P_{damp}) parameter is specified in time units and determines how rapidly the temperature/pressure is relaxed. If the damping factor is too small, the temperature, pressure and volume can fluctuate wildly; if it is too large, these quantities will take a very long time to equilibrate. So the proper damping factor has to be chosen carefully. In most situations, the microscopic equations of motion obeyed by the system are no longer Hamiltonian. In fact, it is often possible to model the effect of the surroundings simply positing a set of non-Hamiltonian equations of motion which are designed to generate positions and velocities sampled from the canonical (NVT) and isothermal-isobaric (NPT) ensembles (Tuckerman 2010). This updates the position and velocity for atoms in the group at each time step (Plimpton 1995).

2.3 The Empirical Interatomic Potential

The physical fidelity of the MD simulation ultimately depends on the accuracy of the potential used for the simulation. The empirical inter-atomic potential is the most critical quantity in MD modelling and simulation; it essentially controls the numerical and algorithmic simplicity (or complexity) of MD simulation. Pair potentials are the simplest form of potentials in which the potential energy of interaction between two non-bonding atoms or molecules are based on their distance of separation. A typical example of pair potential is the Lennard-Jones potential (Jones 1924) that considers only two-atom interactions and neglects all others. The Lennard-Jones potential, $U_{LJ}(r)$, expressed in terms of interatomic distance, r, with two parameters as:

$$U_{LJ}(r) = 4\varepsilon \left[\left(\frac{\sigma}{r} \right)^{12} - \left(\frac{\sigma}{r} \right)^{6} \right], \tag{2.10}$$

where ε is the lowest energy of the potential curve and parameter σ is the inter-atomic distance at which the potential is zero. The advanced bond-order potential consists of a new set of potential parameters associated with the existing empirical interatomic potentials and that depend on the local chemical environment in the reactive simulations.

A good potential energy model should be able to balance both the radial forces and angular forces in the system which resist a change in the bond length from the equilibrium value and resist the shape of the bond angle at the unstrained equilibrium state respectively. Then, a classical potential takes the form :

$$E_{pot} = \sum_{i} V_1(r_i) + \sum_{i,j} V_2(r_i, r_j) + \sum_{i,j,k} V_3(r_i, r_j, r_k) + ... \tag{2.11}$$

where, V is the total potential energy of the system, V_1 represents a single particle potential which corresponds to an external potential, V_2 is a pair-potential (or two body potential) and only depends upon the distance between the atoms i and j. V_3 is the three-body interaction in the system and may contain the torsional and angular dependent terms. Three-body and higher order potentials are grouped into a category called many-body potentials. It is also a common practice to put a cut-off function for a potential energy to avoid massive computation due to long-range forces beyond the first nearest neighbor atoms. Hence $V(r_{ij}) \to 0$ for $r_{ij} > r_c$ where r_c is the cut-off radius. To prevent the discontinuity and unphysical behaviour in the second derivatives of this cut-off function at $r_{ij} = r_c$, a trigonometric smoothing function is usually introduced in the interval $r_c < r_{ij} < (r_c + \Delta r)$, which makes the potential and the force continuous.

2.3.1 Tersoff Potential

A proper interatomic potential function which is capable of describing accurately the interactions in the material system is of crucial importance. Classical empirical force fields can be used in large-scale atomistic simulations with low computational cost. Recently, a new approach named as bond-order potentials emerged that depend on the local chemical environment in reactive simulations. In contrast to classical empirical potential, bond-order potentials capture bond formation and breaking, saturated and unsaturated bonds, dangling and radical bonds, as well as single, double or triple bonds (Grotendorst et al. 2009).

The interatomic potentials can be divided into two formats: a separated format and an integrated format. The first format consists of two-body and three-body (and higher) energy terms separately such as the Finnis-Sinclair, embedded-atom method (EAM), modified EAM (MEAM), and Stillinger-Weber (SW) potentials. In the integrated format, the potential energy has integrated many-body effect and two-body interaction via a bond order term such as Tersoff and reactive empirical bond order (REBO) potentials.

A considerable improvement has taken place in the development and evolution of empirical interatomic potentials for the large scale atomistic simulations of covalent materials, in particular silicon, carbon, semiconductors and hydrocarbons. Stillinger-Weber (SW) type potentials (Stillinger and Weber 1985, Bazant et al. 1997, Justo et al. 1998), Tersoff type bond order potentials (BOPs) (Tersoff 1986, 1988b,a,a, 1986, Brenner 1990, Brenner et al. 2002), embedded atom models (EAMs) for metals and metal alloys (Finnis and Sinclair 1984, Baskes 1987, Baskes et al. 1989, Cai and Wang 2001) and higher bond order potentials derived from tight binding models (TBBOPs) (Pettifor 1989, Pettifor and Oleinik 1999, Oleinik and Pettifor 1999), etc. are meant to give a good description of the energy landscape for any possible realistic configuration characterized by the set of atomic positions r_i.

Among all these potentials, Tersoff (Tersoff 1988b,a, 1989) and Tersoff-type (Brenner 1990, Brenner et al. 2002) empirical potentials are considered as the most successful ones for the study of carbon and boron-nitride nano systems. Tersoff-Brenner pair potentials are structurally similar to that of Tersoff potentials, but the functional forms of the attractive and repulsive parts of these potentials are different.

In 1986, J. Tersoff has introduced an empirical interatomic potential energy function (Tersoff 1986) for silicon systems. The main idea of this kind of potential was to incorporate the bond order term (i.e., the strength of each bond) in it, which depends upon the local environment (Abell 1985). Usually an atom with many neighbors forms weaker bonds than an atom with few neighbors. Due to the crucial role of bond order and its dependence upon local geometry, it seems attractive to include an environment dependent bond order explicitly into the potential. In general, in a Tersoff type potential, the total energy E of a collection of atoms can be written as,

$$E = \frac{1}{2}\sum_{i}\sum_{j\neq i} V_{ij} \tag{2.12}$$

where,

$$V_{ij} = f_c(r_{ij})\left[f_R(r_{ij}) + b_{ij} f_A(r_{ij})\right] \tag{2.13}$$

Here, V_{ij} is the potential energy of the pair of atoms situated at $\vec{r}_i$ and $\vec{r}_j$. Their interaction energy V_{ij} depends on the environment of both the atoms through the bond-order term b_{ij}. f_R and f_A are the repulsive and attractive pair potentials respectively. $f_c(r)$ is the cut off function which depends on distance r in such a manner that the potential energy and the force experienced by the atoms taper of to zero at the cutoff distance without any discontinuity. The summations in the formula are over all neighbors j and k of atom i within a cut off radius. r_{ij} is the bond distance between atoms i and j and b_{ij} is the many body order parameter that describes how the bond formation energy is affected by the local atomic arrangement due to the presence of other neighboring atoms. The repulsive and attractive pair potentials f_R and f_A are represented respectively as,

$$f_R(r) = A(r)e^{-\lambda_1 r} \quad \text{and} \quad f_A(r) = -B(r)e^{-\lambda_2 r} \tag{2.14}$$

$$f_c(r) = \begin{cases} 1, & \text{if } r_{ij} < R_{ij}, \\ \frac{1}{2} + \frac{1}{2}\cos\left[\frac{\pi(\mathrm{r_{ij}} - \mathrm{R_{ij}})}{\mathrm{S_{ij}} - \mathrm{R_{ij}}}\right], & \text{if } R_{ij} < r_{ij} < S_{ij}, \\ 0, & \text{if } r_{ij} > S_{ij} \end{cases} \tag{2.15}$$

which is a continuous function with a continuous derivative for all r, and goes smoothly from 1 to 0 in a small range around R. The value of R has to be chosen in such a manner to include only the nearest-neighbors. The function b_{ij} is a measure of the bond order. The terms which act to limit the range of interaction to the first neighbors are included in b_{ij}.

$$b_{ij} = \left(1 + \beta^n \zeta_{ij}^n\right)^{\frac{-1}{2n}} \tag{2.16}$$

$$\zeta_{ij} = \sum_{k \neq i,j} f_c(r_{ik}) g\left(\theta_{ijk}\right) e^{-\lambda_{ij}^m (r_{ij} - r_{ik})^m} \tag{2.17}$$

$$g\left(\theta_{ijk}\right) = 1 + \frac{c^2}{d^2} - \frac{c^2}{\left[d^2 + \left(h - \cos\theta_{ijk}\right)^2\right]}, \tag{2.18}$$

where θ_{ijk} is the bond angle between bonds ij and ik.

In the present work, a Tersoff interatomic potential developed by Kinaci et al., has

Table 2.1: Tersoff-type inter atomic potential parameters optimized for hexagonal boron nitride.

A (eV)	1380.0	c	25000
B (eV)	340.0	$\beta(10^{-7})$	1.25724
λ_1(Å^{-1})	3.568	d	4.3484
λ_2(Å^{-1})	2.199	cosθ or (h)	-0.89000
λ_3(Å^{-1})	0.000	R (Å)	1.950
n	0.72751	S (Å)	0.050

been used to investigate the various structural, thermodynamic, mechanical and elastic properties of monolayer pristine and defective h-BN (Kinaci et al. 2012) and the values of the parameters used are shown in table 2.1. Further details about the parameterisation are available in references (Kinaci et al. 2012, Sevik et al. 2012).

Chapter 3

Temperature Dependent Structural and Thermal Properties

This chapter explains the temperature dependent structural and thermal properties of h-BN. Temperature dependence of lattice parameter, radial distribution function, specific heat at constant volume, linear thermal expansion coefficient and height correlation function of the thermally excited ripples on pristine as well as defective h-BN sheet have been investigated. Specific heat shows considerable increase beyond the Dulong-Petit limit at high temperatures, which is interpreted as a signature of strong anharmonicity present in h-BN. Analysis of the height fluctuations shows that the bending rigidity and variance of height fluctuations are strongly temperature dependent and this is explained using the continuum theory of membranes. It is also seen that the variance of the height fluctuations increases with defect concentration.

3.1 Introduction

This chapter investigates the structural and thermodynamical properties of monolayer pristine and defective 2D h-BN in a wide temperature range by carrying out atomistic simulations using a tuned Tersoff-type inter-atomic empirical potential. We have used the potential parametrization of Kinaci et al., that is reported in Sevik et al (Sevik et al. 2011) and available with LAMMPS (Large scale Atomic/Molecular Massively Parallel Simulator) (Plimpton et al. 2007) package without any modification. Simulation with this potential gives a value of lattice parameter comparable to the experimental result, which prompted us to use this potential for calculations of the structural and thermal properties of h-BN. To the best of our knowledge, the structural integrity analysis of h-BN, the vacancy defect, Stone-Wales (SW) defect and height fluctuations with respect to temperature have not been studied so far with the well established parameterized Tersoff potential (Kinaci et al. 2012). In this thesis work, high temperature studies have been performed for the computation of temperature dependence of lattice parameter, radial distribution function, specific heat at constant volume, linear thermal expansion coefficient, correlation function of the thermally excited ripples and formation of defects. The influence of defects on the bending rigidity is also analyzed. Even though h-BN sheet is stable only up to $\sim$ 1500 $^\circ$C in air, studies using Tersoff type empirical potentials show an increase in its melting point to $\sim$ 2700 -3000 $^\circ$C with pressure. This enhanced thermal stability makes h-BN a material with potential for applications under high temperature-high pressure conditions.

3.2 Methodology

The simulations are carried out using LAMMPS (Large Scale Atomic/Molecular Massively Parallel Simulator) (Plimpton et al. 2007) package. Periodic boundary conditions were employed for the simulation to avoid the spurious surface effects in h-BN. The standard Velocity-Verlet time stepping algorithm is used to solve the equations of motion with an integration time step of 0.1 fs. A Nose-Hoover type chain thermostat is used in order to control the system temperature. Simulations are carried out in the canonical ensemble to compute the pair correlation function of h-BN. The number of atoms used in a simulation depends on the objective of the simulation. We have used cells with up to 125000 atoms in our study of various properties of hexagonal BN. We have optimized the system size before every calculation so that the computed structural and thermal properties are system size independent. Simulation box with 12800 atoms was found to be good enough for study of lattice constant and nearest neighbour distance of h-BN. We found a cell with about 20000 atoms to be large enough for study of specific heat and defects. Properties of thermally excited ripples were studied with larger number of atoms. Micro canonical (NVE), canonical (NVT) and isobaric-isothermal (NPT) ensembles are used to derive the required physical quantities. The inter atomic potential is the main ingredient of any successful MD simulation. More details about the Tersoff type empirical potential used for the present study can be found in section 2.3.1.

3.3 Results and discussions

3.3.1 Structural Properties

In h-BN, the distance between nearest neighbour boron and nitrogen atoms R_{xy} is 1.46 Å, which is the average of the B-N covalent σ bonds. h-BN has a unit cell consisting of two atoms, referred to as Boron (B) and Nitrogen (N) atoms. After repeating the unit cell, these atoms form two triangular lattices called the B- and N-lattice, located such that each B- atom is directly neighboured by three N-atoms, as is shown in figure 3.1 and $\mathbf{a_1}$ and $\mathbf{a_2}$ are the primitive unit cell with primitive translation vectors. Then the angle between corresponding σ orbital (in plane) derived from s, p_x, p_y is 120°. By using the law of cosines, we can derive $a = \sqrt{3}R_{xy}$ from the triangle ABC as:

$a^2 = R^2 + R^2 - 2 \times R \times R \times Cos(120)$

$a^2 = R^2 + R^2 - 2 \times R \times R \times Cos(90+30)$

$a^2 = R^2 + R^2 + R^2$

$a = \sqrt{3}R$

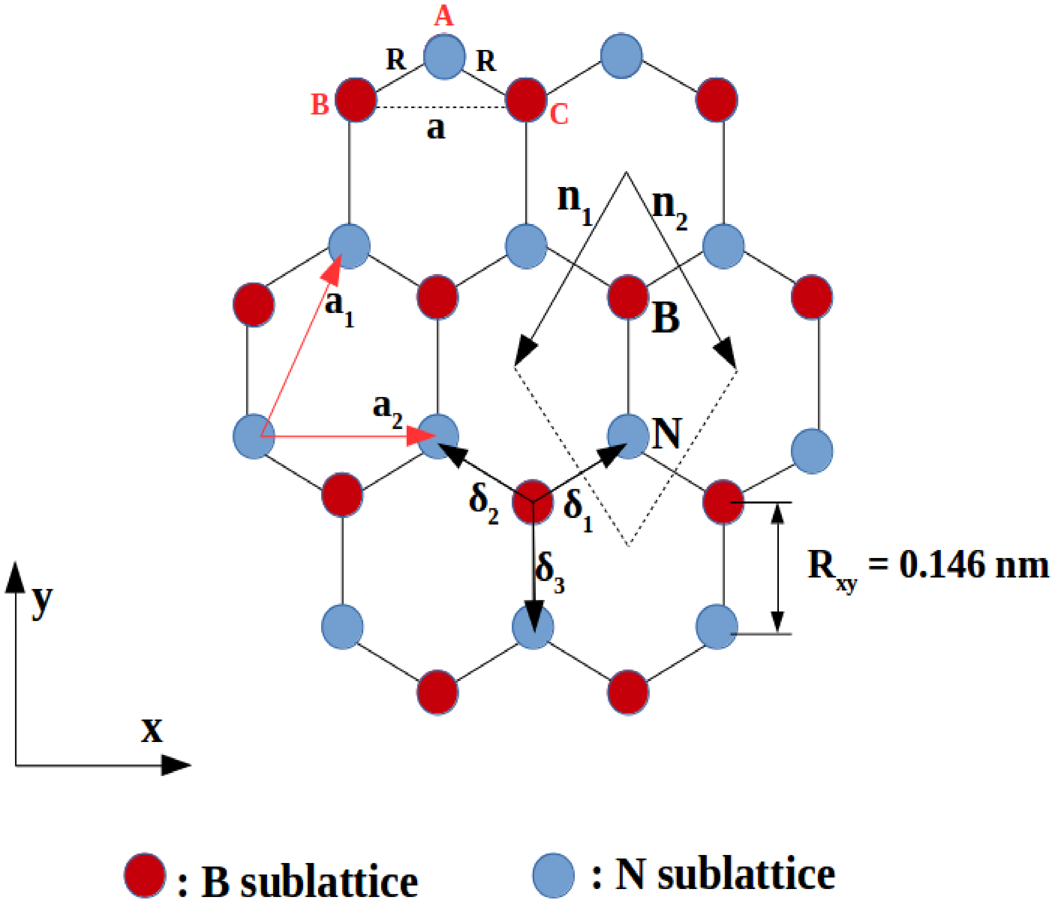

Figure 3.1: The two triangular sublattices (the B- and N-lattice) creating the honeycomb structure, and the defining vectors in h-BN.

We have observed that the lattice parameter of h-BN is not equal to $\sqrt{3}R_{xy}$ ($R_{xy} = a/\sqrt{(3)}$ is the in-plane nearest neighbor separation and) at any other temperatures other than zero, due to the thermally excited ripples in the out-of-plane direction, which determines the stability of 2D crystals. Ideally, the perfect lattice matching of graphene and h-BN with almost similar structural properties is used to explore the possibility of multilayers (Graphene on h-BN) for various potential applications. The equilibrium lattice parameter of h-BN sheet obtained from the previous theoretical investigations based on various formalisms, and experimental studies are shown in table 3.1. The value tabulated from reference (Paszkowicz et al. 2002) is at room temperature and all the other results shown in table 3.1 correspond to zero Kelvin. The equilibrium lattice parameter of h-BN obtained from the present study at zero Kelvin is in good agreement with the previous *ab initio* results. In fact, the potential chosen for the present study gives a value of lattice parameter closer to the experimentally observed value. Experimentally observed lattice parameter of h-BN at room temperature is a=2.504 Å with an average B-N interatomic distance of 1.44 Å (Paszkowicz et al. 2002). Molecular Dynamics simulations using a modified Albe, Moller and Heining interatomic potential gives the equilibrium lattice parameter as a=2.532 Å at zero Kelvin (Slotman and Fasolino 2012, Albe et al. 1997) with an average B-N interatomic distance as 1.46 Å. In the present study, at zero Kelvin, the lattice parameter is observed as a=$\sqrt{3}R_0$=2.505 Å with an interatomic B-N distance R_{xy}=1.44 Å.

Table 3.1: Comparison of lattice parameter of Monolayer h-BN Sheet reported during various calculations.

Reference	**Year**	**Method**	**a (Å)**	**R_{xy} (Å)**	**E_{Coh} (eV/atom)**
Present Study	2015	Molecular Dynamics	2.505	1.445	7.49
Greenwood	1997	Experiment	-	-	7.41
Paszkowicz et al	2002	Experiment	2.504	1.440	-
Sevik	2014	*ab initio* QHA-GGA	2.519	-	-
Sevik	2014	*ab initio* QHA-LDA	2.495	-	-
Slotman et al	2013	Molecular Dynamics	2.532	1.462	-
Kaloni et al	2011	DFT-LDA	2.480	-	7.91
Hamdi et al	2010	*ab initio* DFT-LDA	2.486	-	-
Furthmüller et al	1994	Ab-*initio*	2.486	-	8.81
Xu et al	1991	*ab initio* DFT-LDA	2.494	-	-

An attempt has also been made to calculate the variation of the in-plane lattice constant (a) and the B-N nearest neighbour distance (R_{xy}) with temperature using equilibrium MD simulations. The variation of a and R_{xy} with temperature is shown in figure 3.2. The pressure of the system is maintained at a constant level at P=0. In the current simulation we have considered a sample of N= 12800 atoms. The lattice parameter a (marked in the left y-axis) and B-N interatomic distance in the xy-plane R_{xy} (marked in the right y-axis), which differ by a factor of $\sqrt{3}$, are tabulated. It is found that a and R_{xy} first decrease with increase in temperature upto 1700 K. Beyond this temperature, considerable change in the lattice parameter is observed as a is no longer equal to $\sqrt{3}R_{xy}$ due to the thermal fluctuations in the out of plane direction. Thereafter they increase with temperature upto 3000 K, the highest temperature considered in this study. However, their values never exceed the corresponding values at T=0 K. The h-BN shows negative thermal expansion at low temperatures due to presence of low frequency bending modes in its phonon spectrum. Until the temperature becomes sufficiently large to excite the in-plane modes, the amplitude of the bending modes would go on increasing which leads to a reduction in the in-plane interatomic distances. As the temperatures further increases, the in-plane phonon modes also get excited. These modes would cause an increase in the in-plane distance. Thus a non-monotonic variation in the lattice constant as shown in figure 3.2 can be anticipated (Zakharchenko et al. 2009, Pozzo et al. 2011, Mounet and Marzari 2005). Both the mechanisms are operative in the temperature range 1700-3000 K. However, anharmonic effects are more important in this temperature regime.

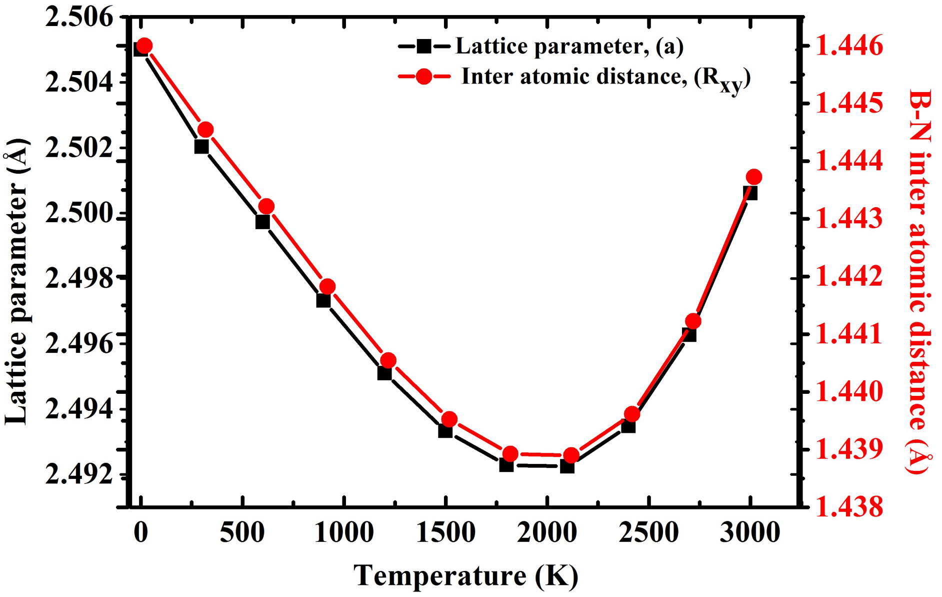

Figure 3.2: Temperature dependence of lattice parameter a (marked in the left y-axis) and B-N interatomic distance in the xy-plane R_{xy} (marked in the right y-axis) of h-BN sheet with 12800 atoms calculated at different temperatures with zero external pressure.

3.3.2 Radial distribution function

Radial distribution function (RDF) or pair correlation function is a powerful tool to analyze the structural information of a material. It is estimated by considering distance between all pairs of atoms. In general, if $g_{AB}(r)$ is the radial distribution function, then $g_{AB}(r)\Delta r$ is proportional to the probability of finding an atom of type B at a distance between r and $r+\Delta r$ from an atom of type A. For a two dimensional system, it is given by

$$g_{AB}(r) = \frac{\Delta n_{AB}}{2\pi r \Delta r \rho_B}, \tag{3.1}$$

where, ρ_B is the average density of species B in the entire material and Δn_{AB} is the average number of particles of type B present in the annular region between r and r+Δr with an A atom at the center. The averaging is over all the A atoms present in the simulation volume. The radial distribution functions must be delta functions at 0 K, as there are unique values for the radii of the various neighbour shells. However, due to thermal vibrations, these distances become blurred as the temperature of the system increases and the delta functions broaden into smooth peaks. The peak width increases with temperature. The width is in fact proportional to the root mean squared displacement of the atoms from their equilibrium position. The position of the n^{th} peak in $g_{AB}(r)$ would correspond to the mean distance of the B atom from the A atom in n^{th} neighbour positions. Thus the value of RDF at any r decreases as the temperature increases due to thermal broadening.

The peak positions of first, second and third neighbor of h-BN sheets correspond to 1.45 Å, 2.511 Å and 2.85 Å respectively as shown in figure 3.3. In order to obtain the RDF of h-BN sheet at various temperatures, the material is heated by using a Nose-Hoover thermostat with 20000 atoms and 1 fs time step. The peak positions of the RDF correctly give the various distances between the atoms which can also be obtained by analysis of geometry and structure using other techniques such as full width at half maximum (FWHM) of an RDF (Yuan and Liew 2014, Barnard et al. 2007). When the temperature increases, the atoms start moving from their equilibrium position. As the positional spread increases with increase in temperature, the probability of finding a particular atom in the vicinity of the reference atom decreases with increase in temperature. The different contributions (B-B, B-N and N-N) to RDF in BN sheet at various temperatures are shown in figure 3.3 (a), (b) and (c) as a function of distance *r*.

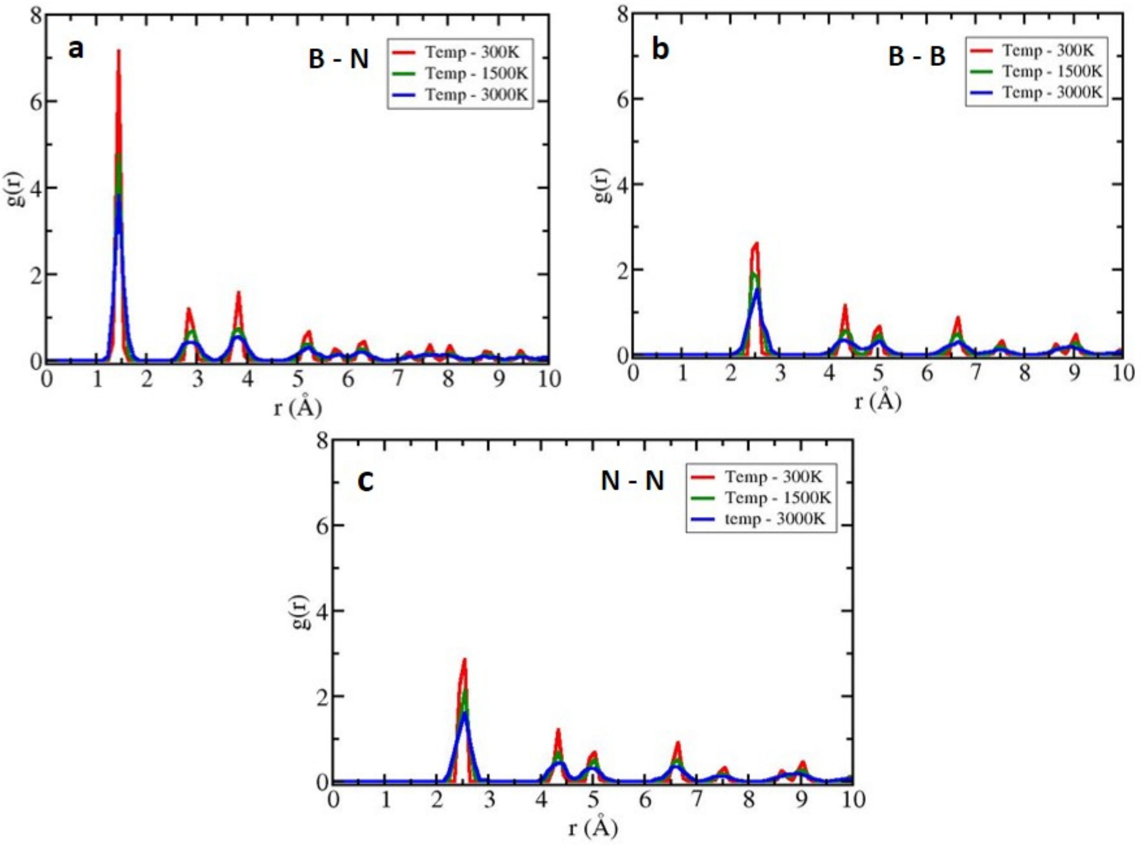

Figure 3.3: Figure (a), (b) and (c) shows the Radial distribution function of B-N, B-B and N-N pairs in h-BN sheet at various temperatures. The value of RDF at any *r* decreases as the temperature increases due to thermal broadening.

3.3.3 Specific heat at constant volume

This section explains how to calculate the specific heat at constant volume $C_V(T)$ of hexagonal BN. It is well known that the heat capacity is a temperature dependent quantity and it will decrease considerably when the temperature is decreased below Debye temperature due to quantum mechanical effects. However, while the classical molecular dynamics simulations give the correct high temperature limit, they fail in the lower temperature region. Quantum corrections are significant in any material when the temperature become very low. Moreover, the classical approximation is rather poor for light elements. Quantum corrections are often superimposed on the classical description of motion given by MD to get the correct results. In the present thesis work, we calculate C_V in the temperature range 200-3000 K, which is sufficiently high for quantum effects to be not significant, in two ways.

First, we consider the formula

$$C_V = \left(\frac{\partial U}{\partial T}\right)_{\mathrm{V}}, \tag{3.2}$$

to calculate $C_V(T)$ from the internal energy U. The total energy $U(T)$ of the h-BN sheet is shown in figure 3.4 (a) as a function of temperature. Here, the black solid squares in the figure correspond to the MD study of hexagonal BN taken from reference (Singh et al. 2013) and the red circles represent the results of the present study. The total energy appears to vary linearly with temperature. Detailed analysis using NVT ensemble shows that it actually has a nonlinear dependence on temperature. It is seen that the $U(T)$ vs T data can be fit to a quartic polynomial with the fractional residual less than 10^{-6} as shown in figure 3.5. The solid line in figure 3.4 (b) represents the specific heat calculated in this manner. The specific heat obtained using the formula $C_V = \left(\langle E^2\rangle - \langle E\rangle^2\right)/(k_B T^2)$ relating energy fluctuations in the canonical ensemble to the specific heat is also shown in figure 3.4 (b). Energy fluctuations over 100 ps after attaining equilibrium was used for the calculation. The percentage of error associated with the C_V estimated in this manner is large. Temperature fluctuations over longer time duration, of the order of ns, may be needed to reduce the error in the calculation.

Density functional studies of Xiao et al., showed that the specific heat at constant volume (C_v) of boron nitride nanotube is larger than that of Carbon nanotube (Xiao et al. 2004). In the present work, the estimated value of C_V/atom is 25.18 $\mathrm{Jmol^{-1}K^{-1}}$ at room temperature and within a range of temperature from 200-3000 K, C_v/atom varies in the range 24.8-28.2 $\mathrm{Jmol^{-1}K^{-1}}$. Thus there is a considerable increase in the specific heat beyond the Dulong-Petit value of 24.942 Jmol^{-1}K^{-1}, which is due to strong anharmonicity present in hexagonal BN. In fact anharmonic effects on thermodynamic properties are seen in hexagonal BN not only at very high temperatures but also at room temperature. Since the increase in C_V continues even at high temperatures, we conclude that the quartic term in the potential also gives a positive contribution to specific heat, even though it can be negative in some materials (da Silva et al. 2014, Katsnelson 2005, Keller and Wallace 1962).

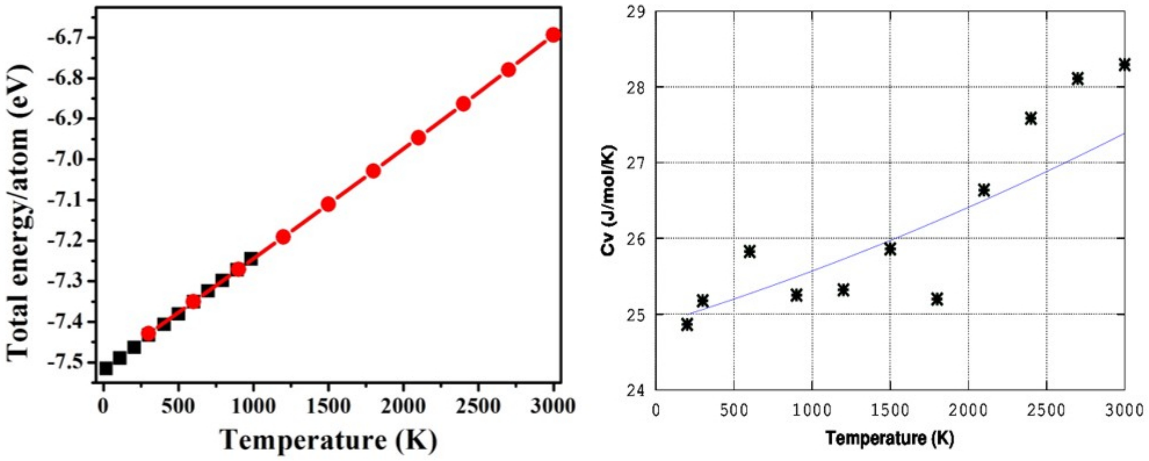

Figure 3.4: (a) Variation of the total energy (per atom) of the monolayer h-BN sheet as a function of temperature. (b) The variation on specific heat capacity at constant volume with temperature of h-BN sheet at a time step of 0.1 fs using NVT simulation. We have chosen 20000 atoms for the simulation.

3.3.4 Linear thermal expansion coefficient

Materials possessing both positive and negative thermal expansion coefficients are of practical importance due to the fact that they can be used to make composites with very little thermal expansion/contraction. In general, if $a(T)$ is the equilibrium lattice parameter and T is the temperature, then the linear thermal expansion coefficient ($\alpha(T)_l$) can be calculated using the equation,

$$\alpha_l(T) = \frac{1}{a(T)}\left(\frac{\partial a(T)}{\partial T}\right)_P \tag{3.3}$$

h-BN shows negative thermal expansion (α_l) at low temperatures due to presence of low frequency bending modes in its phonon spectrum. Until the temperature becomes sufficiently large to excite the in-plane modes, the amplitude of the bending modes would go on increasing which leads to a reduction in the in-plane interatomic distances. As the temperatures further increases, the in-plane phonon modes also get excited. These modes would cause an increase in the in-plane distance. Thus a non-monotonic variation of the lattice constant with temperature can be expected.

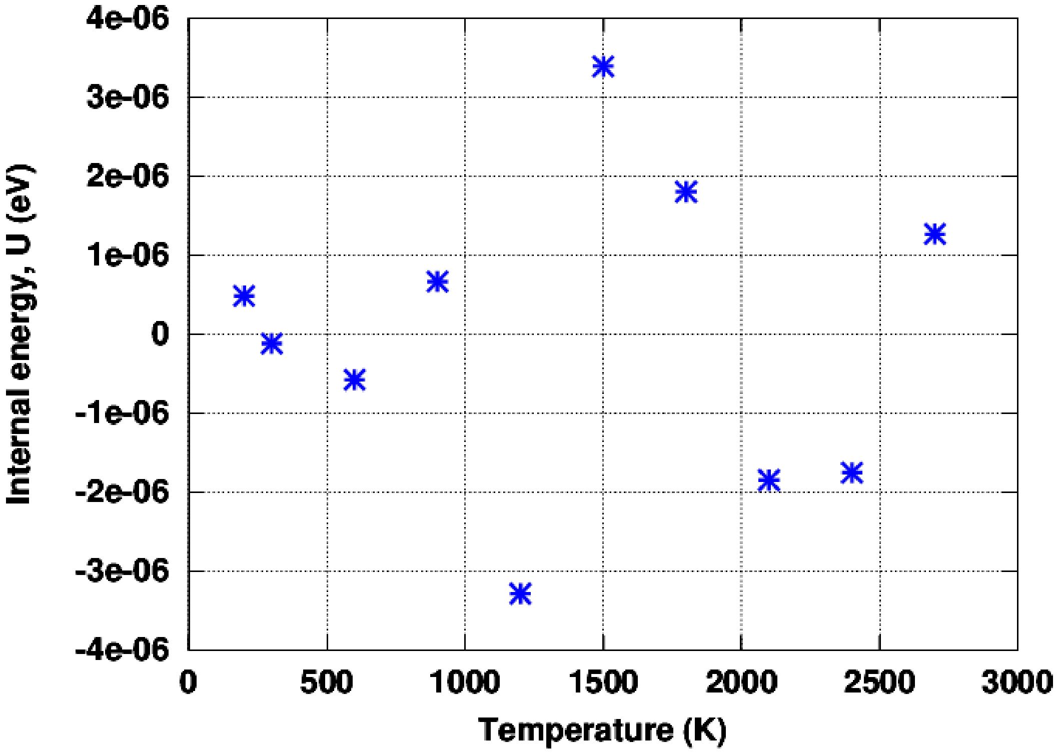

Figure 3.5: The nonlinear dependence of total energy with temperature. The $U(T)$ vs T data is fitted to a quartic polynomial with the fractional residual less than 10^{-6}.

By using quasi harmonic approximation, Sevik (Sevik 2014) has reported that the linear thermal expansion coefficient of h-BN is considerably negative below 300 K and it gradually increases in the temperature range 300-1500 K. Yates et al (Yates et al. 1975) have reported a value of -3.75×10^{-6}K^{-1} at room temperature. Belenkii et al (Belenkii et al. 1985) have experimentally observed that α_l decreases considerably as the temperature increases from 0 K to 400 K. In the present study, the negative values of α_l is observed upto 1000 K and this is comparable with the results of *ab initio* calculations using quasi harmonic approximation-generalized gradient approximation (QHA-GGA) and QHA-local density approximation (QHA-LDA) methods (Sevik 2014). Results of studies using X-ray diffraction and interferometry techniques (Paszkowicz et al. 2002) show that h-BN possesses an anisotropic thermal expansion due to its anisotropic bond strength. Our studies show a positive value of linear thermal expansion coefficient at higher temperatures which is comparable to earlier studies (Sevik 2014) in the range 1000-1500 K. The present work shows a steady increase in α_l beyond this temperature upto 3000 K as shown in figure 3.6. The results of the present study are compared with those obtained from QHA-GGA and QHA-LDA studies (Sevik 2014) and experimental studies on hexagonal BN (Paszkowicz et al. 2002, Yates et al. 1975, Belenkii et al. 1985).

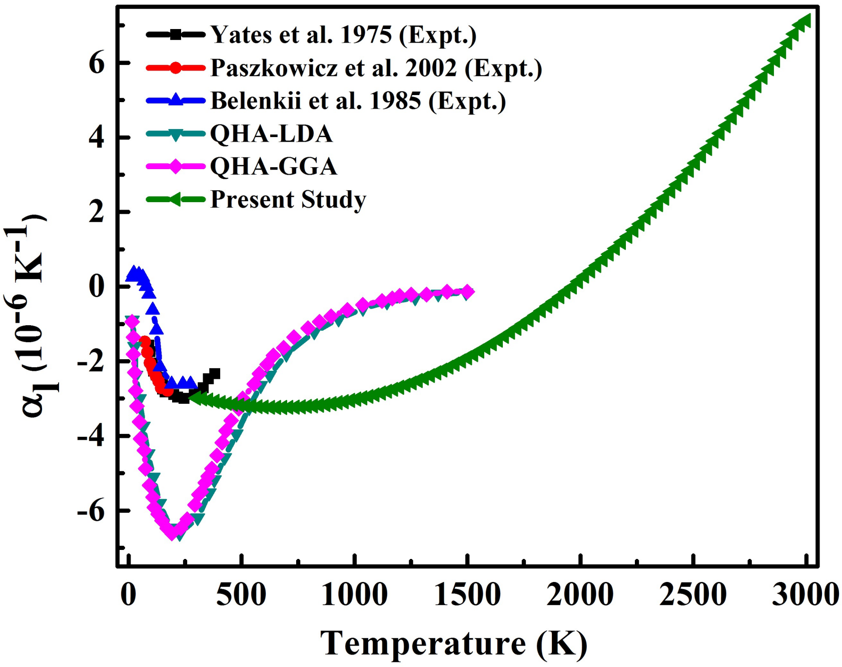

Figure 3.6: Variation of linear thermal expansion coefficient of h-BN sheet. h-BN shows negative thermal expansion at low temperatures due to presence of low frequency bending modes in its phonon spectrum. The results obtained from the present study are in qualitative agreement with the overall trend suggested by the results obtained from experimental and QHA based investigations.

We are of the opinion that the results obtained from the present study are in qualitative agreement with the overall trend suggested by the results obtained from experimental and QHA based investigations. The experimental data available up to temperatures $\sim$ 400 K shows the thermal expansion coefficient to be negative in this regime of temperatures, and the magnitude of the contraction decreases with increase in temperature. Had this tendency continued, the contraction would have paved way for an expansion at a sufficiently high temperature. The *ab initio* calculations based on QHA are expected to be good for low and intermediate temperatures. Since QHA does not explicitly incorporate anharmonicity, it cannot properly describe the shift in phonon frequencies, and coupling between the phonon modes leading to sharing of thermal energy between the various vibrational modes. Thus QHA based results cannot be used to obtain quantitatively correct results at high temperatures. One of the ways of overcoming this limitation of QHA is to carry out *ab initio* molecular dynamics simulations. However this is computationally intensive. A simpler solution is to use classical Molecular Dynamics with a good empirical potential, which incorporates the anharmonicity of the interatomic interaction in its entirety. That is the rationale behind the present work.

3.3.5 Defects in h-BN

The usual defects observed in the h-BN sheet are vacancies and Stone-Wales (SW) defects. Vacancies and SW defects are randomly created in the h-BN sheet and the variation of total energy/atom with concentration is an indicator of the structural changes. The number of atoms remains the same for the case of SW defects whereas the number of atoms decreases when vacancies are created. Stone-Wales defect or 5-7-7-5 defect (Stone and Wales 1986) is a kind of topological defect that can be observed in h-BN sheet when a 90 degree rotation of a pair of atoms alters the group of four hexagons into two pentagons and two heptagons as shown in figure 3.7.

It has been observed that the total energy/atom increases with increase in defect concentration when SW and vacancy type defects are incorporated in the h-BN sheet as shown in figure 3.8. By analyzing the results in table 3.2, it is observed that the formation energy of a SW defect is twice that of a single atom vacancy. Theoretical studies have been done to incorporate SW defects in graphene like 2D layered structures and also in nanotubes and monolayer h-BN. Slotman et al (Slotman and Fasolino 2012) studied the structural properties, vacancy defects and Stone-Wales defects of h-BN sheet using classical molecular dynamics simulation. Different experimental studies had been done to investigate the impact of defects in the BN sheet (Lehtinen et al. 2011, Alem et al. 2009, Zobelli et al. 2007).

Table 3.2: Formation energy of various defects in h-BN calculated for 0 K. N_V is the number of vacancies required for creating the defect.

Defect	N_v	E^{form} **(eV)**
V_B	1	5.04344
V_N	1	5.04344
SW	0	6.20935
V_{B+N}	2	10.09006
V_{2B+2N}	4	17.94495

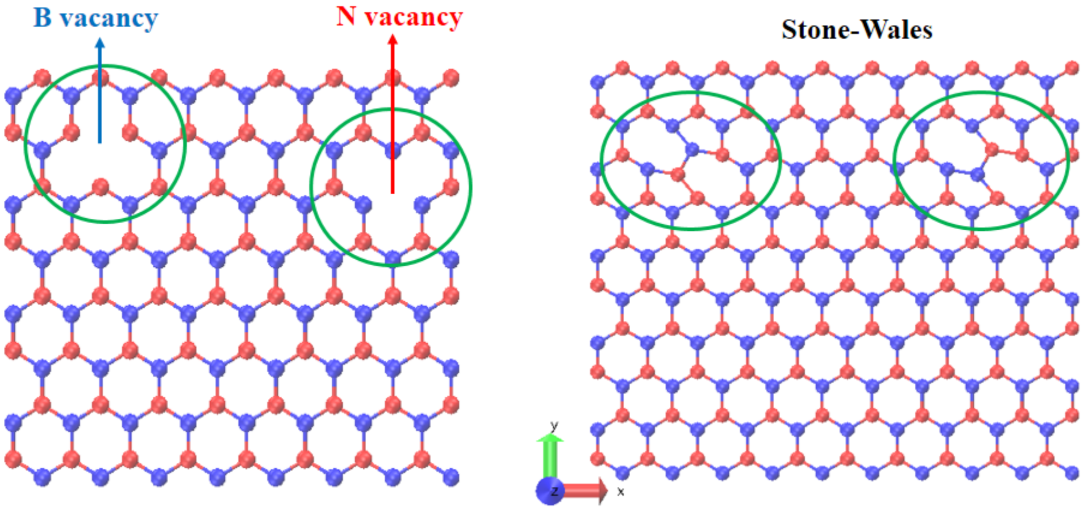

Figure 3.7: Formation of the vacancy and Stone-Wales defect in the h-BN sheet. A SW defect is formed when a pair of atoms is rotated by 90 degrees to form two pentagons and two heptagons.

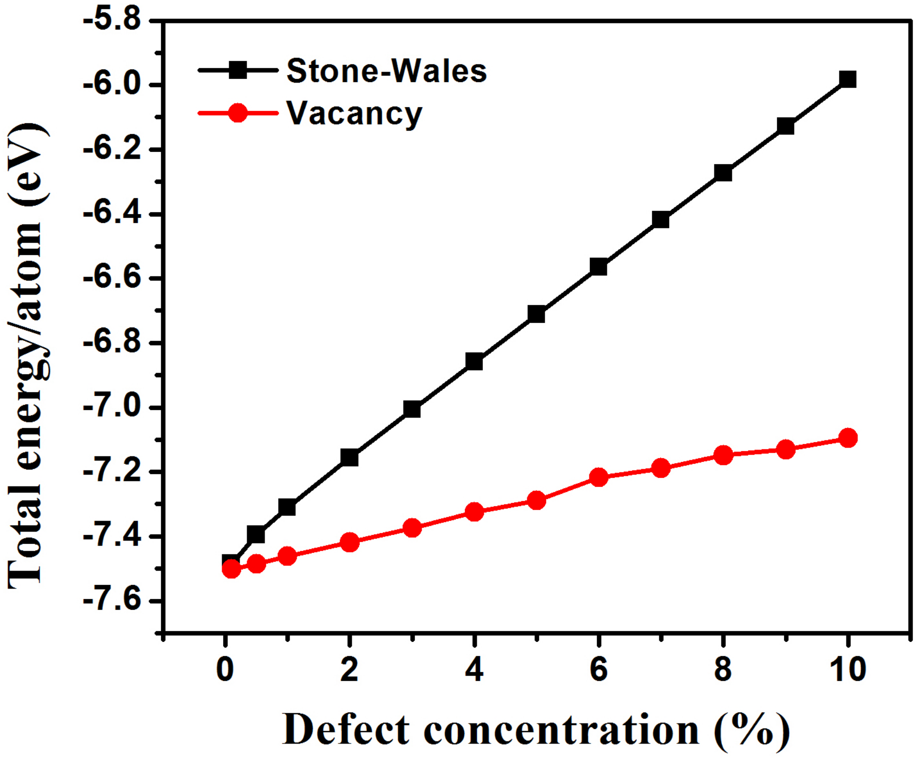

Figure 3.8: Variation of cohesive energy with defect concentration in h-BN sheet. As the percentage of defect concentration increases, energy per atom also increases (equivalently, cohesive energy decreases).

The interatomic potential that is being used in the present molecular dynamics simulations has no one-body term. Hence the total energy that is being calculated represents the change in energy of a collection of atoms when they are brought together. If $E_{perfect}$ is the total energy of a perfect crystal with N atoms, the cohesive energy per particle is

$$E_{Coh} = -\frac{E_{perfect}}{N} \tag{3.4}$$

Since there is no change in the number of atoms when a Stone-Wales defect is created, its formation energy can be calculated as the difference in energy of the system with the defect E_{SW} and the energy of the perfect system $E_{perfect}$

$$E_{SW}^{Form} = E_{SW} - E_{perfect}. \tag{3.5}$$

On the other hand, there is a change in the number of atoms when vacancy type defects are created. If $E(N,N_v)$ is the total energy of a crystal with N lattice sites in which N_V vacancies are created, then the formation energy of this collection of defects is given by

$$E^{Form}_{vacancies} = E(N,N_v) - (N - N_v) * E_{perfect}/N. \tag{3.6}$$

We have considered a sample of 20000 atoms and the observed cohesive energy E_{Coh} = 7.50648 eV. *Ab initio* studies on the formation of vacancies in boron nitride have been reported and concluded that the diatomic vacancy (V$_{BN}$) is more favorable than single vacancy (Okada 2009). The formation energy of all the defects studied in this chapter are given in table 3.2. N_v in table 3.2 is the number of atoms removed to create the defect. The formation energies are calculated for zero Kelvin temperature.

3.3.6 Thermally excited ripples

In two-dimensional (2D) layers and membranes, the dynamical corrugation of the surface due to thermal vibrations has been observed. In many earlier atomistic simulations of 2D hexagonal hybrid structures, the thermally excited ripples, the out of plane motion of atoms, have been observed (Fasolino et al. 2007). Mermin (Mermin 1968) has reported that, long-wavelength fluctuations in 2D crystals will destroy its long-range order. 2D membranes embedded in a 3D space have a tendency to form wrinkles. These height fluctuations can be suppressed by the anharmonic coupling between bending and stretching modes. That is, a 2D membrane can exist, but it will exhibit strong height fluctuations (Fasolino et al. 2007, Nelson and Peliti 1987, Le Doussal and Radzihovsky 1992, Nelson et al. 2004). In our studies also, the presence of thermally excited ripples are observed in the h-BN sheet and the height of the formed ripples are proportional to the applied temperature on the system as shown in figure 3.9.

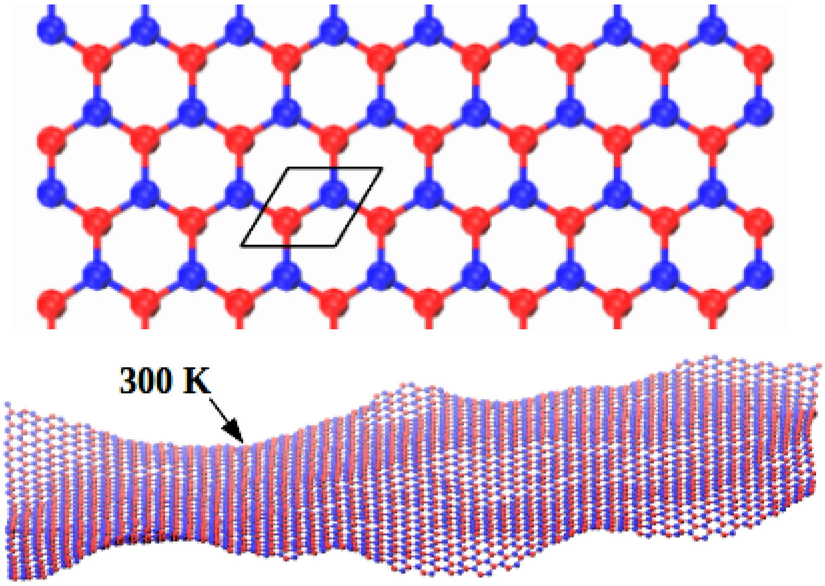

Figure 3.9: Monolayer h-BN sheet at 0 K (top) and the flat surface becomes corrugated due to thermally excited ripples at 300 K (bottom) under periodic boundary condition.

To explain the formation of thermally excited ripples in h-BN, the mean square displacement (MSD) of the out-of-plane fluctuations ($\langle h^2 \rangle$) in the sheet has been calculated. The height-height correlation function can be used to extract the bending rigidity of the material. In this thesis, an attempt has been made to extract the bending rigidity of the pristine and defective h-BN sheet in the harmonic regime. The height-height correlation function ($\langle h^2 \rangle$) of pristine and defect incorporated h-BN sheet is also studied using the continuum theory of membranes. We noticed that the formation of ripples strongly depends on the atomic corrugations. As compared to the sp^2 covalent C-C bonds in graphene, B-N bonds in h-BN are not pure covalent in nature. Because of the electronegativity difference in two atoms, they show partial ionic character. We also observed that the larger corrugations in the out-of-plane direction occur due to the weaker B-N atomic bonds. The ionic character in the h-BN layer increases the inter layer interactions and it leads to a higher value of hardness of 3D bulk h-BN relative to that of graphite. In the case of monolayer h-BN, its stiffness is less than that of graphene (Alem et al. 2009).

The mean square out-of-plane displacement of atoms, in pristine h-BN sheet and also in BN sheet with vacancy and SW defects, has been analyzed. In the case of pristine h-BN sheet, MSD gradually increases with increase in temperature. When the material is connected to a thermostat, the atoms start vibrating from their mean position. When the simulation is carried out for a longer time, the material reaches equilibrium state and the out-of-plane height fluctuations decrease monotonically with time and the value of $\langle h^2 \rangle$ subsides to a constant level. In figure 3.10, the black line corresponds to a temperature of 100 K and the cyan line is for 2400 K. The rest of the lines correspond to temperatures in between 100 K and 2400 K.

The defective h-BN is sheet created from the pristine sheet by the removal of atoms, thus creating an irregularity in the atomic arrangement. After performing the relaxation at zero temperature, the material is subjected to heating and by comparison with the MSD of the pristine h-BN sheet, it is clear that the MSD gradually increases with increase in defect concentration. The MSD shows non-monotonic variation with time when the defect concentration is comparatively high. Presence of high concentration of defects can lead to modification of the effective interatomic interactions in the material and this may lead to nontrivial changes in various physical properties. Variation in mean square displacement ($\langle h^2 \rangle$) as a function of concentration of SW and vacancy defects at room temperature is shown in figure 3.11.

3.3.7 Bending rigidity and scaling property

According to the Mermin - Wagner theorem (Mermin and Wagner 1966), particles having a short range interaction cannot exist in crystalline form in dimensions less than or equal to 2. A way out of this restriction in two dimensions is to have a planar structure with ripples which allows the atoms in the crystal to move in-plane and out of plane directions. Formation of thermally excited ripples in two-dimension can be described on the basis of elasticity theory of continuum membranes. Here suppression of long wavelength fluctuations takes place due to the anharmonic coupling between the out-of-plane bending and in-plane stretching modes. This leads to a characteristic power-law behavior for the height fluctuations. It was believed that graphene, the first experimentally observed two-dimensional

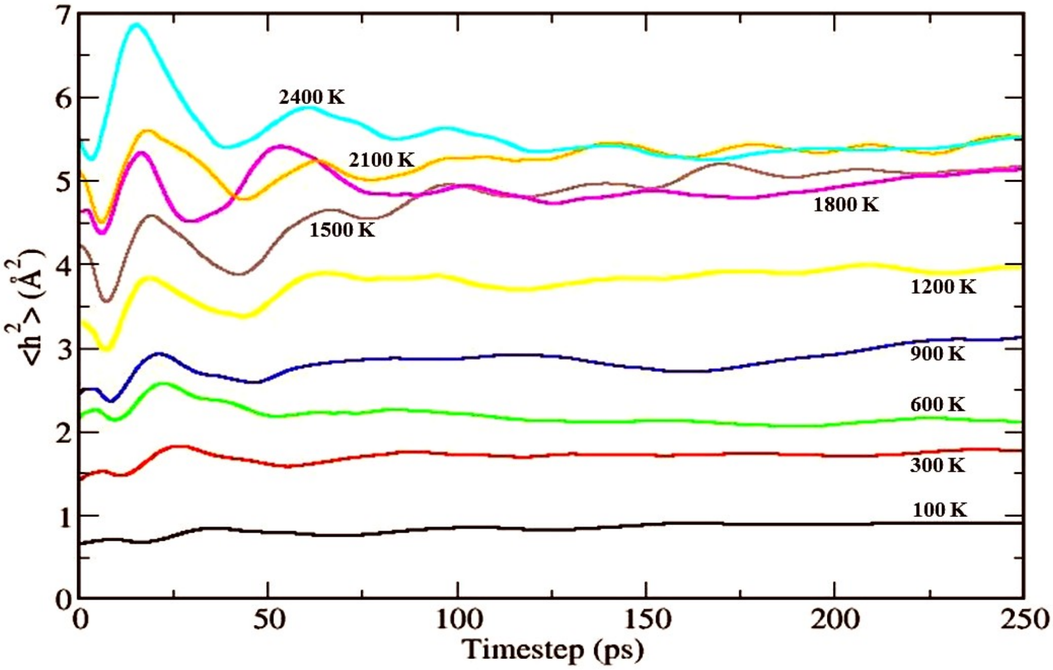

Figure 3.10: Variation in $\langle h^2 \rangle$ with time step for different temperatures in h-BN sheet. When the simulation is carried out for long time, the value of $\langle h^2 \rangle$ stabilizes to a constant level. The black line corresponds to a temperature of 100 K and the cyan line is for 2400 K. The rest of the lines correspond to temperature in between 100 and 2400 K.

crystal, is thermodynamically unstable (Xu and Buehler 2010). In the harmonic approximation, the inter-atomic interactions in a two-dimensional crystal are related to the Fourier components of the height-height correlation function of the out-of-plane vibrations. The correlation function $\langle |h(q)^2| \rangle$ for wave vector $q \sim T/q^4$. This diverges for small wave vectors implying that strictly two-dimensional crystalline order cannot exist. But, the anharmonic coupling between the bending and stretching modes suppresses these long wavelength fluctuations. The resultant out-of-plane ripples become the root cause for the existence of two-dimensional crystals which buckles instead of being flat. The height fluctuations in h-BN sheet are analyzed using the continuum theory of membranes and the key object of study in this theory is the height-height correlation function of the height fluctuation. The correlation function in the harmonic approximation is expressed as (Nelson et al. 2004, Fasolino et al. 2007),

$$H(q) = \langle |h(q)^2| \rangle = \frac{Nk_BT}{\kappa S_0 q^{\beta}} \tag{3.7}$$

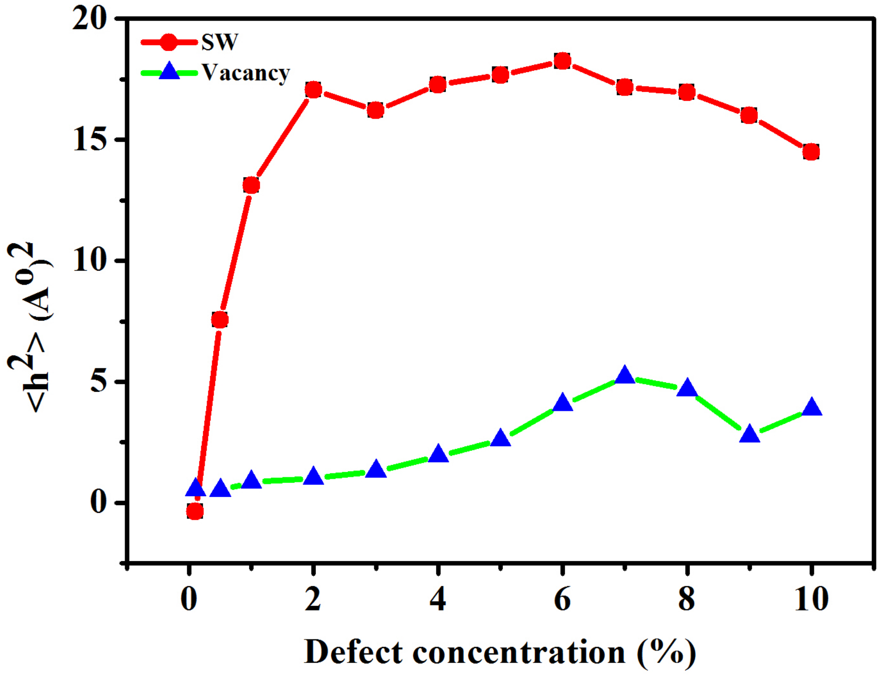

Figure 3.11: The variation in mean square displacement as a function of concentration of SW and vacancy defects at 300 K for h-BN sheet with 20000 atoms.

where, κ is the bending rigidity of the membrane, N is the number of atoms of the sample, S_0 is the surface area per atom and k_B is the Boltzmann constant. The exponent β is universal in this formalism with harmonic approximation, and it takes the value 4. In the large wavelength limit, i.e., for $q \rightarrow 0$, the height fluctuations are suppressed by anharmonic couplings between the bending and stretching modes which gives rise to a re-normalized q dependent bending rigidity. More details about the theory of two dimensional crystalline membrane is detailed in appendix C of the thesis. We have tried to extract the value of bending rigidity by considering the data between q=0.5 Å^{-1} and q=1.0 Å^{-1} to be the harmonic part of $H(q)$ and fitting the data to the function αq^{β}. Such an analysis showed that the scaling exponent β varies from 3.6 to 2.9 as the temperature increases from 200 K to 3000 K.

The results of our study of the exponents of the correlation function shown in figure 3.12 (a) correspond to a simulation cell with 20000 atoms. In figure 3.12 (b) system size dependence of the correlation function is shown with cells containing up to 80000 atoms. Trial runs were done at room temperature with larger cells as well and we found 20000 atoms to be quite large to study the long-wavelength regime. Both in figure 3.12 (a) and 3.12 (b), the x-axis is the wave vector q in units of Å^{-1}. Our work on the correlation function follows the methodology of Zakharchenko et al (Zakharchenko et al. 2010a). In their work on bilayer graphene, Zakharchenko et al., reported that the the correlation function and bending rigidity of smaller sample coincide with that of larger sample. Our studies corroborate this point.

We have determined the value of the critical exponent β, by fitting $\langle|h(q)|^2\rangle$ to a power law αq^{β}. Here q is the norm of the wave vector and $h(q)$ is the Fourier transform of the out of plane excursion of the atoms. The angular bracket represents averaging over several frames. $\langle|h(q)|^2\rangle$ corresponds to the Fourier transform of the height-height auto-correlation function. The fit that is actually carried out is the equivalent linear least square fit $log\left(\langle|h(q)|^2\rangle\right) = \log(\alpha) + \beta \log(q)$ to extract the values of α and β.

The height-height correlation function $H(q)$ and $H(q)/N$ at different temperature and its power law fit are shown in figure 3.12 (a). The fitted solid lines give the harmonic approximation αq^{β} and at the long wavelength limit, the correlation functions have a power-law dependence and is strongly dependent on the value of the exponent. The continuum theory breaks down and deviations from power-law behavior occur if the value of $q \geq 1.0$ Å^{-1}, which is close to the Bragg peak position at $q = 4\pi/\sqrt(3)a$ = 2.8948 Å^{-1}. Earlier studies have reported that the continuum theory breaks down and deviations from power-law behavior occur if the value of $q \geq 1.0$ Å^{-1} (Costamagna et al. 2012) and the same feature is also observed in the present study as shown in figure 3.12 (b). The deviation from power-law behavior is observed at $q \geq 1.0$ Å^{-1}. As the number of atoms increases, the harmonic fit is not showing much variation, but it changes considerably in the case of scaling factor for system dimension.

From the theory of membranes, in the harmonic limit, it has been observed that $\langle h^2\rangle$ is directly proportional to CL^2, where C is a temperature dependent constant. Earlier studies (Costamagna et al. 2012, Lajevardipour et al. 2012) evaluated the spectral modes of graphene by fitting $|h(q)^2|$ to the function αq^{β}. The value of β

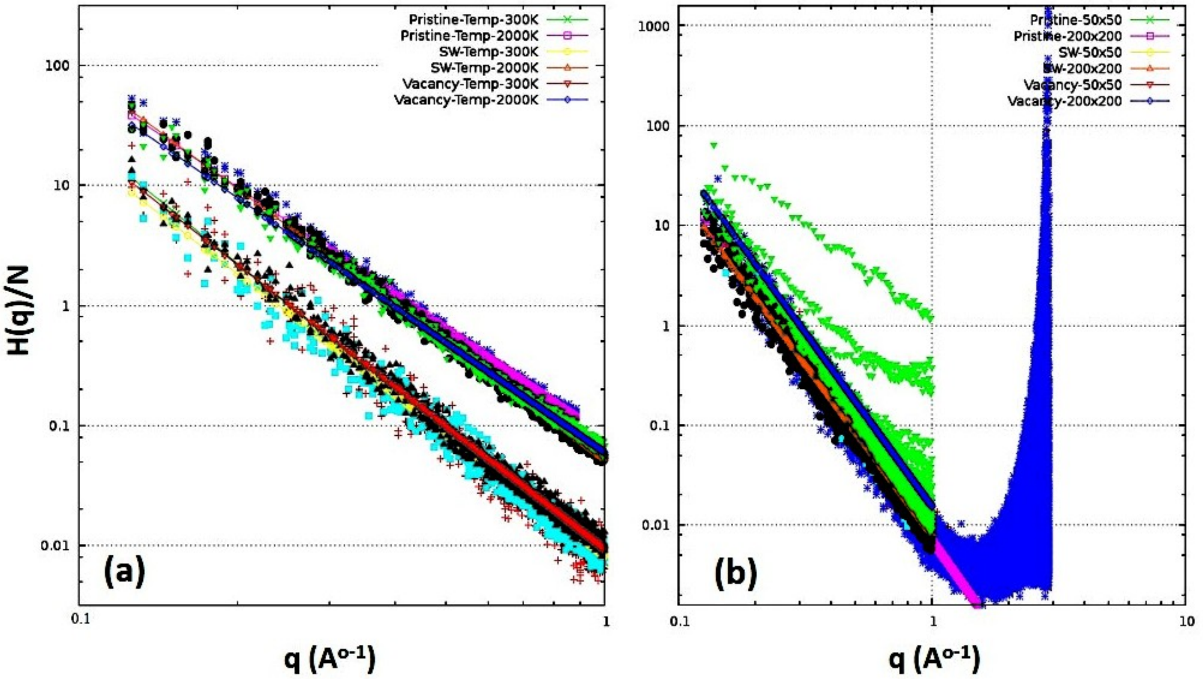

Figure 3.12: (a) Height-height correlation function $H(q)/N$ of pristine and defective h-BN sheet with 20000 atoms at different temperatures. Both Stone-Wales and vacancy type defects are considered. The solid line corresponds to power law fit q^{β} for small values of q, namely 0.1 to 1 Å^{-1}. The exponent is found to be dependent on temperature. Its value differs from the value of 4 that is expected from the harmonic theory of membranes. (b) System size dependence of the correlation function is shown with cells containing up to 80000 atoms. The continuum theory breaks down and deviations from power-law behaviour occur if the value of $q \geq 1.0$ Å^{-1}, which is close to the Bragg peak position at $q = 4\pi/\sqrt{(3)}a = 2.8948$ Å^{-1}.

obtained is different from 4 and hence the height fluctuations do not strictly follow the predictions of harmonic theory of membranes. The discrepancy increases with increase in temperature as observed by Zakharchenko et al (Zakharchenko et al. 2010b). A study of the height fluctuations in graphene by Los et al (Los et al. 2009) at 300 K showed a similar departure from the harmonic theory of membranes. The exponent β that was obtained in their study was 3.15, which is distinctly different from 4 given by the harmonic theory. We have studied the variation of the exponent for a range of temperatures.

One of the properties of h-BN that we have studied is the bending rigidity. In the present work, we aimed at a comparison of the bending rigidity of hexagonal BN with and without defects. The study of defects is particularly important in material like h-BN. Following the works on graphene, we carried out preliminary investigations in this regard by considering the commonly occurring defects like vacancy and Stone-Wales. In the light of the work of Slotman and Fasolino (2012), it is now clear that unlike in the case of graphene, SW defects are not the defects with the lowest formation energy in hexagonal BN. The bending rigidity (κ) of pristine and defective h-BN is calculated by a least squares fit of the slope of the calculated $H(q)$ to equation (3.7) in the range of q vectors, where the harmonic approximation applies.

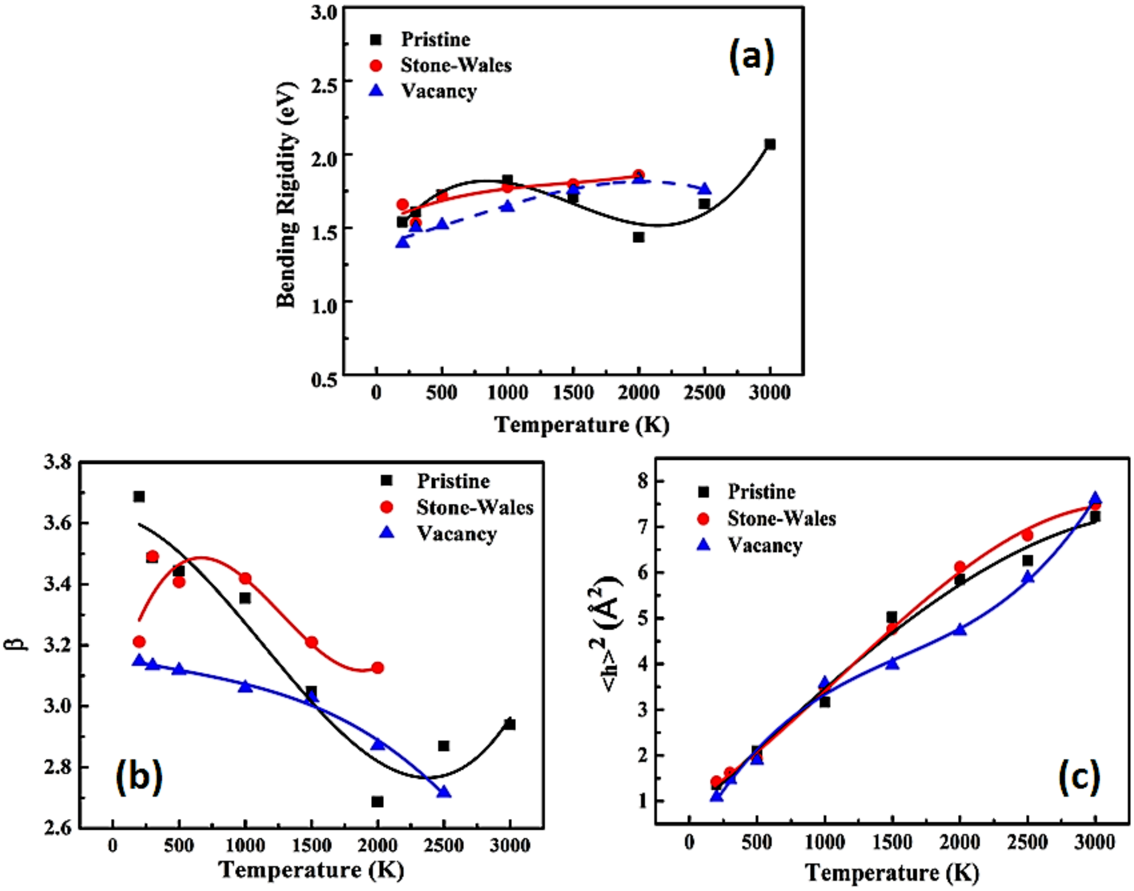

Figure 3.13: (a) Bending rigidity (κ) of pristine and defective h-BN sheet as a function of temperature, (b) variation of scaling exponent with temperature for pristine and defective h-BN sheets and (c) the variation of height-height correlation function with temperature for pristine and defective h-BN sheets. The bending rigidity calculated using the continuum formula increases monotonically with temperature in pristine h-BN sheet and the bending rigidity starts decreasing above 2000 K in defective h-BN sheet.

The temperature dependence of the bending rigidity thus obtained is shown in figure 3.13 (a). The bending rigidity is calculated using the continuum formula given as equation (3.7) increases monotonically with temperature in pristine h-BN sheet and it decreases above 2000 K in defective h-BN sheet. The exponent β decreases from 3.7 to 2.7 as the temperature increases from 200 K to 3000 K in the cases of both pristine and defective sheets. It is observed that the $\langle h^2 \rangle$ increases with increase in temperature in both pristine and defective h-BN sheet. The obtained value of bending rigidity is relatively less compared to the results of the previous studies. The value of bending rigidity strongly depends on the scaling factor (theoretically $\simeq 4$) (Fasolino et al. 2007). As compared to graphene's bending rigidity, (0.82 eV) (Fasolino et al. 2007), h-BN has lower value of bending rigidity of 0.56 eV at 0 K, which implies that h-BN is more vulnerable to fluctuations and bending. The variations in the scaling factor (β) and the height fluctuations are shown as a function of temperature in figure 3.13 (b) and (c) for both pristine and defective h-BN sheets.

Since β changes considerably from continuum limit 4, the expected power-law scaling behavior of $\langle h^2 \rangle$ with system size L also vary accordingly to $\langle h^2 \rangle = C' L^{-2+\beta}$, where C' is a temperature dependent constant. The variation in $\langle h^2 \rangle$ against L=$\sqrt{L_x L_y}$ of pristine and defective sheets are shown in figure 3.14 (a). System size dependence of bending rigidity is shown in figure 3.14 (b) for various system sizes. In the case of the sheet with SW defects the number of atoms remains the same. For the cases with SW and vacancy defects the bending rigidity decreases with increase in system size. It has been noticed that, bending rigidity and height fluctuations vary with increase in the system size and temperature. The system size dependence of scaling exponent is shown in figure 3.14 (c). A correlation between the scaling factor and bending rigidity is observed in both the pristine and defective h-BN sheets. Both of them vary with temperature from 200 K to 3000 K and system size and the results are shown in table 3.3.

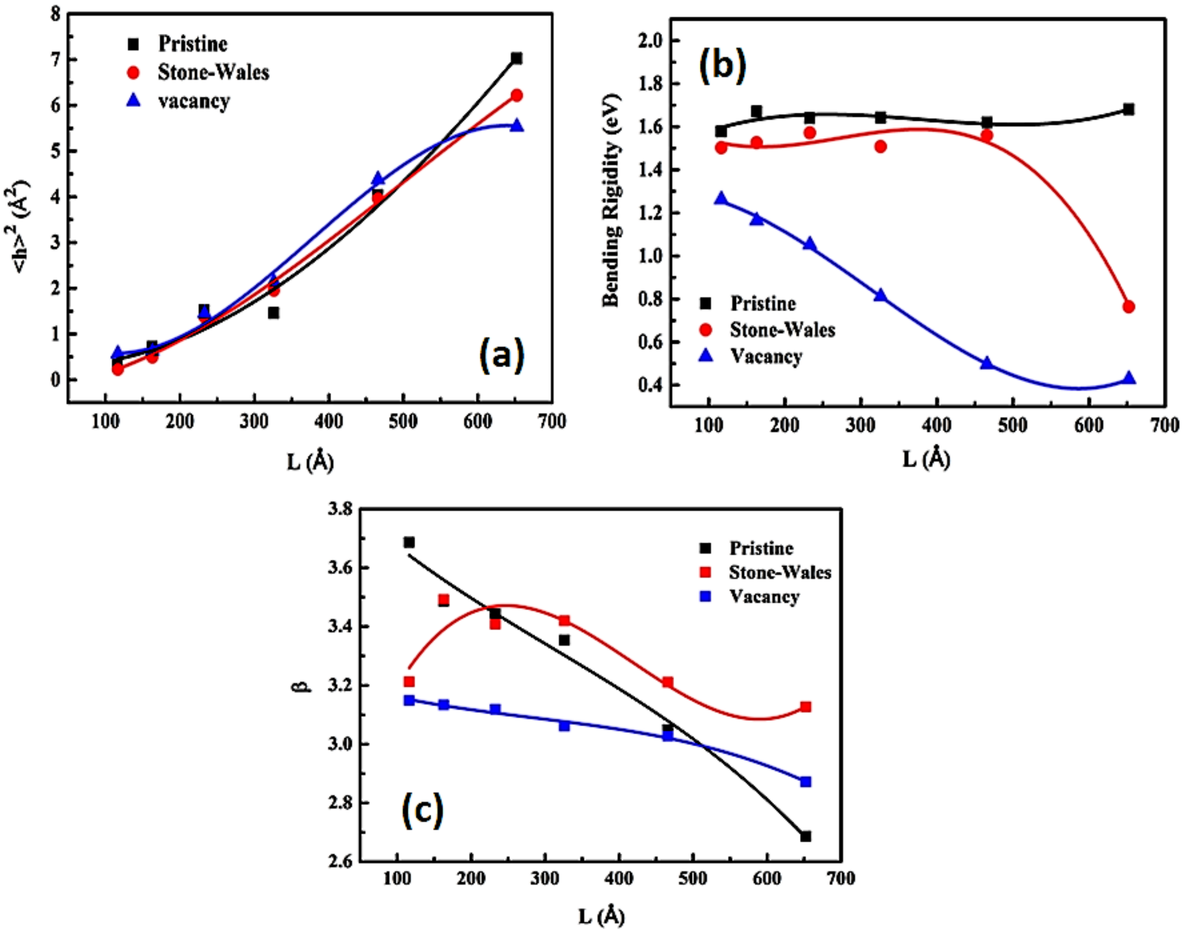

Figure 3.14: Room temperature (a) variation in $\langle h^2 \rangle$ against L=$\sqrt{L_x L_y}$ of pristine and defective sheets, (b) system size dependence of bending rigidity and (c) variation of the scaling exponent β with system size.

Table 3.3: Bending rigidity κ and scaling exponent β at different temperatures for pristine and defective h-BN sheet.

			$\langle h^2 \rangle = \alpha q^\beta$			
T (K)	κ (eV)	β	κ (eV)	β	κ (eV)	β
	Pristine		Stone-Wales		Vacancy	
200	1.5397	3.6863	1.6582	3.2110	1.3940	3.1473
300	1.6094	3.4861	1.5348	3.4913	1.5013	3.1329
500	1.7237	3.4441	1.7191	3.4076	1.5185	3.1180
1000	1.8213	3.3540	1.7771	3.4187	1.6399	3.0601
1500	1.7074	3.0489	1.7955	3.2099	1.7580	3.0272
2000	1.4354	2.6865	1.8573	3.1260	1.8295	2.8706
2500	1.6612	2.8697	1.4574	2.3312	1.7581	2.7154
3000	2.0662	2.9385	0.8856	1.11841	0.1103	0.3461

3.4 Conclusions

It is found that the lattice parameter (a) and B-N nearest neighbor distance (R_{xy}) in h-BN vary considerably at higher temperatures due to the height fluctuations in the out-of-plane direction and the observed lattice parameter is not equal to $\sqrt{3}R_{xy}$. As temperature increases the amplitude of the peaks in RDF decreases due to thermal broadening. The obtained results for linear thermal expansion coefficient and specific heat at constant volume of hBN are in good agreement with the earlier atomistic studies. Specific heat shows considerable increase beyond the Dulong-Petit limit at high temperatures, which is interpreted as a signature of strong anharmonicity present in h-BN. Presence of defects leads to increase in the height fluctuations. Stone-Wales defects cause a larger height fluctuation as compared to vacancy type defects. The height-height correlation function and bending rigidity, calculated within the frame work of continuum theory of membranes, vary with increase in temperature and defect concentration. The power-law exponent β for the height-height correlation function shows deviation from the harmonic limit of 4 predicted by membrane theory. It decreases from 3.7 to 2.7 as the temperature increases from 200 K to 3000 K. The non-universality of the scaling exponent β is also an indication of the important role played by anharmonicity in h-BN. The system size and temperature dependence of the bending rigidity and the power-law exponent are derived. Comprehensive study of properties of h-BN incorporating all types of energetically favorable defects is necessary for many of the potential applications of h-BN to become a reality.

Chapter 4

Directional Anisotropy, Finite Size Effect and Elastic Properties

---

This chapter explains the details of the calculation of zero Kelvin elastic constants of 2D-hBN using energy method. We present a systematic study of h-BN for various system sizes. The Young's modulus and Poisson ratio are found to be anisotropic for finite sheets whereas they are isotropic for the infinite sheet due to the presence of transverse displacement waves in it. Both of them increase with system size in accordance with a power law. It is concluded from the computed values of elastic constants that h-BN sheets, finite or infinite, satisfy Born's criterion for mechanical stability. Due to the the strong in-plane sp^2 *bonds and the small mass of boron and nitrogen atoms, h-BN possesses high longitudinal and shear velocities. The variation of bending rigidity with system size is also calculated.*

4.1 Introduction

The mechanical robustness of h-BN is an important requirement for the manufacturing of nano-devices and also in nano and opto-electronics applications. To the best of our knowledge, the elastic constants of a free standing 2D h-BN have not been studied so far using the framework of classical molecular dynamics. In this thesis, one of our aims is to calculate the elastic constants of a finite and infinite 2D sheet of h-BN using the energy method (Krishnan and Ghosh 2014, Xiong and Tian 2015). We also extracted the sound velocities using the derived elastic constants and calculated the variation of bending rigidity with system size. The obtained results of the mechanical properties of 2D h-BN sheet are expected to provide better ideas for the development of potentially and technologically important integrated devices. It has been reported that, h-BN is considered as the thinnest 2D material with ionic bonds and it can be used as a part of graphene like structures for the design of novel nano-electro mechanical systems (NEMS) (Boldrin et al. 2011). Various research groups have investigated the mechanical properties of h-BN using experimental tools (Bosak et al. 2006) as well as atomistic simulation using *ab initio* method (Kudin et al. 2001, Ohba et al. 2001, Green et al. 1976, Peng et al. 2012a, Mirnezhad et al. 2013) and molecular dynamics (Mortazavi and Rémond 2012, Zhao and Xue 2013, Han et al. 2013).

4.2 Molecular dynamics modelling

In the present study we created a rectangular simulation cell of BN and subjected it to different type of deformations to evaluate the energy, forces, etc., from the simulated output data file and extracted the values of various properties using the developed script. The number of atoms used in a simulation depends on the objective of the simulation. We have carried out MD simulations on h-BN to mimic two types of systems: (1) system of infinite spatial extent and (2) a series of systems with finite system size. There is a finite size effect even in simulations mimicking an infinite system. This is because the neighbors of atoms near the edge of a cell are exactly the same as the atoms in the other side of the very same cell, and hence their motion are correlated when the system size is small. These correlations would decrease when the system size is increased. For this geometry, we have optimized the system size so that the properties are independent of the system size. In the case of simulations intended to mimic a finite sheet, the simulation cell is taken to be a finite sheet surrounded by a sufficiently large vacuum space so that the interaction between the atoms in the simulation cells and the atoms in its replicas is negligible. Here, the properties are expected to be system size dependent, and this aspect is systematically studied by varying the system size from 400 atoms to 90000 atoms.

We have carried out calculations pertaining to the two dimensional h-BN sheet of infinite spatial extent (in the x and y directions) as wells as sheets of various finite sizes. Ideally, a simulation box with periodic boundary conditions in the x and y directions and fixed boundary condition in the z direction (with sufficiently large height for the simulation box) should suffice for the two dimensional sheet of infinite size, whereas fixed boundary conditions in all the three directions would be appropriate for sheets of finite size. However, there is a practical difficulty of losing atoms across the boundary while using LAMMPS package for calculations involving deformation if such boundary conditions are employed. A simple way out is to augment the simulation box with vacuum spaces of adequate size in one or more directions paying attention to following details.

In the case of simulation of the infinite sheet, we have to add the vacuum space in the z-direction. The calculations done in this manner correspond to a system comprising of infinite number of parallel sheets. The thickness of the vacuum space has to be sufficiently large so that the interaction between the atoms in the sheet of our interest with those in the replicas is negligibly small. We have found that a vacuum space of 20 Å thickness is sufficient for this purpose. We have to add vacuum spaces in the x and y directions too while carrying out simulation of finite films. If the system is allowed to relax for a sufficiently long time after stretching the box, the atoms can come back to their initial position at equilibrium if the boundary atoms are not kept fixed. To do this, we have separated out the edge atoms and imposed zero force constraint on the edge atoms.

In our study, the observed equilibrium lattice parameter of 2D BN nanosheet of infinite spatial extent at zero Kelvin using NVE ensemble is obtained as 2.505 Å with a nearest boron-nitrogen bond length as 1.45 Å. Our results are comparable to the experimentally observed value a=2.504 Å (Bosak et al. 2006, Solozhenko et al. 1995) and the nearest boron-nitrogen bond length is 1.45 Å (Zeng et al. 2010). The zigzag and armchair directions were taken to be oriented along the X and Y axes respectively. Bond length and bond angles of an infinite unstrained and strained pristine BN sheet with different orientation is shown in figure 4.1. The simulations with finite sheets show considerable changes in the bond length and bond angle while applying strain compared to an infinite sheet with the same strain. For example, when a longitudinal strain $\varepsilon_{yy} = 0.05$ is applied to a sheet of size 400 atoms, the B-N interatomic distance at the edge of the sheet is 1.52 Å as compared to 1.50 Å for the bond length in an infinite system subjected to the same strain. Similarly there is a difference in the bond angles as well. It is 121.98° for the infinite system, whereas it is 121.22° for the finite system upon imparting the same strain.

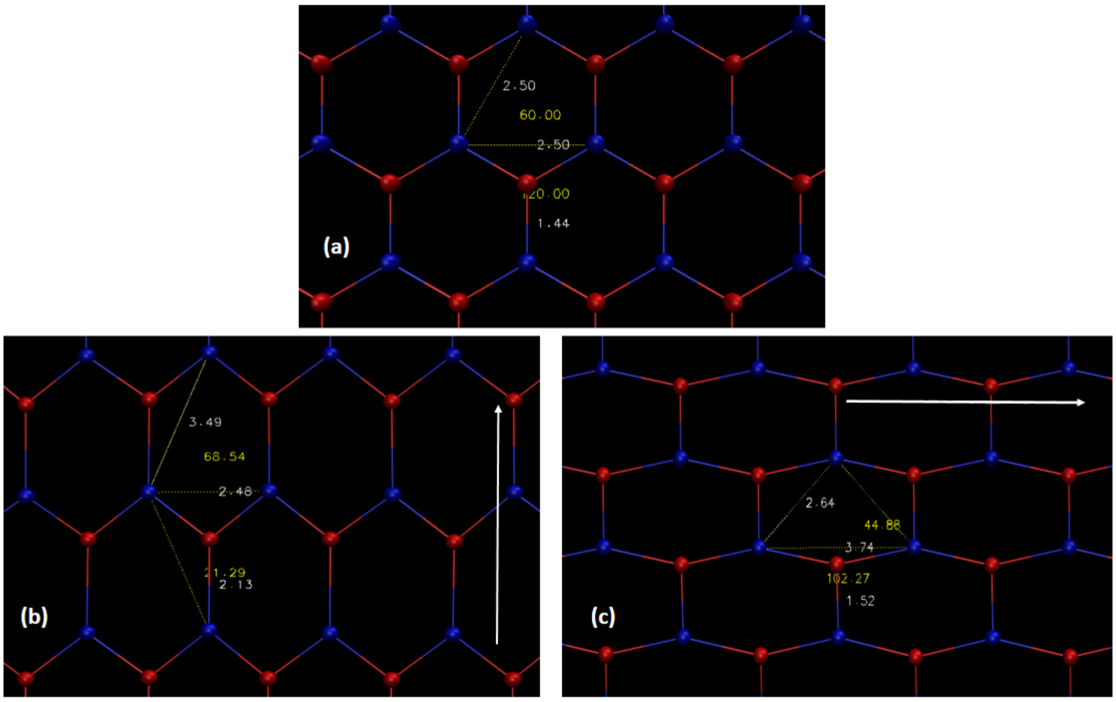

Figure 4.1: Bond length and bond angles of an infinite (a) unstrained pristine BN sheet. Considerable change in the bond length and bond angle has been observed after applying a deformation to the (b) armchair and (c) zigzag direction. The white arrow in fig (b) and (c) represents the direction of deformation in armchair and zigzag chirality.

Structural relaxation of 2D h-BN has been performed using the conjugate-gradient (CG) minimization algorithm. In CG algorithm, in each iteration, the force gradient is combined with the previous iteration information to compute a new search direction conjugate to the previous search directions. Newton's equations of motion of the atoms are solved using the standard Velocity - Verlet algorithm (Swope et al. 1982). We observed that 0.1 fs is a reasonably good timestep for the structural and thermal studies of h-BN (Thomas et al. 2015) and the same is used for the elastic constant analysis. In this chapter we explains the calculation of zero temperature elastic constants, even though this method can be used for calculating temperature dependent elastic constants. All the calculations are done in the micro-canonical ensemble (constant NVE) with energy kept constant within one part in 10^7 for times of the order of 100 ps. In hexagonal boron nitride, boron and nitrogen atoms experience strong covalent bonding within the layers, whereas they experience a weak van der Waal's interaction across the layers. The strength of the inter-layer van der Waal's interaction is such that the distance between the hexagonal layers is 3.34 Å. In order to calculate the elastic constants of 2D h-BN, we studied change in energy of a rectangular sheet of atoms as a function of magnitude of strain for various types of deformations.

4.3 Results and discussions

4.3.1 Elastic Constants

To calculate the elastic constants of h-BN, a rectangular simulation cell is considered in which one of the basis vectors of the honeycomb lattice is taken to be the basis vector along X direction. The other basis vector is in the Y directions and its magnitude is $\sqrt{3}$ times the lattice parameter of the honeycomb lattice. The changes in the energy upon deformation of the simulation cell are extracted, and the elastic constants are calculated by processing this data.

When the applied stress is small, the stress and strain tensors are related by the equation of linear elasticity, namely, σ_{ij}=$C_{ijkl}\varepsilon_{kl}$ (summation over repeated indices implied). Here, σ_{ij} and ε_{kl} are the symmetric second rank stress tensor and strain tensor respectively. The fourth rank tensor C_{ijkl} is known as the elasticity tensor and its components are called the elastic moduli or elastic constants. 3D hexagonal structures like graphite have five independent elastic constants, which are C_{11}, C_{12}, C_{13}, C_{33} and C_{66}, in the Voigt notation (Anees et al. 2014). These are again categorized in to three different classes, depending on the nature of the bonding in the material. C_{11} and C_{12} belong to the first class and they are related to the strong in-plane covalent bonding, C_{33} and C_{66} form the second class in which they depend on the weak van der Waal's bonding across the layers and C_{13} corresponds to inter layer binding along with C_{33} and C_{66}. Every crystal would be mechanically stable if the energy of the deformed system is larger than that of the perfect crystal. Mathematically, this implies that the elastic constant matrix must be positive definite. This is the famous Born stability criterion.

The elastic behavior of a 2D system is described by the in-plane interactions which is considered as isotropic and its matrix of second-order elastic constants is given by:

$$C_{ij} = \frac{1}{A_0 d_0}\left(\frac{\partial^2 E}{\partial \varepsilon_i \partial \varepsilon_j}\right),$$

where, E is the energy of the system, A_0 is the equilibrium area of the 2D system, d_0 is the van der Waals's distance (which represents the effective thickness of the layer) and ε is the strain tensor. The elastic energy $E(\varepsilon)$ of the two-dimensional sheets can be expressed using polynomial form as $E(\varepsilon) = \frac{1}{2}C_{11}\varepsilon_{xx}^2 + \frac{1}{2}C_{22}\varepsilon_{yy}^2 + C_{12}\varepsilon_{xx}\varepsilon_{yy} + 2C_{66}\varepsilon_{xy}^2$. The longitudinal strain applied along the x direction is ε_{xx}, that along y direction is ε_{yy} and the shear strain in the xy plane is ε_{xy}. These are denoted by the symbols ε_1, ε_2 and ε_6, respectively, in the Voigt notation. Here, the x (y) axis is along the zigzag (armchair) direction, ε_{ij}'s are the infinitesimal strain tensors, and the C_{ij}'s are the corresponding linear elastic constants (Ding and Wang 2013).

For the case of an isotropic two-dimensional sheet, the linear elastic constants satisfy the relations of $C_{11} = C_{22}$ and $2C_{66} = C_{11} - C_{12}$ (Zhou and Huang 2008).

Then, the Born mechanical stability criterion for a 2D system like h-BN reduces to $C_{11} > C_{12}$. The 2D in-plane stress-strain relation for the h-BN system in terms of stiffness matrix can be written as,

$$\begin{pmatrix} \sigma_1 \\ \sigma_2 \\ \sigma_6 \end{pmatrix} = \begin{pmatrix} C_{11} & C_{12} & 0 \\ C_{21} & C_{22} & 0 \\ 0 & 0 & \frac{C_{11}-C_{12}}{2} \end{pmatrix} \begin{pmatrix} \varepsilon_1 \\ \varepsilon_2 \\ \varepsilon_6 \end{pmatrix}, \tag{4.1}$$

and the elastic energy for small deformation is given by

$$U(\varepsilon) = \frac{1}{2} \begin{pmatrix} \varepsilon_1 & \varepsilon_2 & 2\varepsilon_6 \end{pmatrix} \begin{pmatrix} C_{11} & C_{12} & 0 \\ C_{21} & C_{22} & 0 \\ 0 & 0 & \frac{C_{11}-C_{12}}{2} \end{pmatrix} \begin{pmatrix} \varepsilon_1 \\ \varepsilon_2 \\ 2\varepsilon_6 \end{pmatrix} \tag{4.2}$$

Finite size scaling: Usually the system size effect is studied by fitting the results of simulations as a function of inverse system size. A power law like expression $C(N) = A - B/N^{\nu}$ is used to fit the data derived from the finite system size (N, the number of atoms) and extrapolate the results to an infinite system limit (where A, B and ν are positive constants). We have systematically varied the system size of the simulation cell to understand the effect of system size on the calculated properties. For the case of simulations mimicking an infinite system, we used simulation cells without any vacuum space at the boundaries of the cell. Here we found that about 10000 atoms in a simulation cell is good enough to obtain convergence, with respect to system size, in the values of the various properties of the material. Since all the atoms are surrounded by atoms, there are no surface effects in the above mentioned simulations.

However, in the context of nanomaterials, an appreciable fraction of the atoms are in the surface region. Hence it is necessary to do simulations of such systems with simulation cells with free surfaces. One of the ways of doing this is to attach vacuum regions at the surfaces of the simulation cell to form a new simulation cell, and continue to use periodic boundary conditions along all the three directions. The thickness of the vacuum regions can be chosen in such a manner that the interaction between an atom in the boundary of the new cell with another in the replica of the new simulation cell is practically negligible. We can then consider series of such systems with various system sizes to study the system size dependence of physical properties of finite systems.

In the normal case of minimization, one would expect the system to come back to the original configuration when it is allowed to relax after changing the length of the simulation box to induce the necessary strain. To avoid this, we have tagged the edge atoms and enforced a constraint of zero force on them. Thus the fractional coordinates of the inner atoms would readjust to come to new equilibrium position. Thus, we can extract the energy required to calculate the elastic constants. In the present study, we varied the system size of a finite h-BN sheet from 400 to 3,60,000 atoms and we found that the finite system very well mimics an infinite system when the system size becomes ∼90,000 atoms or more.

We know that the atomic lattice of h-BN is six-fold-rotation symmetric, and the in-plane orientation of h-BN in the X-Y plane is typically described by a chirality angle θ: $0^\circ \leq \theta \leq 30^\circ$, where $\theta = 0^\circ$ corresponding to the zigzag chirality and $\theta = 30^\circ$ that of armchair chirality (Cao 2014). Then, using the calculated elastic constants, one can calculate the Young's modulus and Poisson's ratio along an arbitrary orientation θ as Ding and Wang (2013), Cadelano and Colombo (2012),

$$E(\theta) = \frac{C_{11}C_{22} - {C_{12}}^2}{C_{11}s^4 + C_{22}c^4 + \left(\frac{C_{11}C_{22} - {C_{12}}^2}{C_{66}} - 2C_{12}\right)c^2s^2} \tag{4.3}$$

and

$$\nu(\theta) = -\frac{\left(C_{11} + C_{22} - \frac{C_{11}C_{22} - {C_{12}}^2}{C_{66}}\right)c^2s^2 - C_{12}(c^4 + s^4)}{C_{11}s^4 + C_{22}c^4 + \left(\frac{C_{11}C_{22} - {C_{12}}^2}{C_{66}} - 2C_{12}\right)c^2s^2}, \tag{4.4}$$

where $c = cos\theta$ and $s = sin\theta$. Our simulations shows that in the above equations (4.3) and (4.4), if we use Cauchy relations $C_{11} = C_{22}$ and $C_{66} = (C_{11} - C_{12})/2$ for an isotropic sheet, then

$$E(\theta) = Y = \left(\frac{{C_{11}}^2 - {C_{12}}^2}{C_{11}}\right) \tag{4.5}$$

and

$$\nu(\theta) = \nu = \left(\frac{C_{12}}{C_{11}}\right) \tag{4.6}$$

We observed that the calculated elastic constants depend on boundary of the used sheets. In the present study, the obtained elastic constants of a system with infinite sheet size without vacuum space are C_{11} = C_{22} = 823.28 GPa, C_{12} = 245.23 GPa and C_{66} = 289.45 GPa, which clearly depicts the isotropic nature of the material. A direct comparison has made with the theoretical value and the obtained value of C_{66} using the Cauchy relation for a hexagonal system as $2C_{66}$ = $C_{11} - C_{12}$ = 289.025 GPa, which validate our efforts to calculate the elastic constants of 2D h-BN using classical molecular dynamics simulation.

The finite system size simulations are carried out with finite simulation cells surrounded by vacuum space of appropriate thickness on all sides. We have analyzed the system size dependence on the anisotropy of Young's modulus and Poisson's ratio of h-BN using equations (4.3) and (4.4) and the θ=0 gives the zigzag direction and θ=30 that of armchair direction. Figure 4.2 shows the variation of Young's modulus with inverse system size. Even though the Young's modulus for the arm chair and zigzag configurations are substantially different for small system sizes, they converge to almost the same value of $\sim$ 750 GPa when the system size become higher. Thus the anisotropy of the Young's modulus progressively decreases when the system size increases.

A similar trend is seen in the behaviour of Poisson ratio as well, shown in figure 4.3. The second order linear elastic constants ($C_{ij}, i, j = 1,2$) of 2D h-BN are investigated by calculating the change in internal energy E_j while applying certain specific type j of small deformations. For example, if only $\varepsilon_6 \neq 0$, the change in energy will be a function only of ε_6. This function is expected to be quadratic in ε_6 only if the maximum deformation that is considered is very small.

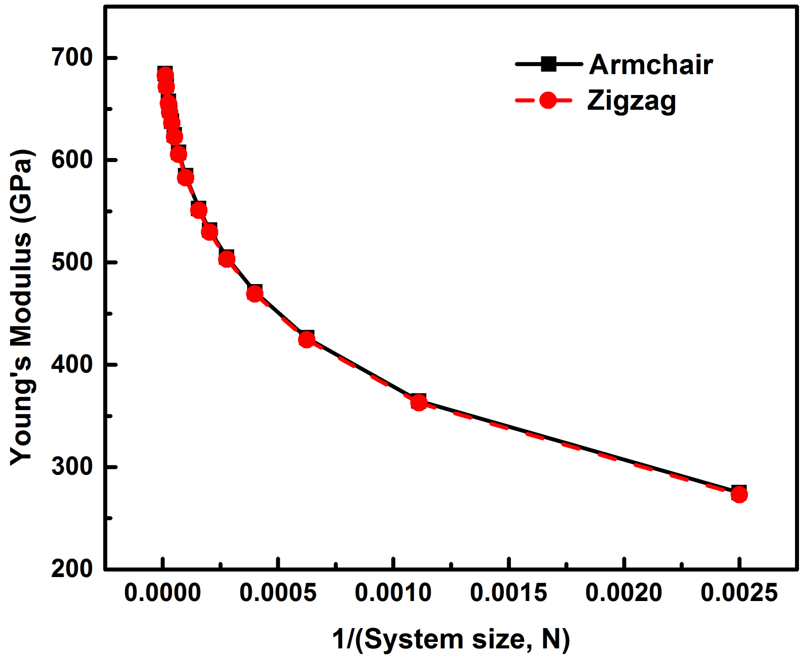

Figure 4.2: Variation of Young's modulus with inverse system size. As the system size become higher, the value of Young's modulus tends to a saturated value in both armchair and zigzag directions.

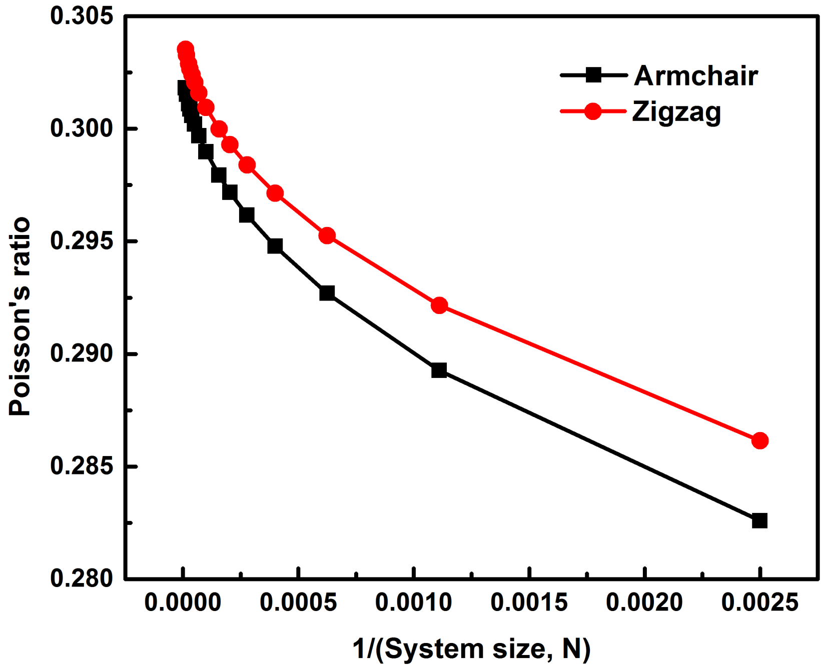

Figure 4.3: The variation of Poisson's ratio with inverse system size in armchair and zigzag chirality.

The strain energy can be fitted to a polynomial of appropriate order in ε_6. The coefficient of quadratic term in this fit gives $2C_{66}$. We determined the optimal order of the fit by an iterative procedure. Figure 4.4 shows the total energy as a function of specific strains, and the corresponding polynomial fit. If we consider a sheet with no vacuum space and is periodically repeating, then 10000 atoms are good enough to evaluate the elastic constants and here $C_{11} = C_{22}$ as shown in figure 4.4 (a). On other hand, if we consider a series of finite systems consisting of 400 atoms onwards, with periodic boundary condition and a vacuum space of 20 Å, considerable variation of the elastic constants with system size is observed. Young's modulus for systems with 400, 25600 and 90000 atoms are found to be 272, 632 and 682 GPa, respectively. The variation in the values of the computed elastic constants is shown in figure 4.4 (b). When the system size increases beyond 90,000 atoms, the finite systems mimic the behaviour of an infinite system as shown in figure 4.4 (c) and (d).

In the current study, the positive values of elastic constants ensure the mechanical stability of h-BN. Using Born-Stability criterion, we observed that the necessary and sufficient condition for the elastic stability of a h-BN system reduced to $C_{11} > 0$ and $C_{11} > |C_{12}|$ (Mouhat and Coudert 2014). The values of C_{11} and C_{12} are found to be very well in agreement with the earlier experimental and *ab initio* DFT studies, which indicates the strong in-plane covalent bonding between boron and nitrogen atoms. The calculated Young's modulus and Poisson's ratio in comparison to the existing data from the literature are tabulated in table 4.1.

Finite size scaling approach is commonly used to quantify the system size dependence of physical properties estimated from simulations employing cells with finite size, and to extrapolate their values in the limit of infinite system size. This analysis begins with the simulation of systems with different size. In this study, we used the finite size scaling method by implementing a power law fit to find the values of the elastic constants C_{11} and C_{12} by observing how these quantities vary with different system sizes. We also noticed that the first class elastic constants C_{11} and C_{12} varied considerably with system size.

As the system size increases, the surface effect become negligible and the values of C_{11} and C_{12} showed a tendency to converge to their respective bulk value.

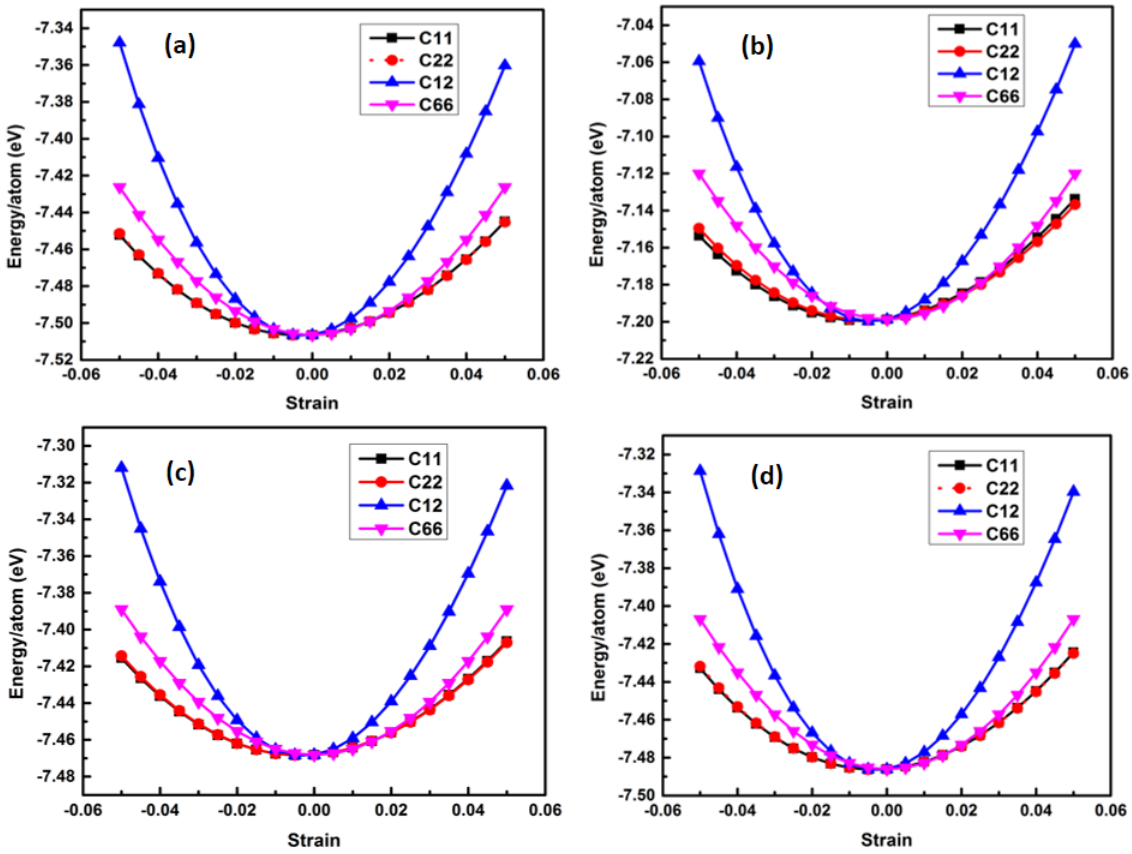

Figure 4.4: The energy-strain response graph for the calculation of elastic constants of h-BN. The total energy is plotted as a function of various specific strains necessary for calculating the elastic constants. (a) Calculations on a sheet with 10000 atoms subject to periodic boundary condition show that $C_{11} = C_{22}$. (b) A finite system consisting of 400 atoms with periodic boundary condition and a vacuum space of 20 Å, shows significant difference in the computed elastic constants. (c) and (d) When the system size increases from 25,600 to 90,000 atoms, respectively, behaviour of the finite system tends to that of an infinite system.

We fitted the values of C_{11} and C_{12} in each system size to the equation $C(N) = A - B/N^{\nu}$ and plotted the results as a function of $1/N$. The value of ν, the scaling exponent, obtained from the fit using the data is 0.4. The constant A represents the asymptotic value of the elastic constant (the value in the limit of system size tending to infinity). The variation of the elastic constants C_{11} and C_{12} with system size, and the fit are shown in figure 4.5 and 4.6. From figure 4.5 and 4.6, it is clear that both C_{11} and C_{12} show a similar increase with system size and reach a saturated value. Our results are comparable to the experimentally determined elastic moduli of single crystal hexagonal boron nitride using inelastic X-ray scattering by

Bosak et al (Bosak et al. 2006) and the *ab initio* DFT calculations by Hamdi et al (Hamdi and Meskini 2010). An exclusive study was done to compare the elastic constants of BN nanosheet using ab-initio DFT calculations(Peng et al. 2012b). Density functional theory calculations(Peng et al. 2012b, Milowska et al. 2013) predicted the elastic properties of h-BN, with an accuracy comparable to the present work, other experimental and atomistic simulation methods.

Table 4.1: Calculated elastic properties of the infinite h-BN and comparison with the experimental and other theoretical calculations. Young's modulus (Y) [in GPa] and Poisson's ratio (ν) are tabulated.

	Reference	**Year**	**Method**	**Results**
Young's Modulus (GPa)	Present study	2016	Molecular Dynamics	750
	Han et al	2014	Molecular Dynamics	881
	Milowska et al	2013	Ab-*initio*	756
	Zhao et al	2013	Molecular Dynamics	716
	Mirnezhad et al	2013	Ab-*initio*	829
	Peng et al	2012	Ab-*initio*	802
	Topsakal et al	2010	First-principle studies	769
	Bosak et al	2006	Inelastic X-ray scattering	811
	Kudin et al	2001	Ab-*initio*	781
Poisson's ratio	Present study	2016	Molecular dynamics	0.297
	Milowska et al	2013	Ab-*initio*	0.216
	Peng et al	2012	Ab-*initio*	0.217
	Mirnezhad et al	2013	Ab-*initio*	0.213
	Eun-Suok Oh	2010	Continuum lattice approach	0.413

4.3.2 Acoustic wave velocity using elastic constants

In the present study, the used bond order potential has an ability to describe not only the structural stability around equilibrium, but also the anharmonic as well as possible bond breaking mechanism and sp^2 to sp^3 phase transitions (Karssemeijer and Fasolino 2011). From the obtained elastic constants, the C_{11} and C_{12} are independent due to the symmetry of the hexagonal structure. The in-plane stiffness Y of an infinite system can be obtained from the elastic moduli C_{11} and C_{12} as $Y = (C_{11}^2 - C_{12}^2)/C_{11}$. The Poisson's ratio ν of the infinite system can be described

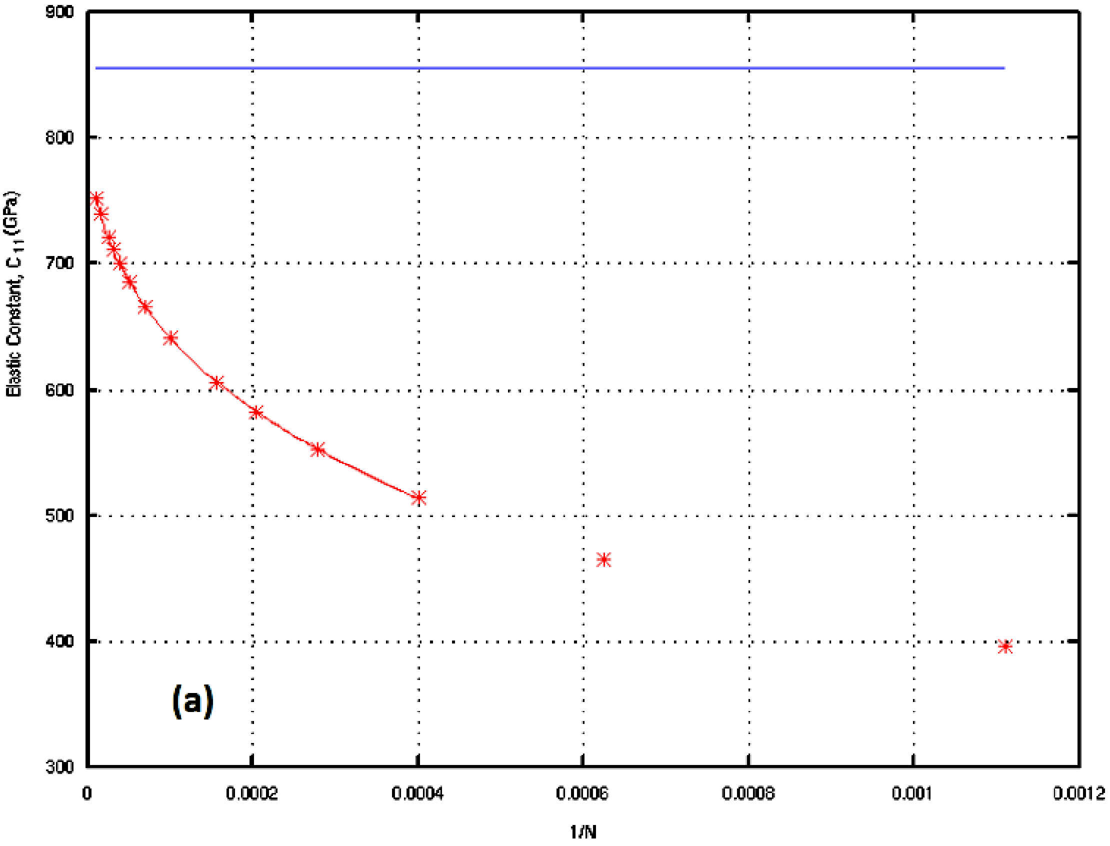

Figure 4.5: Dependence of the elastic constants C_{11} on the inverse system size. We fitted the values of C_{11} in each system size to the equation $C(N) = A - B/N^{\nu}$ and plotted the results as a function of $1/N$, where N is the number of atoms in the simulation cell. The value of the scaling exponent ν obtained from the fit is 0.4. The blue line represents the value of the respective elastic constant extrapolated to infinite system size limit.

as the ratio of the transverse strain to the axial strain and is related to the elastic moduli as $\nu = C_{11}/C_{12}$. We also have calculated the in-plane stiffness of a 2D h-BN with finite and infinite sheets. In the case of a finite sheet, we keep a vacuum spacing of 20 Å to avoid the surface effects.

In the case of a finite sheet, as shown in figure 4.5 and 4.6, both the C_{11} and C_{12} increases with system size. We have observed that C_{11} is the dominant factor in computing the in-plane stiffness as compared to C_{12}. The study of elastic properties gives a better understanding of the mechanical behaviour of the material. In the case of h-BN structures, the presence of a non-zero stiffness in both volumetric and shear deformations helps to generate the sound waves with different

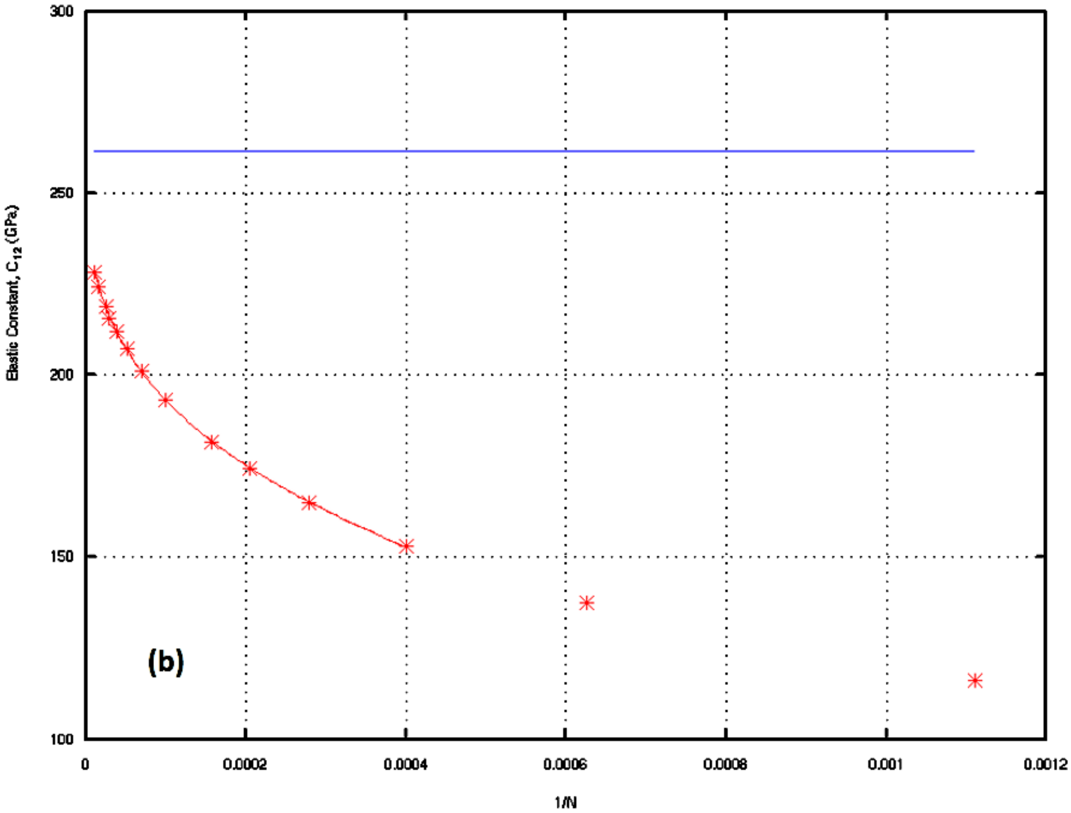

Figure 4.6: Dependence of the elastic constants C_{12} on the inverse system size is shown in figure. We fitted the values of C_{12} in each system size to the equation $C(N) = A - B/N^{\nu}$ and plotted the results as a function of $1/N$, where N is the number of atoms in the simulation cell.

velocities depending on the deformation mode. Thus, the sound waves generated due to volumetric deformations (compressions) are called longitudinal waves (p-waves) and that of shear deformations are called shear waves (s-waves). Using the in-plane elastic modulus (Young's modulus) Y, Poisson's ratio ν, two dimensional mass density ρ_m, in-plane elastic constants C_{11} and C_{12}, the longitudinal and shear wave velocities can be expressed as (Kinsler et al. 1999):

$$V_p = \sqrt{\frac{Y(1-\nu)}{\rho_m(1+\nu)(1-2\nu)}} \tag{4.7}$$

$$V_s = \sqrt{\frac{C_{12}}{\rho_m}} \tag{4.8}$$

The two dimensional mass density of h-BN can be written as $\rho_{2D} = 4m_{BN}/(\sqrt(3)a^2)$, where a is the in-plane lattice parameter of h-BN and m_{BN} is the atomic mass of boron nitride. In the present study, the observed mass density is 15.180×10^{-7} kg/m^2, which is twice the mass density of graphene. Due to the the strong in-plane sp^2 bonds and the small mass of boron and nitrogen atoms, 2D h-BN possess high group velocities. We noticed that the longitudinal wave velocity is more as compared to shear wave velocity which is consistent with earlier *ab-initio* studies (Peng et al. 2012b). Using equation (4.7) and (4.8), the observed longitudinal and shear wave velocities of a system with infinite boundary are 14.898 km/s and 7.3628 km/s respectively. Figure 4.7 (a) shows that, as the system size increases, the total energy of the sample decreases and the Young's modulus increases, which leads to an increase of longitudinal and shear wave velocities as shown in figure 4.7 (b). Peng et al., reported that the experimental measurement of the group velocities of 2D h-BN is possible for the practical engineering applications. The sound frequency and ranging channel can be formed using a velocity gradient which is the functional mechanism of surface acoustic wave sensors and wave guides (Peng et al. 2012b).

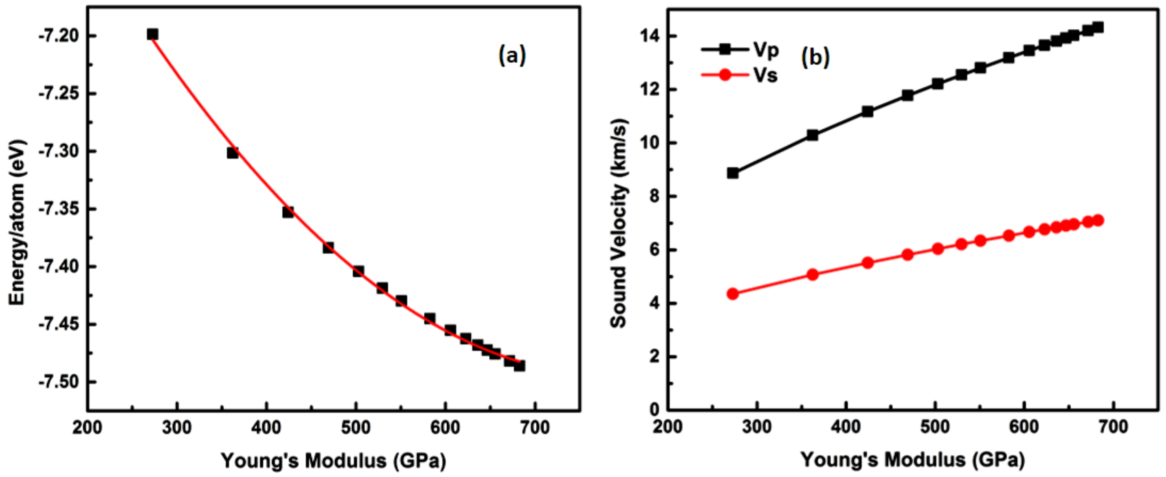

Figure 4.7: As the system size increases, the Young's modulus of h-BN system increases, leading to an increase in longitudinal and shear wave velocities.

4.3.3 Thin shell thickness and bending stiffness

In order to analyze the tensile and out-of-plane mechanical behaviors of 2D materials, an effective thickness has to be defined and is entirely different from the inter-layer distance. The thin shell thickness (t_s) of 2D material is a key parameter which characterizes the structural flexibility. This is used to investigate the non linear structural deformation mechanism and is directly related o the Foppl-von Karman approach (Gao and Xu 2015). In this approach, the bending stiffness can be extracted by coupling the in-plane stretching and out-of-plane bending modes. Young's modulus is the one of the most fundamental mechanical properties of materials to establish a relation between the tensile stress, energy, strain, etc.

The bending stiffness or bending rigidity (κ) is one of the important physical properties of membranes and layered structures, which determines the elastic properties and mechanical stability (Nelson et al. 2004). In layered materials, acoustic phonon mode is the lowest out-of-plane mode (ZA) and is used to determined the bending rigidity from the coefficient of the quadratic dispersion relation. The ZA mode in 2D h-BN is a bending mode and in the long wavelength range, the two atoms in the unit cell move in the out-of-plane Z direction, which results the bending of the surface leads to the formation of ripples in the h-BN sheet. We have noticed that the bending rigidity of h-BN has a strong dependency on temperature and it increases with temperature (Thomas et al. 2015).

In general, tensile stiffness is a structural property of a material which is greatly influenced by its geometry and composition whereas the Young's modulus is a material property. In h-BN, the strong chemical bonding leads to a high tensile stiffness. Experimentally, the tensile stiffness D can be calculated and is related to the Young's modulus Y and the shell thickness t_s, and can be expressed as, $D = Yt_s$. The bending rigidity or bending stiffness can be extracted from the mechanical tests or vibrational analysis using the equation $\kappa = Yt_s^3/12(1-\nu^2)$. Here, ν is the in-plane Poisson's ratio, then the shell thickness t_s can be written as:

$$t_s = \left(\frac{\kappa[12(1-\nu^2)]}{Y} \right)^{1/3} \tag{4.9}$$

Slotman et al., reported that the zero Kelvin bending modulus of a finite h-BN sheet is 0.54 eV (Slotman and Fasolino 2012). Using the equation $\kappa = Yt_s^3/12(1-\nu^2)$, we calculated the thin shell thickness (t_s) value of h-BN as 1.1304 Å, which is comparable to the earlier reported value of 0.94 Å, using density functional theory studies (Gao and Xu 2015). In general, the thin shell thickness is always much smaller than that of the inter-layer spacing d=3.4 Å of 2D h-BN (Hod 2012). We have calculated the zero temperature bending modulus of 2D h-BN with different system size. The obtained zero Kelvin bending rigidity of a system with infinite boundary is 0.62 eV and we already calculated the room temperature bending rigidity of h-BN is 1.6 eV (Thomas et al. 2015), obtained using the approach continuum theory of membranes. It is seen that κ, Y and ν monotonically increase with system size at zero Kelvin.

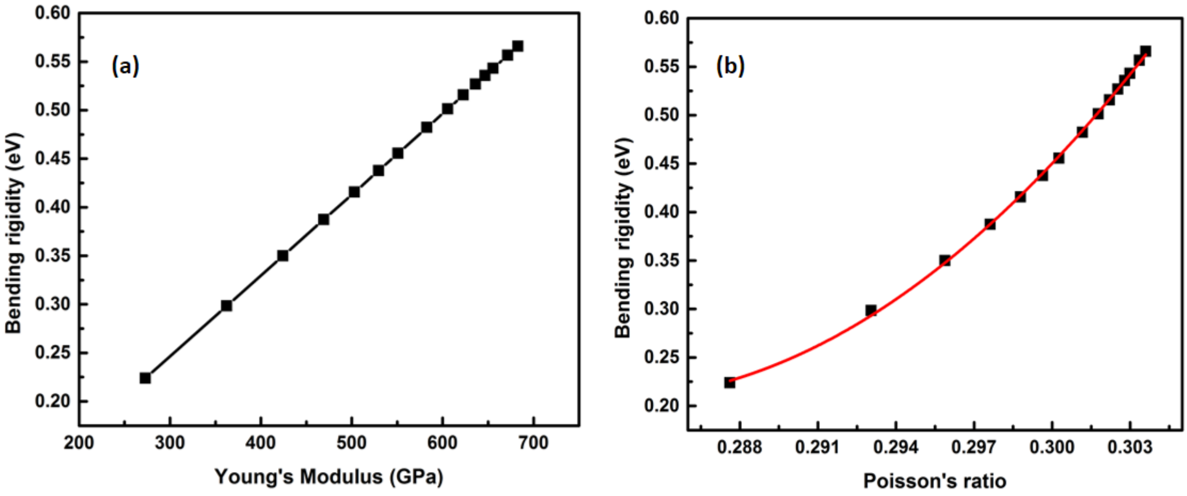

Figure 4.8: As the Young's modulus and Poisson's ratio increases, the bending rigidity also increases to a saturated value of 0.56 eV.

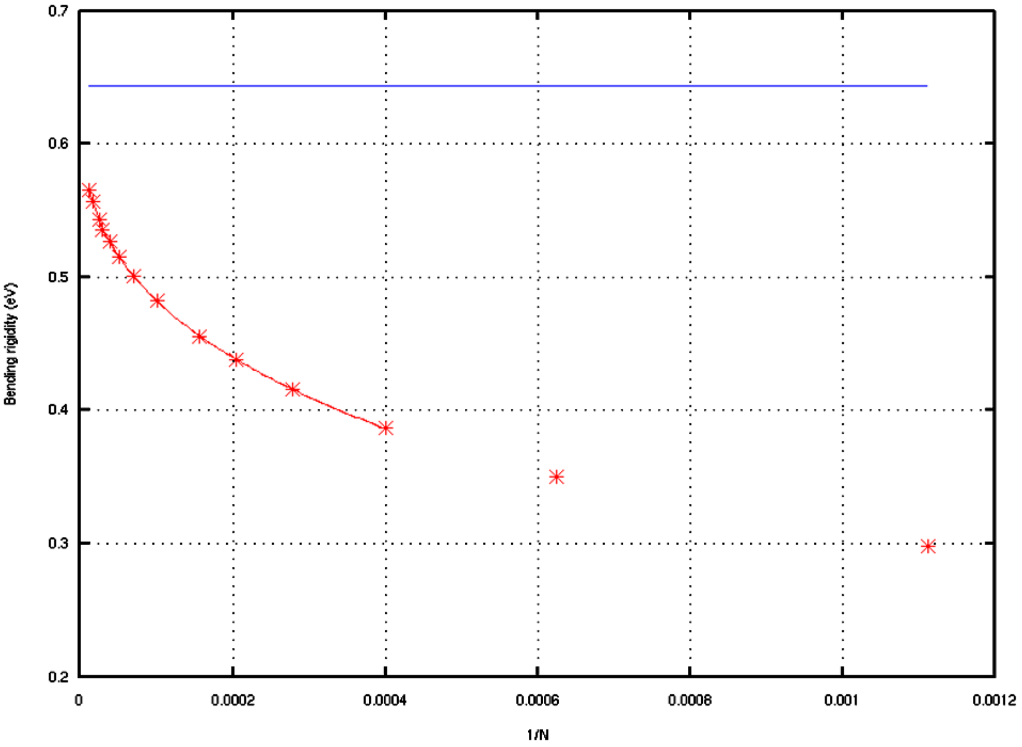

Figure 4.9: The calculated bending rigidity and its scaling with inverse system size. The blue line represents the value of the respective bending rigidity extrapolated to infinite system size limit.

However, the increase of ν with system size is less significant compared to that of κ and Y. When the system size changes from 400 to 360000, ν increases monotonically from ~ 0.288 to ~ 0.304. This shows that the lateral deformation consequent upon deformation in any direction is slightly less in small systems as compared to big systems. For the system size variation mentioned above, $1/(1-\nu^2)$ increases from 1.09 to 1.10, whereas κ and Y increase by more than 250%. Assuming a fixed plate thickness t_s, we thus see that κ is proportional to Y for all practical purposes. We see that Y treated as a function of ν can be fitted to an accuracy of 1% with the expression $Y(\nu) = Y_0 + Y_1\nu + Y_2\nu^2$. Since $\nu^2 << 1$ for the entire range of system sizes that is studied here, the relation $\kappa(\nu) = Y(\nu)t_s^3/12(1-\nu^2)$ can be rewritten as $\kappa = \left(t_s^3/12\right)\left(Y_0 + Y_1\nu + (Y_0 + Y_2)\nu^2\right)$ to the order in ν^2. The graph of κ vs ν in figure 4.8 (b) shows exactly this dependence.

In this thesis work, we reported that a finite sheet with large system size, the material possess a constant value of bending rigidity. As the Young's modulus and

Poisson's ratio increases, the bending rigidity also increases to a saturated value of 0.56 eV as shown in figure 4.8 (a) and (b). The obtained value of bending rigidity using the method of plate theory is consistent with the value obtained using continuum theory of membranes, which validate the effort of present study. The bending rigidity of h-BN with different system size is calculated using the equation obtained from Foppl-von Karman approach, and its scaling behaviour with inverse system size is depicted in figure 4.9.

4.4 Conclusions

The observed elastic moduli of a finite h-BN sheet are different for the armchair and zigzag directions, thereby demonstrating its anisotropic linear elastic behavior. The values of the independent elastic constants C_{11} and C_{12} are such that Born's criterion for mechanical stability of h-BN is satisfied. It has been noticed that there is a strong system size dependency for the in-plane stiffness and Poisson's ratio for finite sheets. These properties show a power law convergence to the bulk values when the system size tends to infinity. Due to the the strong in-plane sp^2 bonds and the small mass of boron and nitrogen atoms, 2D h-BN possess high group velocities. As the system size increases, the Young's modulus also increases, which leads to an increase in the longitudinal and shear wave velocities. This information could highly useful for the design of future graphene based nano-devices. The variation of bending rigidity with system size is also investigated.

Chapter 5

Effect of Ripples on the Finite Temperature Elastic Properties using Strain-fluctuation Method

---

This chapter investigates the temperature dependent elastic constants of h-BN between 100 and 1000K for the first time using the strain fluctuation method. The Young's, bulk and shear moduli and Poisson's ratio are calculated from the computed values of elastic constants and are found to decrease with increase of temperature. The thermal rippling in h-BN leads to strong anharmonic behavior that causes large deviation from the isotropic elasticity. A detailed study shows that the strong thermal rippling in large systems is also responsible for the softening of elastic constants in h-BN. The variation of longitudinal and shear velocities with temperature is also calculated from the computed values of elastic constants and elastic moduli. The obtained results provide an indication of the general trend of the variation of elastic constants with temperature in the anharmonic regime.

5.1 Introduction

Knowledge of temperature dependent properties are essential for sophisticated device fabrication. Since classical MD can incorporate the full anharmonicity of the interatomic potential and can handle millions of atoms, it will be a proper and efficient tool to probe the anharmonic as well as temperature dependent mechanical and elastic properties of materials.

Even though graphene/h-BN based micro devices have the potential for improved performance, the heat removal is a crucial issue in these devices (Anees et al. 2016). Since hexagonal boron nitride is stable in air and BN coatings can withstand ultra high temperatures, it can be used as a part of high temperature oxidation resistant coatings and also as a protective material against high temperature oxidation damage in aerospace applications and micro-electromechanical systems. The space-based technologies would experience harsh environments and large temperature fluctuations which will lead to changes in material properties such as thermal expansion, thermal and electrical conductivity, elastic and mechanical properties, etc. Thus, the effect of temperature on various physical properties of 2D materials need to be elucidated.

To the best of our knowledge, the temperature dependent elastic constants of a free standing monolayer hexagonal boron nitride have not been studied so far using the framework of classical molecular dynamics. In this thesis work, an attempt has also been made to calculate the temperature dependent elastic constants of h-BN using the strain-fluctuation method derived from the fluctuation-dissipation theorem (Landau and Lifshitz 1958) by varying the size and shape of the simulation cell and is described in the following section. We extracted the Young's modulus and sound velocities from the derived elastic constants. The obtained results of the mechanical and elastic properties of 2D h-BN sheet are expected to provide better ideas for the development of potentially and technologically important integrated devices as well as the manipulation of h-BN for engineering applications.

5.2 Methodology

The effect of temperature on various material properties can be effectively evaluated using Molecular dynamics (MD) simulation due to the explicit inclusion of temperature (Gao et al. 2006). In general, there are different methods to calculate the elastic constants of materials which include direct method (Lovett 1999), the strain-fluctuation method (Ray 1988, Parrinello and Rahman 1982) and the stress-fluctuation method (Ray 1982, Ray and Rahman 1984, 1985, Ray et al. 1985, Lutsko 1989). The stress and strain fluctuation methods use the ensemble averages of the fluctuations in either strain or stress. The C_{ijkl} represents the fourth-rank elastic stiffness tensor and ε_{kl} is the kl element of the second-rank strain tensor. The fourth rank tensor C_{ijkl} is known as the elasticity tensor and its components are called the elastic moduli or elastic constants. Generally, the relation between stress and strain is given by the Hooke's law and is represented as,

$$\sigma_{ij} = C_{ijkl}\varepsilon_{kl} \tag{5.1}$$

In order to convert from tensor notation to matrix notation, a pair of indices is changed to a single number using the following rules: 11 → 1, 22 → 2, 33 → 3, 23 and 32 → 4, 13 and 31 → 5, and 12 and 21 → 6. Furthermore, in matrix notation the indices 1, 2, and 3 map to x , y and z respectively. Crystals with 2D hexagonal symmetry, such as graphene and h-BN, have only three independent elastic constants which are C_{11}, C_{12} and C_{66}, in the Voigt notation.

In the case of elastic properties, if $f(t)$ is a mechanical force (or stress) acting on a solid body that invokes a deformation (or strain) $x(t)$, then the proportionality factor α between these two quantities is the familiar elastic compliance. In the limit of high temperatures with classical case, $kT >> h\omega/2\pi$ and the fluctuation-dissipation theorem can be simplified to $\langle x^2 \rangle = kT\alpha(0)$, where x represents the mean square of the fluctuations of a general physical quantity x. It has been reported that the stress-fluctuation method converges more rapidly than the strain-fluctuation method and it can also provide insight into the molecular origin of a given mechanical response (Yoshimoto et al. 2005). However, the implementation of stress fluctuation method is challenging for a complex, many-body potential, such as the REBO and Tersoff potential.

Using energy method, we noticed that the tuned Tersoff empirical potential is able to quantitatively reproduce the zero Kelvin elastic constants of h-BN within the framework of classical MD simulation (Thomas et al. 2016). The present thesis work also aimed at elucidating the effect of ripples on the temperature dependent elastic constants of 2D h-BN using the strain fluctuation method. We adopt this method for the non-zero temperature elastic constants calculations and the basic equation employed in the strain-fluctuation method (Ray 1988, Parrinello and Rahman 1982) can be directly derived from the equation $\left\langle x^2 \right\rangle = kT\alpha(0)$ as (Landau and Lifshitz 1958):

$$\left\langle \varepsilon_{ij}\varepsilon_{kl} \right\rangle - \left\langle \varepsilon_{ij} \right\rangle \left\langle \varepsilon_{kl} \right\rangle = \frac{k_B T}{A_0 d_0} S_{ijkl}, \tag{5.2}$$

where k_B is the Boltzmann constant, A_0 is the equilibrium area of the 2D system, d_0 is the van der Waals's distance (which represents the effective thickness of the layer), S_{ijkl} is the elastic compliance tensor, which is the inverse of the elastic stiffness tensor, and $\langle\ \rangle$ represents an ensemble average in a constant particle number, pressure and temperature (NPT) ensemble. It is now generally recognized that equation (5.2) furnishes a satisfactory way of calculating temperature dependent elastic constants using the strain fluctuations in molecular dynamics simulations (Fay and Ray 1992). It has been found that though equation (5.2) is used in Ref. (Parrinello and Rahman 1982), the lack of satisfactory convergence at low temperatures restricted them to incorporate the molecular dynamics simulations results. Later studies also reported essentially the same conclusion (Sprik et al. 1984, Ray 1988). However, this method is still used (John and Klug 1991) for the calculation of the adiabatic elastic constants at temperatures above 100 K, in which, it is possible to obtain results with acceptable accuracy as long as the simulation is run for a sufficiently long time. This method is more acceptable due to the simplicity of the implementation of equation (5.2) compared to the corresponding formulas in the EhN (E is the energy) and ThN (T is the temperature) ensembles (Ray and Rahman 1984, Ray 1988), where h is a tensor constructed from the three vectors forming a parallelepiped, which is the periodically repeating molecular dynamics cell. The statistical ensemble (EhN) is also related to the ($H\sigma N$) or (HtN) ensembles; where, H is the enthalpy, t is a tensor related to σ, the usual stress tensor, and is called tensor of thermodynamic tension.

One of the advantage of using equation 5.2 is that it involves only the fluctuations in the h matrix, which is derived from the three angles and sides of the simulation box and furnishes a method of calculating the elastic constants which does not depend explicitly on the potential (Ray 1988). We have performed MD calculations with a time-dependent metric tensor which allows the volume and the shape of the MD cell to vary with time. The size and shape of the simulation cell of a system of N particles in a periodically repeating MD cell which changes with time in shape and volume is controlled using the method developed by Parrinello and Rahman (Parrinello and Rahman 1980). In these MD simulations, the size and angles of the simulation cell is a dynamic variable. Let the edges of the MD cell be a, b, and c (in a space-fixed coordinate system), and are time dependent. Inorder to perform the simulations we have considered a parallelepiped with triclinic geometry and is represented by three time-dependent vectors $\vec{a}$, $\vec{b}$, $\vec{c}$ and angles α, β, γ. Here, $c_1 = \mathbf{c}cos\beta$, $c_2 = \mathbf{c}[cos\alpha - cos\beta cos\gamma]/sin\gamma$ and $c_3 = \sqrt{\mathbf{c}^2 - c_1^2 - c_2^2}$. The symmetry-equivalent elastic constants are obtained from the fluctuations in the simulation box lengths and angle. Then the h matrix of all parameters at equilibrium is:

$$\mathbf{h} = \begin{pmatrix} \mathbf{a} & \mathbf{b}cos\gamma & \mathbf{c}cos\beta \\ 0 & \mathbf{b}sin\gamma & \frac{\mathbf{c}[cos\alpha - cos\beta cos\gamma]}{sin\gamma} \\ 0 & 0 & \sqrt{\mathbf{c}^2 - c_1^2 - c_2^2} \end{pmatrix} \tag{5.3}$$

Then the symmetry-equivalent elastic constants are obtained from the fluctuations in the simulation box lengths and angle. Then the instantaneous strain tensor ε and the $\mathbf{h}$ matrix is related as (Ray 1988),

$$\varepsilon_{ij} = \frac{1}{2}\left[\left((\mathbf{h}_0^{-1})^T\, \mathbf{h}^T \mathbf{h}\, \mathbf{h}_0^{-1}\right)_{ij} - \delta_{ij}\right], \tag{5.4}$$

where $\mathbf{h}_0$ corresponds to the reference system and is initially averaged over all the frames and $\mathbf{h}$ matrix corresponds to the instantaneous values of the edges of the simulation box with respect to the reference system, and the superscript T denotes the transpose of a matrix.

In order to perform molecular dynamics simulations, periodic boundary conditions are employed in the x and y directions and a non-periodic and shrink-wrapped with a minimum value boundary condition is employed along the z direction. We used a simulation cell of size 100×100×1 (40000 atoms), which is capable of incorporating all long-wavelength rippling effects. We also used simulation cells of various sizes (30×30×1, 40×40×1, 50×50×1, 60×60×1, 70×70×1, 100×100×1, 125×125×1, 150×150×1, 175×175×1, 200×200×1) to incorporate the effect of long wavelength ripples and also to study the system size effect. A vacuum separation of 30 Å is provided along the Z-direction to avoid the un-physical interactions between the periodic images of the 2D h-BN layers. The conjugate-gradient algorithm is used for the initial geometry relaxation and also to avoid the residual stresses. The system has been equilibrated by coupling it to a Nosé-Hoover thermostat.

We have performed the strain-fluctuation method at constant temperature and under ambient pressure (NPT ensemble) for 0.5 nanosecond (ns), in which the thermodynamic tension and external hydrostatic pressure are set to zero. The size and shape of the simulation cell is controlled using a Lagrangian which allows the variation of the shape and size of the periodically repeating molecular-dynamics cell (Parrinello and Rahman 1982). In order to integrate the positions and velocities, a standard Velocity-Verlet time stepping algorithm has been used. We have used an integration time step of 1.0 femtosecond (fs) for solving the equations of motion.

5.3 Results and discussions

In the case of 2D membranes, most commonly used harmonic approximation neglects the interaction between the bending and stretching modes and these two modes are decoupled. But, it is a well known fact that, at sufficiently long scales, the flat phase of 2D h-BN is much larger than the interatomic separation and is well defined by the combination of bending and stretching modes (Nelson et al. 2004). This means that the existence of a 2D membrane is due to the *anharmonic* coupling between the bending and stretching modes. This chapter intents to investigate the temperature dependent elastic constants and elastic (Young's) moduli of 2D h-BN. In order to validate the anharmonic behaviour of hexagonal boron nitride, the variation of lattice parameter (a_{int}) and linear thermal expansion coefficient (LTEC) as a function of temperature has also been studied.

5.3.1 Thermal rippling behavior of h-BN

In harmonic approximation, one neglects the interaction between the in-plane stretching ($u(r)$) and out-of-plane bending ($h(r)$) contributions of the h-BN membrane, and these bending and stretching modes are decoupled. One can calculate the correlation function for the out-of-plane (flexural) displacements $h(r)$ (different from **h** considered earlier) which, in Fourier space, is denoted as $G_0^{harm}(\mathbf{q}) = \langle|h(\mathbf{q})|^2\rangle_{u=0} = \frac{k_B T}{\kappa q^4}$, where k_B is the Boltzman constant, T is the temperature, and the suffix $u = 0$ in the average denotes the absence of any external strain and the subscript 0 indicates that we neglect anharmonic couplings between in-plane and out-of-plane modes. The prediction from harmonic theory states that, divergence in the mean-square amplitude of the out-of-plane displacements will take place and is written as, $\langle h^2\rangle_{harm} \propto L^2$ or $\langle h^2\rangle_{harm} = CL^2$, where L is the size of the sample, C is a temperature dependent constant and $\langle h^2\rangle = \langle|h(q)|^2\rangle$. This is the well known result that harmonic theory of membranes predict the existence of a crumpled membrane rather than a flat one. In particular, the harmonic theory predicts that a 2D membrane or crystal will not be stable. This contradiction is solved by including the anharmonic coupling between bending and stretching modes in the calculation (López-Polín et al. 2015).

In the large wavelength limit, i.e., for small q values, the height fluctuations are suppressed by the anharmonic coupling between bending and stretching modes giving rise to a renormalized q-dependent power law scaling behavior and is $\langle h^2 \rangle_{anh} = C' L^{2-\eta}$, where C' is a constant and is not equal to C (Costamagna et al. 2012) (More details given in appendix C). We observed that the height of the ripples formed in the sheet due to thermal fluctuations are proportional to the applied temperature (Thomas et al. 2015) and also noticed that the height fluctuations vary with increase in the system size and temperature.

The large reduction of elastic constants at high temperature is due to the increase of thermal fluctuation, which leads to the enhancement of the entropic contribution. In addition, as temperature increases, the location of the maximum slope moves toward a higher strain because a larger strain is needed to flatten the enlarged ripples at higher temperature (Lee 2015). As the temperature and system size increases, mean square out-of-plane displacement amplitude also increases. We have considered the membrane theory for h-BN and estimated the variation in mean square out-of-plane displacement amplitude ($\langle h^2 \rangle$) with temperature and system size ($L = \sqrt{L_x L_y}$) at 300 K (Thomas et al. 2015). The value of universal scaling exponent η at room temperature is obtained as 0.52. In this chapter, we investigate qualitatively to which extent membrane theory can be applied to the description of finite temperature elastic constants of h-BN from thermally excited ripples.

In the harmonic regime (short wavelengths), the Young's modulus is not affected by the interactions between bending and stretching modes, and it is well approximated by $E_{2D}^{har}(q) \approx E_{2D}^{0}$. But, if we consider the anharmonic region in the h-BN spectrum, all the physical quantities such as linear thermal expansion coefficient, elastic constants and specific heat show a scale dependence. It has been reported that the Young's modulus is a scale dependent parameter and one can define an effective Young modulus of a 2D h-BN (considering anharmonicities) as $E_{2D}^{anh}(\mathbf{q}) = \frac{E_{2D}^{0}}{1+E_{2D}^{0}b(\mathbf{q})}$, where $b(\mathbf{q})$ can be obtained by using a Feynman-diagram technique by coupling the lowest order in the in-plane displacements $u(r)$ and the out-of-plane displacements $h(r)$ of h-BN membrane (Roldán et al. 2011, López-Polín et al. 2015). In the anharmonic regime (long wavelengths), the effective elastic moduli become $E_{2D}^{anh}(q) \approx \frac{1}{b(\mathbf{q})}$ (Roldán et al. 2011). Here, the Young modulus is highly dependent on the wave-vector k which follows a power law behaviour $E_{2D} \sim q^{2-2\eta}$.

When the ripple amplitude increases, it effectively softens the elastic moduli of the material due to the anharmonic coupling between the bending and stretching modes. The inverse system size $(1/N)$ dependence of elastic constants C_{11} and C_{12} at 300 K is shown in figure 5.1 (a) and (b) respectively. Here, we fitted the values of C_{11} and C_{12} in each system size using a polynomial function, where N is the number of atoms in the simulation cell. Variation of Young's modulus with inverse system size at 300 K is shown in 5.1 (c). As the system size become higher, the value of Young's modulus decreases considerably with the variation of elastic constants due to the thermally excited ripples.

From our analysis of the zero Kelvin elastic constants of h-BN using molecular statics, we found that the elastic constants and Young's modulus increase with system size (Thomas et al. 2016). It has been noticed that the influence of temperature shows thermal rippling behaviour which effectively reduces the elastic constants, and such reduction is completely absent in the zero Kelvin calculations.

5.3.2 Temperature dependence of lattice parameter and thermal expansion coefficient

Molecular dynamics simulations are done for a 2D h-BN sheet containing 40000 atoms, and the dimensions of the simulation boxes are L_x = 250.00Å, L_y = 433.0127 Å and L_z = 30 Å. The internal lattice parameter (a_{int}) of h-BN is associated with the average sp^2 bond length, which indicates the actual size of the system.

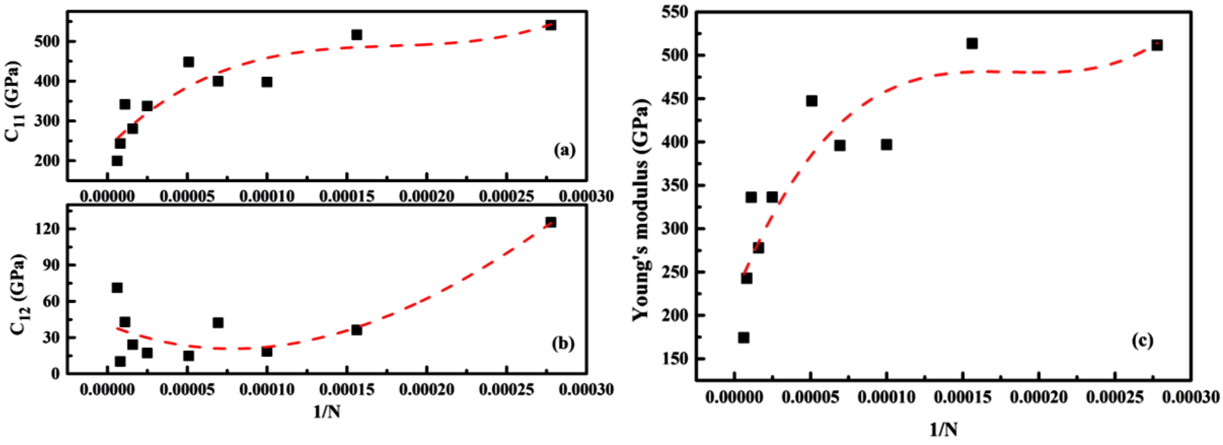

Figure 5.1: Dependence of the elastic constants C_{11} and C_{12} on the inverse system size ($1/N$) at 300 K is shown in (a) and (b) respectively. Here, we fitted the values of C_{11} and C_{12} in each system size using a polynomial function, where N is the number of atoms in the simulation cell. Variation of Young's modulus with inverse system size at 300 K is shown in (c). As the system size become higher, the value of Young's modulus decrease consistently with the variation of elastic constants due to the thermally excited ripples.

The internal lattice parameter shows no obvious size dependence and changes linearly with temperature. Mathematically it can be expressed as, $a_{int} = \sqrt{3}R_{xy}$, where R_{xy} is the average bond length. Figure 5.2 (a) shows that the internal lattice parameter decreases with an increase in temperature and its magnitude reduces to 1.32% of the equilibrium value at 1000 K and is consistent with the previous predictions (Anees et al. 2016). The linear thermal expansion coefficient (LTEC) is computed by the direct numerical differentiation of the internal lattice parameter and is shown in figure 5.2 (b). It has been reported that the fluctuation amplitude follows a power-law scaling with respect to the linear dimension of the 2D h-BN due to anharmonic interactions between bending and stretching modes. Such thermal fluctuation or rippling is found to be responsible for the effectively negative in-plane thermal expansion of graphene at relatively low temperatures (Gao and Huang 2014).

In h-BN, at low temperatures negative in-plane thermal expansion and at high temperatures, a transition to positive thermal expansion is observed. The negative thermal expansion of h-BN is more prominent at low temperatures, and this is due to the large negative Grüneisen parameter of the out-of-plane bending mode

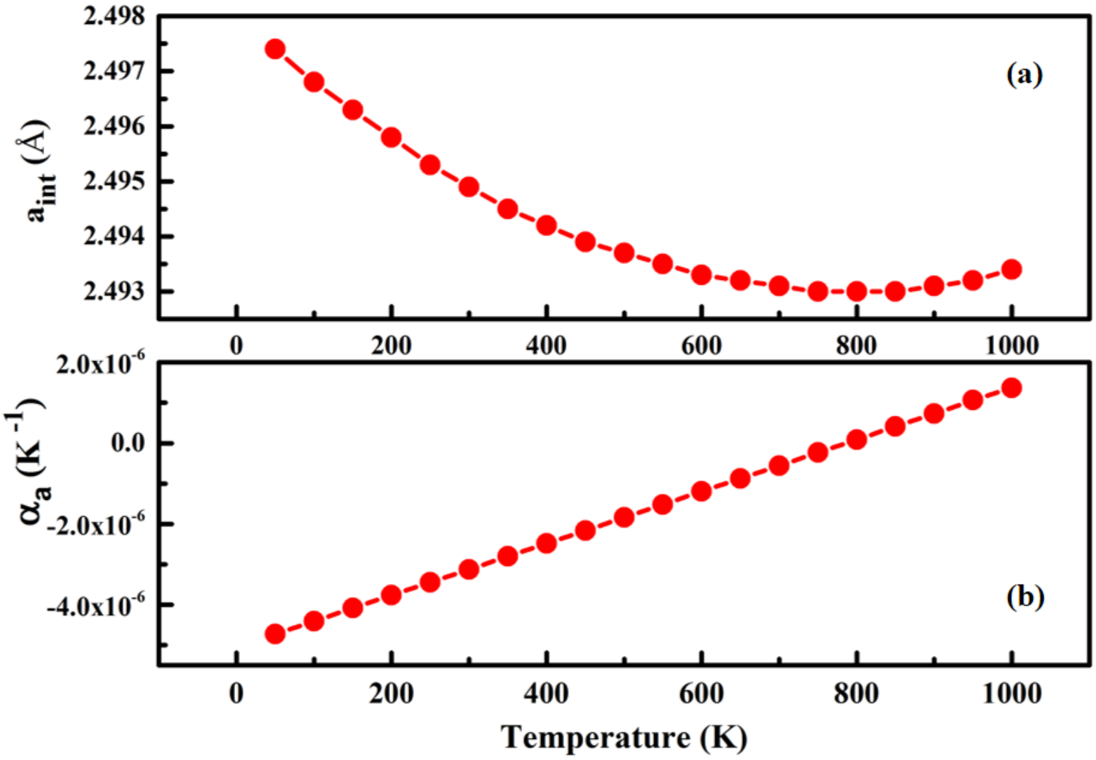

Figure 5.2: (a) Variation of in-plane lattice parameter (a_{int}) of h-BN with temperature; (b) The linear thermal expansion coefficient (LTEC) as a function of temperature.

(ZA) (Sevik 2014). The obtained room temperature LTEC is $-3\times10^{-6}K^{-1}$, which is comparable with the other MD studies (Anees et al. 2016) and quasi harmonic predictions (Sevik 2014). The deviations from harmonic behavior can be characterized by examining the radial distribution function as well (Zakharchenko et al. 2009).

5.3.3 Elastic constants

The strong anharmonic behavior of h-BN leads to unusual temperature dependence of the elastic moduli. The study of temperature dependence of elastic constants provide the intrinsic thermodynamic properties of materials at low and high temperatures. Mermin-Wagner theorem (Mermin 1968, Mermin and Wagner 1966) states that at any finite temperature, the spontaneously developed out-of-plane thermal fluctuations will eventually destroy the long-range translational symmetry of the 2D hexagonal lattice and a 2D crystal would not exist in the thermodynamic limit. However, we observed the existence of h-BN sheet at finite temperatures with significant thermal ripples. These out-of-plane intrinsic buckling (ripples) in h-BN is a highly nonlinear phenomenon that profoundly influences the elastic properties of h-BN. The ripples can effectively soften the elastic moduli, in the sense that stretching a crumpled h-BN sheet requires less force than stretching a flat one (Chen 2012). It is well known that elastic modulus of a crystalline solid is, in general temperature dependent and in particular, linear temperature dependence has been predicted under the harmonic approximation (Weiner 2002). However, we observed a nonlinear temperature dependence with significant anharmonic effect for the elastic modulus of h-BN sheet.

Gao et al., (Gao and Huang 2014) reported that the amplitude of thermal fluctuation depends on the membrane size. The observed elastic constants are significantly reduced with out-of-plane thermal fluctuation and the reduction in the elastic constants also depends on the size of h-BN membrane. In the case of small h-BN membrane, the elastic constants possess high values and the value become small for larger membranes and such reduction also increases with system size. Our MD simulations of h-BN predicted that the elastic modulus depends on the temperature and in-plane thermal expansion, and changes from low value to a high value as the temperature increases. In the present study, we tried to emphasize the intimate relationship between thermal rippling and thermoelasticity of h-BN within the anharmonic limit (Zakharchenko et al. 2009).

We also noticed that the elastic modulus of h-BN is size dependent, which is attributed to the in-plane contraction, meaning that lower modulus for larger h-BN sheet is due to more significant rippling. The effect of temperature can also lead to a variation in box lengths and angles of h-BN sheet. Figure 5.3 shows the variation in (a) simulation cell size and (b) angle γ of h-BN as a function of MD time step at different temperatures. When the simulation is carried out for a long time, the value of box lengths and angles stabilises to a constant level and it is clear from the analysis of these data that this method is slow to converge. A description of the second order elastic constants, elastic energy, etc. of 2D h-BN is detailed in section 4.3.1. Using equation (4.5) and (4.6), Young's modulus and Poisson's ration is calculated. The corresponding Bulk modulus (K) and shear modulus (G) are related to the Young's modulus and Poisson's ratio using the equations:

$$K = \frac{Y}{3(1-2\nu)} \tag{5.5}$$

$$G = \frac{Y}{2(1+\nu)} \tag{5.6}$$

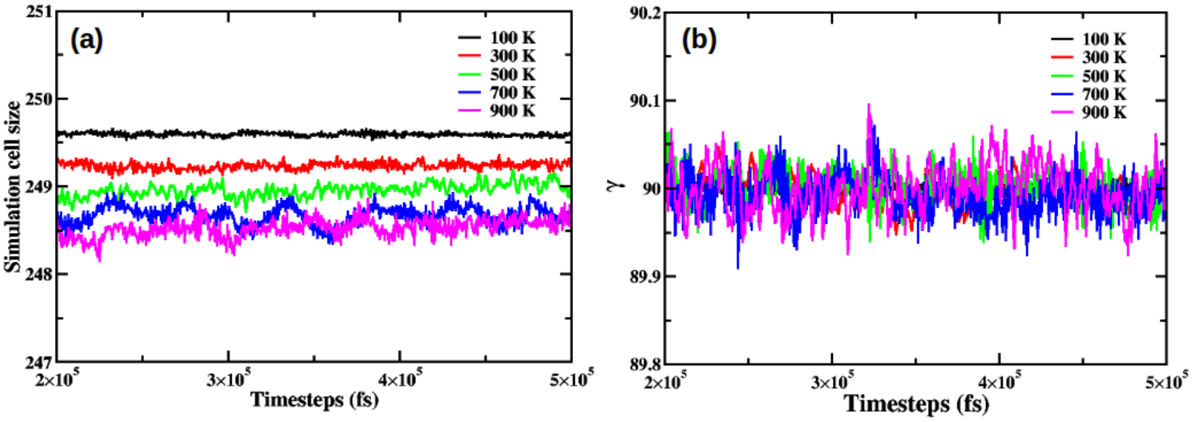

Figure 5.3: Variation in (a) simulation cell size and (b) angle gamma of h-BN as a function of MD timestep at different temperatures.

We have extracted the box lengths and angle from the MD simulation after performing the strain-fluctuation method in which the thermodynamic tension and the external hydrostatic pressure are set to zero. In order to obtain the initial $\mathbf{h}_0$ matrix, the size and shape of the simulation cell of a system of N particles in a periodically repeating MD cell is considered and is initially averaged over all the frames. The instantaneous values of the **h** matrix are obtained by averaging the length and angles of the simulation box over the course of simulation. These instantaneous values of the **h** matrix are used for the calculation of the instantaneous strain tensor using the matrix shown in equation 5.3. By using these values of instantaneous strain, the elastic constants can be calculated using the equation (5.2) and (5.4). Using the values of instantaneous strain, the independent elastic constants C_{11} and C_{12} of h-BN sheet at various temperatures is calculated using the strain-fluctuation method and is shown in figure 5.4 (a) and (b) respectively. The Young's modulus and Poisson's ratio are calculated using equations (4.3) and (4.4) and the careful polynomial fitting shows a decreasing behaviour of these quantities with an increase of temperature and are shown in figure 5.5 (a) and (b) respectively. The computed elastic constants satisfy Born mechanical stability criterion in the studied temperature range.

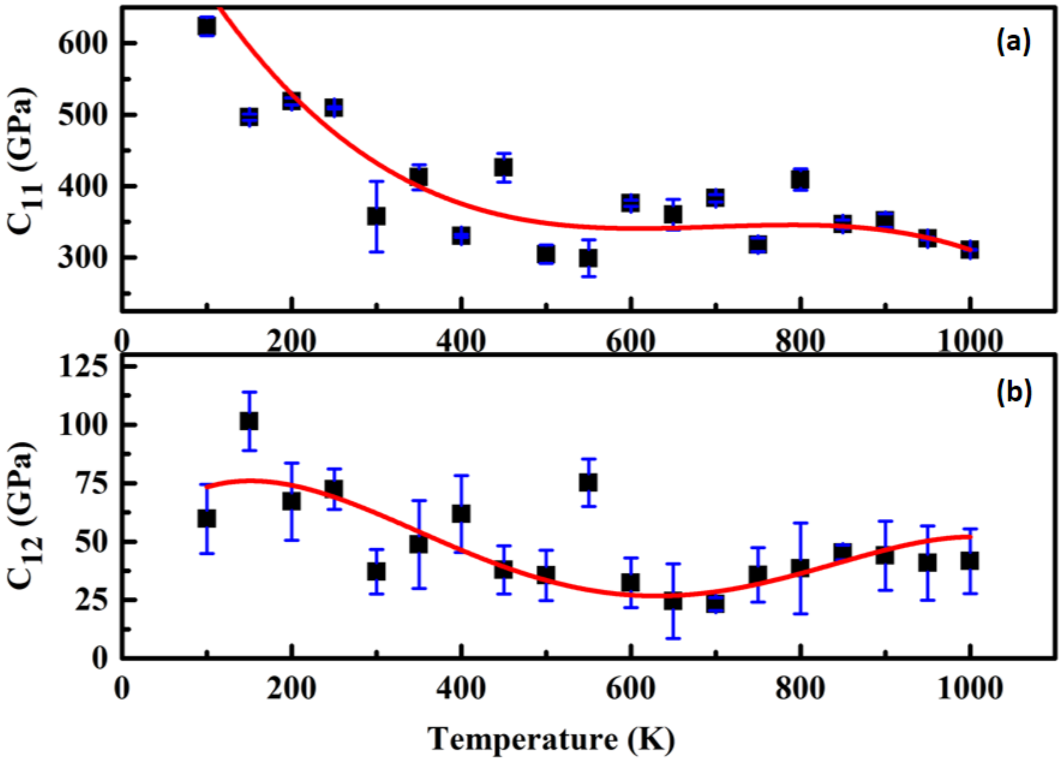

Figure 5.4: Temperature dependent elastic constants of h-BN calculated using strain-fluctuation method. Independent elastic constants (a) C_{11} and (b) C_{12} are calculated using the values of instantaneous strain.

It has already been reported the slow convergence of strain-fluctuation method for the calculation of elastic constants (Gusev et al. 1996). In order to obtain results with acceptable accuracy, the simulation are run for a sufficiently long time. Gao et al., reported the difficulties of strain-fluctuation method to obtain a reliable data of elastic constants at temperatures below 100 K (Gao et al. 2006) and they claim that the stress-fluctuation method is a much more effective way to calculate the elastic constants than the strain-fluctuation method because it converges more quickly and all the components of the stress tensor are expected to be obtained from a single simulation. However, the stress-fluctuation method is more difficult to implement because it requires the analytic second derivative of the potential energy function with respect to strain. But in the case of potential energy functions with complicated functional forms, this term can be difficult to obtain.

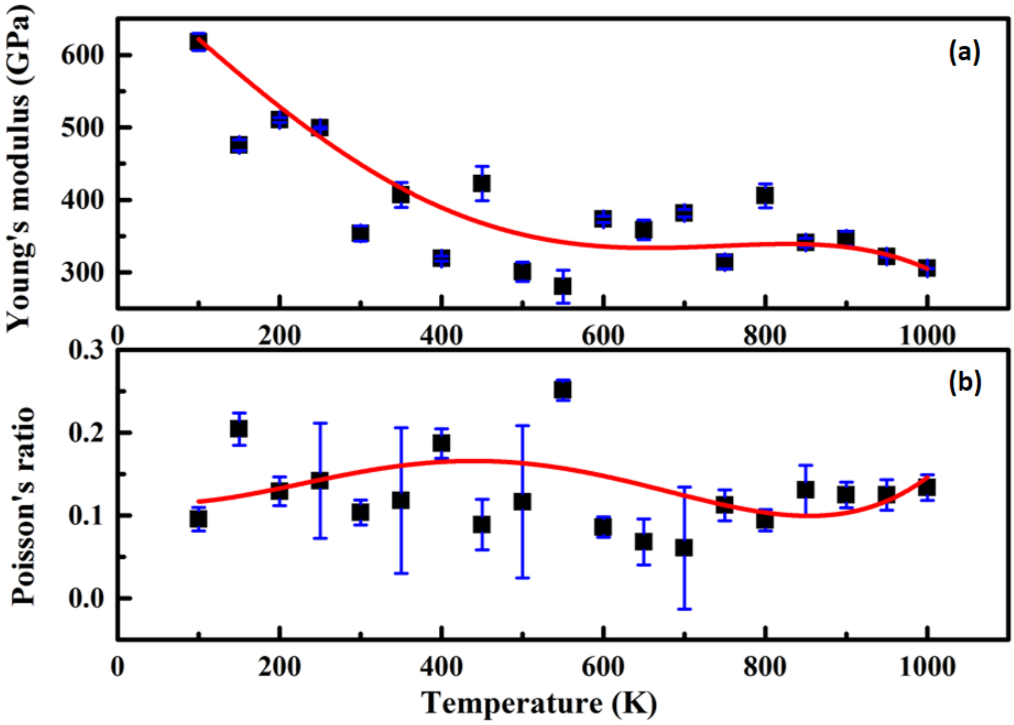

Figure 5.5: Temperature dependent (a) Young's modulus and (b) Poisson's ratio are calculated from the computed values of elastic constants.

In addition, we present results for bulk and shear moduli in figure 5.6 (a) and (b), the magnitude of which can be easily calculated using Young's modulus and Poisson's ratio, employing formulas (5.5) and (5.6) respectively. Both bulk and shear moduli retains the behavior of decreasing values with an increase of temperature. It has been reported that the shear deformations play an important role in the winkling and rippling nature of graphene and we could expect the same in h-BN as well due to the structural similarity and the formation of out-of-plane fluctuations in graphene and h-BN (Liu et al. 2012, Katsnelson and Geim 2008).

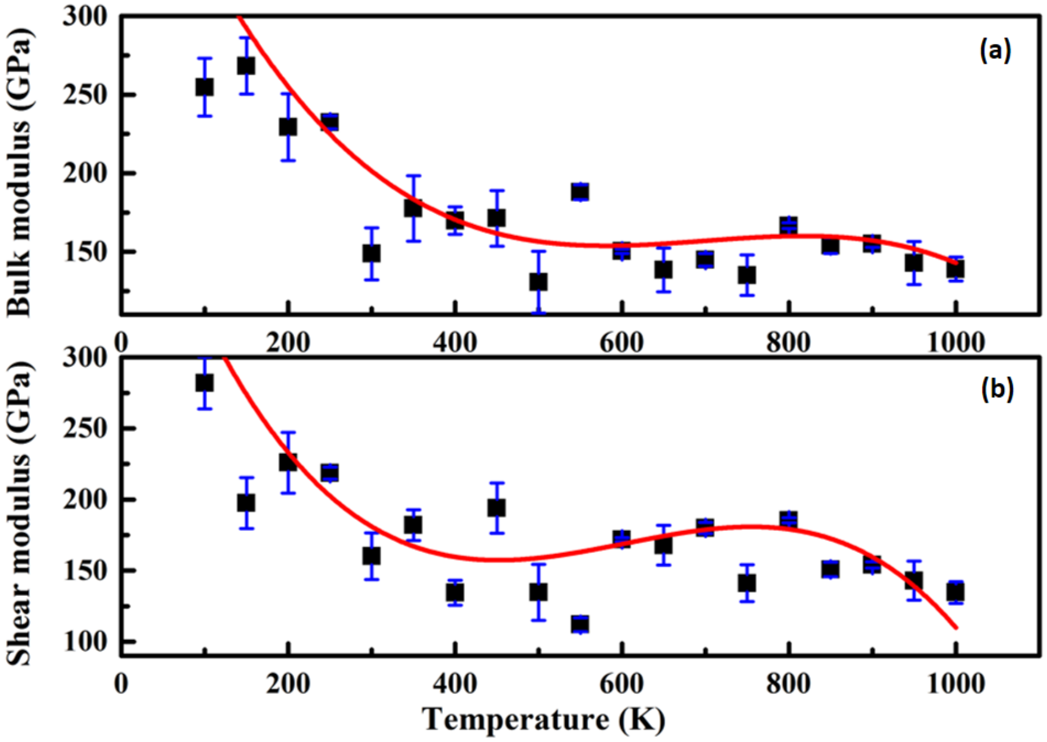

Figure 5.6: Variation of computed (a) bulk and (b) shear modulus using strain-fluctuation method for h-BN as a function of temperature.

While extrapolating and comparing to zero Kelvin elastic constants, it is clear that the obtained values well agree with our calculated zero Kelvin elastic constants C_{11} = 823 GPa and C_{12} = 245 GPa (Thomas et al. 2016). The obtained zero Kelvin Young's modulus, Poisson's ratio, bulk and shear moduli are in good agreement with the earlier theoretical studies (Milowska et al. 2013). The calculated value of C_{11} decreases as a function of temperature more markedly in comparison to C_{12}. It should be noted, however, that there has been no experimental and theoretical work that has been reported on the study of finite temperature elastic constants of h-BN, which limits the direct comparison of the obtained results. We believe that the obtained results quantitatively agree with the general behaviour. The considerable decrease of the elastic constants and Young's modulus with increasing temperature is the direct consequence of the effect of ripples, low thermal expansion and negative Grüneisen parameter of the out-of-plane bending mode (ZA) (Sevik 2014).

5.3.4 Sound velocities

The h-BN and most of the 2D materials show strong anisotropy and in an anisotropic medium there are only certain directions along which elastic waves can propagate in pure longitudinal and transverse modes (Yang et al. 2017). The anisotropy of mechanical properties can be investigated from the independent elastic constants by evaluating the anisotropic factors or elastic constants. The sound waves responsible for the compressional (longitudinal) deformations (p-wave) are called longitudinal waves (p-waves) in which the vibration of particles is parallel to the direction of propagation. The waves generated due to the speed of shear modes are called shear waves (s-wave) in which the polarizations are normal to the direction of propagation. Using the in-plane elastic modulus (Young's modulus) Y, Poisson's ratio ν, two dimensional mass density ρ_m and the in-plane elastic constants C_{11} and C_{12} one can calculate the longitudinal and shear wave velocities using the equations (4.7) and (4.8)(Kinsler et al. 1999, Thomas et al. 2016).

Using the in-plane lattice parameter a and the atomic mass of boron nitride m_{BN}, the two dimensional mass density can be defined as $\rho_{2D} = 4m_{BN}/(\sqrt{(}3)a^2)$. The observed mass density of h-BN is 15.180×10^{-7} kg/m^2, which is twice the mass density of graphene. We observed that the longitudinal wave velocity (V$_p$) is more as compared to shear wave velocity (V$_s$) which is consistent with earlier *ab-initio* studies (Peng et al. 2012b). Using the equations (4.7) and (4.8), we calculated the temperature dependent longitudinal and shear wave velocities of h-BN.

The observed room temperature longitudinal wave velocity is 8.9486 km/s and that of shear wave velocity is 2.640 km/s respectively. The variation of sound wave velocities with temperature is shown in figure 5.7 (a) and (b) respectively. As the temperature increases, the Young's modulus of the sample decreases, which leads to the decrease of longitudinal and shear wave velocities as shown in figure. Since sophisticated experimental facilities are available for the investigation of sound velocities, we can easily calculate the finite temperature elastic constants from the calculated sound velocities. We believe that our calculations on the temperature dependent elastic constants would throw more light on the basic functional mechanism of acoustic wave guides and surface acoustic wave sensors (Peng et al. 2012b).

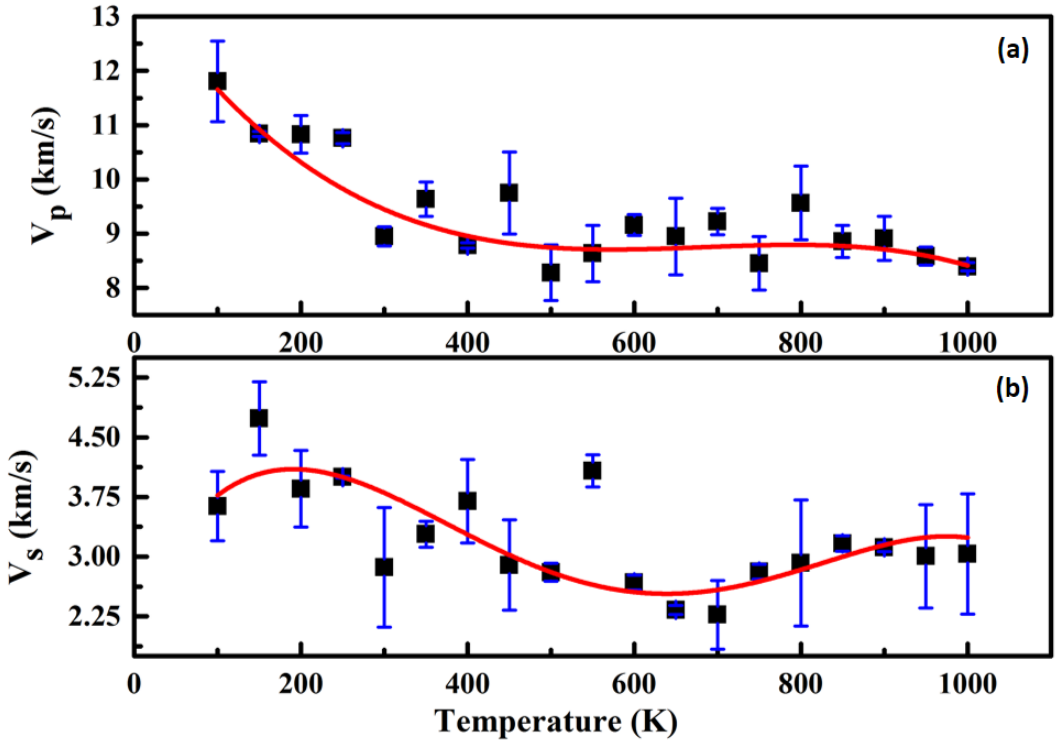

Figure 5.7: Variation of calculated (a) longitudinal and (b) shear wave velocities of h-BN using strain-fluctuation method with temperature.

5.4 Conclusions

The effect of ripples on the temperature dependent elastic constants of monolayer hexagonal boron nitride have been investigated for the first time using strain fluctuation method. The Young's, bulk and shear moduli, Poisson's ratio, sound velocities, etc. are calculated from the computed values of elastic constants and are found to decrease with increase of temperature. It has been observed that the out-of-plane intrinsic ripples responsible for strong anharmonic behavior of h-BN leads to large deviation from the isotropic elasticity. Because of the strong thermal rippling in large systems, the h-BN sheet may have a negative thermal expansion coefficient at relatively low temperatures, with a transition to positive thermal expansion at high temperatures and this also soften the elastic constants. This transition is a result of two competing effects: positive thermal expansion due to in-plane modes and negative expansion due to out-of-plane fluctuation. The calculations show that h-BN sheet satisfy Born's criterion for mechanical stability. As the system size become larger, the value of Young's modulus decrease consistently with the variation of elastic constants due to the thermally excited ripples. As the temperature increases, the Young's modulus of h-BN decreases, which leads to the decrease of longitudinal and shear wave velocities.

Chapter 6

Effect of temperature and defects on the mechanical properties

---

This chapter explains the effect of changing the cut-off distance in the empirical potential on the stress-strain relation and also the temperature dependent Young's modulus of pristine and defective hexagonal boron nitride. As the temperature increases, the computed Young's modulus shows a significant decrease along both the armchair and zigzag directions. The computed Young's modulus shows a trend in keeping with the structural anisotropy of h-BN. As the temperature increases, the computed stiffness decreases and the system with zigzag edge possesses a higher value of stiffness as compared to the armchair counterpart and this behaviour is consistent with the variation of Young's modulus. The defect analysis shows that presence of vacancy type defects leads to a higher Young's modulus, in the studied range with different percentage of defect concentration, in comparison with Stone-Wales defect.

6.1 Introduction

This chapter explains the temperature dependent tensile behavior of pristine and defective boron nitride nanosheets. Here, we have attempted to optimize the cut-off function of the used empirical interatomic potential for a better understanding of the mechanical properties using the framework of classical MD. To the best of our knowledge, no conclusive study has so far been reported on the analysis of temperature dependence on the tensile properties of pristine and defective free-standing h-BN using the tuned Tersoff potential. We have also investigated the influence of vacancy and Stone-Wales type defects on the Young's modulus of h-BN.

6.2 Methodology

Classical MD simulations have been performed with a finite rectangular h-BN sheet of approximate size 50×86 Å containing 1600 atoms. The MD simulations are carried out in NVT ensemble, with a Nose-Hoover thermostat for proper thermal equilibration of the system. All the simulations have been performed using a time step of 0.001 picoseconds. In order to eliminate the residual stress of the h-BN structure, a conjugate gradient minimization algorithm is used for the initial geometry relaxation. The direction along which force is applied to deform the h-BN sheet will be designated as x. Then periodic boundary condition will be applied along this direction (the sheet is infinite in extent along x-direction). The cell has finite size in the perpendicular direction (designated as y), and it may be terminated with either armchair or zigzag edge. Shrink-wrapped boundary condition has been used in the y direction. After ensuring proper equilibration and relaxation, uniaxial tension was applied along the x-direction for both armchair and zigzag terminations (or configurations) at a strain rate of 10^9 s^{-1} for various temperatures and defect concentration. To investigate the tensile properties, the entire simulations are done for 500 picoseconds.

The detailed description and explanation of the Tersoff parameterization can be found in section 2.3.1. The cut-off function plays a crucial role in the bonding characteristics of a material. The process of breaking a bond between a pair of atoms will be influenced by the choice of the cut-off distance - the strength of the bond between a pair of atoms depends on the neighbourhood of both the atoms. Larger the cut-off distance, more the possibility of incorporating the bond order correctly. Calculations with original potential cut-off function gave an anomalous behaviour in stress-strain graph which made us to tune the cut-off parameter in the original potential file. In the present work, we have used the original as well as optimized cut-off distances to bring out the crucial role played by it. As shown in figure 6.1, while the stress-strain behaviour computed with the original cut-off parameter is un-physical, a physically meaningful stess-strain characteristic is obtained with the modified cut-off distance. Here, we have varied the cut-off distance between 1.75 Å and 2.35 Å which lies between the lower cut-off distance R_{ij} and the higher cut-off value S_{ij} of the original potential file. In this regard equation (2.15) can be rewritten as (Dilrukshi et al. 2015)

$$f_c(r) = \left\{ \begin{array}{ll} 1 & \text{if } r_{ij} < R_{ij}, \\ 0 & \text{if } r_{ij} > S_{ij} \end{array} \right\} \tag{6.1}$$

6.3 Results and discussions

6.3.1 Effect of original cut-off parameter on the mechanical behaviour

We have created a rectangular simulation cell of BN and subjected it to uniaxial deformations along the zigzag and armchair directions (which are oriented along the X and Y directions), respectively. The obtained equilibrium lattice parameter of 2D h-BN at 300 K using NVT ensemble is 2.498 Å with a nearest boron-nitrogen bond length of 1.45 Å. Results of our calculations on the structure is comparable to the experimentally observed values, a=2.504 Å, c=6.66 Å (Bosak et al. 2006) with a nearest boron-nitrogen bond length of 1.45 Å.

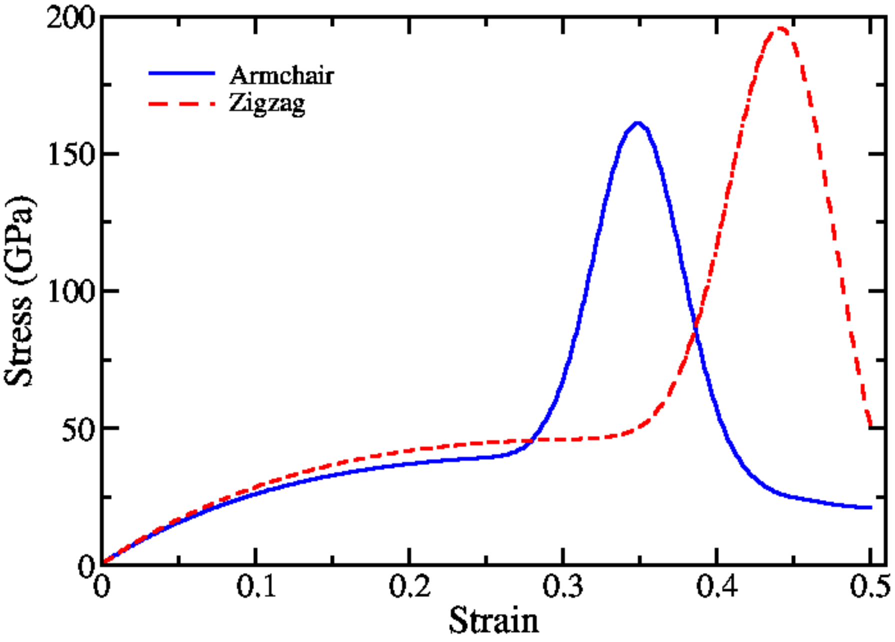

Figure 6.1: Variation of engineering stress due to the bond stretch with bond strain of armchair and zigzag deformation direction of h-BN sheet using the original Tersoff potential cut-off parameter of 1.95 Å.

At first, we studied the tensile properties of pristine h-BN and analyzed the temperature dependence on physical properties using the original cut-off parameter. Later, the vacancy and Stone-Wales type defects were incorporated in h-BN and the direction dependent Young's modulus at room temperature has been calculated. We have focused on the uniaxial strain, and the stress-strain characteristics are shown in figure 6.1 for the cases in which force is applied along the armchair and zigzag deformation directions, respectively, of the pristine h-BN using the original cut-off parameter (1.95 Å). Please note that it is the engineering stress that is shown as a function of the engineering strain. In this procedure, when the engineering strain is applied to the atomic system, the bonds between boron and nitrogen atoms were stretched or compressed, and the potential energy as a function of bond strain is evaluated.

The variation in potential energy with strain for different potential cut-off values of armchair and zigzag configuration is shown in figure 6.2. In the simulation using the original high and low cut-off parameters, we observed a sudden rise in the engineering stress at a strain of about 0.3. It has also been observed that the potential energy shows a sudden decrease of slope beyond the very same strain value of 0.3. These twin observations can be understood once we realize that the distance between some of the neighbouring particles exceed the upper cut-off parameter S_{ij} when the strain exceeds a critical value. At this stage of deformation, the force on all these particles become zero as $f_c(r)$ becomes zero, and hence the potential as well as the force becomes zero, by definition of the cut-off. Hence these particles have no restoring force, and hence there is a run-away situation. Simultaneously, since the potential energy contribution of these atoms is zero, and not negative, there is a sudden increase in the average potential energy. When the cutoff parameter is increased, this run-away situation starts manifesting at larger strains when the average distance between neighbouring atoms exceed the new upper cut-off parameter. Figure 6.2 very clearly depicts this point.

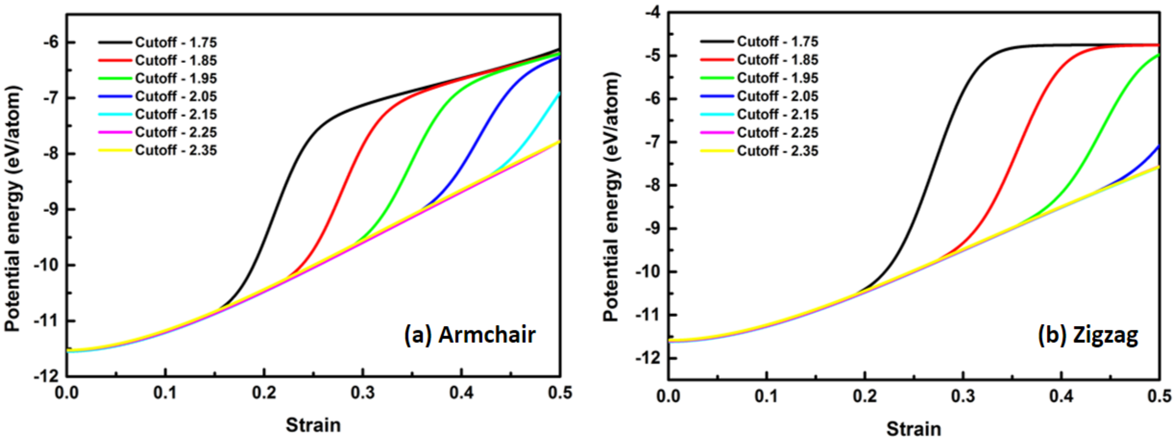

Figure 6.2: The variation in potential energy of pristine h-BN at room temperature with different potential cut-off parameter for armchair and zigzag configurations. It has been observed that the potential energy shows a sudden decrease of slope beyond a strain value of 0.3. Using the original and lower cut-off parameters, we observed a sudden rise in engineering stress corresponding to a small amount of engineering strain. This can be understood from the fact that the force is zero for all the particles whose nearest neighbour distance exceeds the upper cut-off distance S_{ij} in the expression for the potential. Since the potential energy of these atoms is zero, instead of a negative value if the interaction was calculated with a larger cut-off, the average potential energy increases. The nonzero kinetic energy of these particles manifests as an outward pressure which leads to increase in stress and leads to a run-away situation.

To understand the influence on the cut-off function on the potential energy, the variation in the stress-strain relation with strain is noted for different cut-off distances and is shown in figure 6.3 and the observed variations in potential energy curves are reflected in the corresponding stress-strain graph. Our observations on this unphysical stress-strain relation qualitatively similar to the earlier studies of h-BN (Kumar et al. 2016) and carbon nanotubes (Dilrukshi et al. 2015).

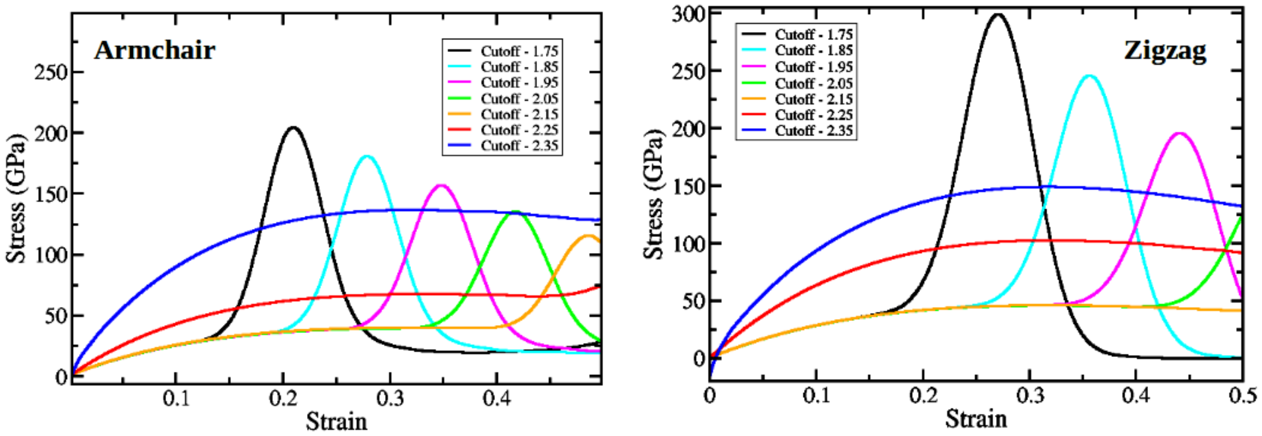

Figure 6.3: The variation in stress-strain relationship of h-BN at room temperature with different potential cut-off function for armchair and zigzag configurations. Due to this sharp rise in stress value using the original (1.95 Å) and below original (< 1.95 Å) cut-off parameter, h-BN shows an unphysical as well as fictitious fracture behavior. This is due to the failure of the smoothing function in the empirical potential and at the stage of deformation, the force on all these particles become zero as $f_c(r)$ becomes zero, and hence the potential as well as the force becomes zero, by definition of the cut-off.

6.3.2 Influence of optimized cut-off parameter on the anisotropic mechanical behavior

Young's modulus is a measure of the stiffness of an elastic material and is one of the prominent considerations in engineering design. In this section, we report analysis of tensile test of h-BN using an optimized cut-off parameter (2.25 Å) of the potential function. The insight gained on the underlying mechanism of deformation is expected to be valuable in the context of fabrication of h-BN materials with specified mechanical applications. Most of the mechanical and elastic properties of crystalline solids are strongly anisotropic in nature. In general, the inter-atomic potentials for real crystals are not harmonic, and they possess strong anharmonicity. When the atomic displacements of these atoms are not very small compared to the interatomic spacing, the anharmonicity of crystal lattices becomes prominent (Hiki 1981).

To calculate the value of Young's modulus, first derivative of the straight line portion of the stress-strain curve is considered and the data with engineering strain of 1% is used. Simulations have been performed separately for armchair and zigzag configurations. The variation in engineering stress corresponding to the applied engineering strain of armchair and zigzag configuration at various temperatures is shown in figure 6.4. The stress-strain graph shows a smooth variation in the entire studied temperature range. The stress-strain graphs obtained using the optimized cut-off parameter (2.25 Å) are devoid of the unphysical sharp increase in stress. In both armchair and zigzag configurations, the observed maximum strain value lies between 0.25 and 0.35. It is interestingly observed that by using the original cut-off value (1.95 Å), the material shows a higher engineering stress and strain value.

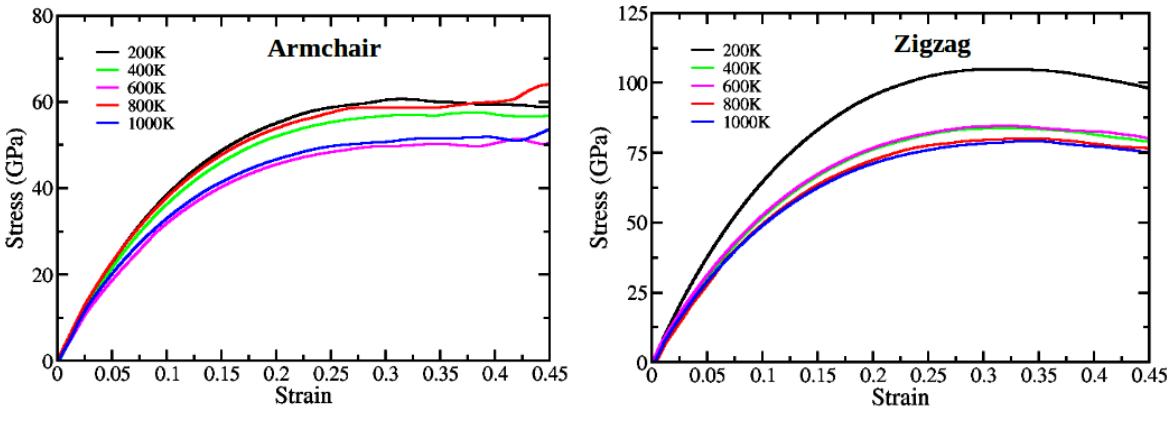

Figure 6.4: Variation in engineering stress corresponds to the applied strain of armchair and zigzag configurations at various temperatures of pristine h-BN using the optimized cut-off parameter (2.25 Å) of the potential.

In order to investigate the system size dependence on the computed Young's modulus of h-BN, we used finite rectangular simulation cells of various sizes (10×10×1, 20×20×1, 30×20×1, 50×50×1, 70×70×1, 100×100×1). We noticed that, at a temperature of 300 K, the system size does not have significant effect on the Young's modulus value, but h-BN possesses strong directional anisotropy as shown in table 6.1. The variation in Young's modulus of pristine h-BN at different temperatures is shown in figure 6.4. Here, as the thermal energy increases, the atoms starts vibrating from the mean position and the regular atomic arrangement has altered. The out of plane fluctuations, called ripples, in h-BN increase with temperature which in turn decreases the strength of the material.

Table 6.1: The system size (rectangular sheet) dependence of Young's modulus (YM) of h-BN at 300 K. The variation in Young's modulus with system are negligible as shown in the table.

Simulation cell size	**Armchair YM (GPa)**	**Zigzag YM (GPa)**
10×10× 1 (400 atoms)	693.72	761.43
20×20× 1 (1600 atoms)	755.72	769.73
30×30× 1 (3600 atoms)	687.44	783.50
50×50× 1 (10000 atoms)	692.95	767.12
70×70× 1 (19600 atoms)	635.63	781.02
100×100× 1 (40000 atoms)	623.32	785.86

The observed room temperature Young's modulus of armchair and zigzag configuration are 755 GPa and 769 GPa respectively, the zigzag configuration shows a higher value of Young's modulus as compared to its armchair counterpart. The decrease of Young's modulus with increase of temperature has also been observed and are consistent with the earlier studies on graphene (Mirnezhad et al. 2013). A comparative study of the elastic modulii of pristine h-BN using various experimental, theoretical and computational methods are given in table 6.2.

6.3.3 Stiffness of pristine h-BN

It is important to analyze the stiffness of any material, which is the ability of a material to resist deformation. When a material behaves elastically, the work done to deform the material is stored as the elastic energy. The elastic strain energy is calculated from the area under the linear portion of the stress-strain graph and stiffness is also inferred from the elastic region of the stress-strain curve. In general, a stiff material needs more force to deform compared to a soft material

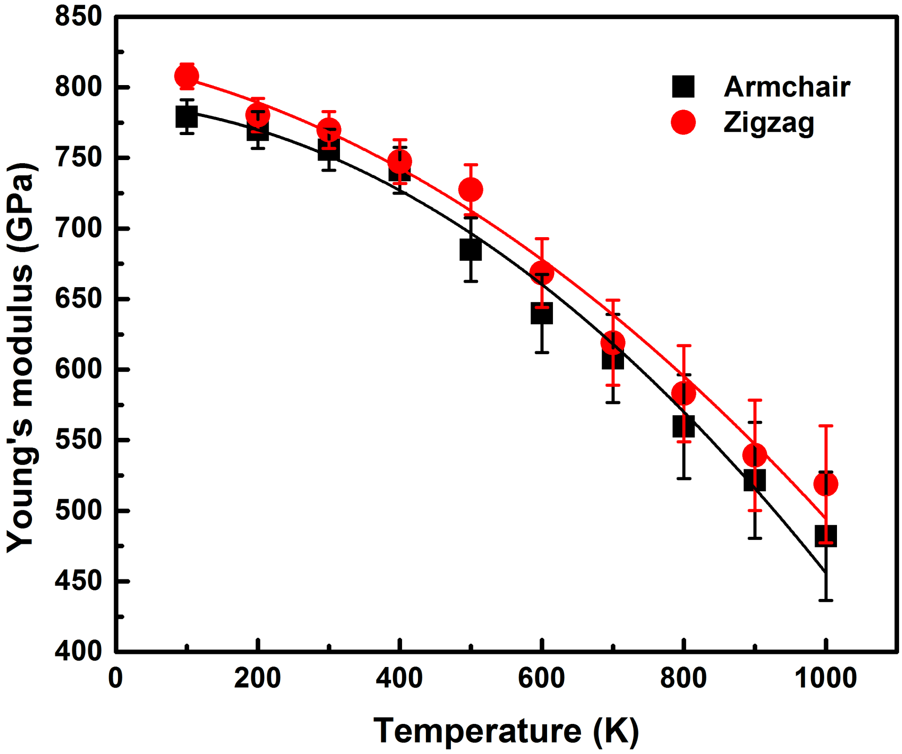

Figure 6.5: Variation of Young’s Modulus with temperature of pristine h-BN along the armchair and zigzag configurations using the optimized cut-off parameter (2.25 Å) of the potential.

and the higher the value of the Young’s modulus, the stiffer the material. Then the stored elastic energy is obtained from the linear portion of the stress-strain curve of the h-BN sheet before the onset of yield. As the temperature increases, the slope of the stress-strain curve shows slight variation as shown in figure 6.4. We have observed that the stored elastic energy of the material decreases with increase in temperature and towards the lower temperatures, the zigzag configuration shows a higher value of elastic energy as compared to the armchair configuration, which is consistent with the values of Young’s modulus shown in figure 6.5. As the temperature increases, the zigzag orientation is less vulnerable to elongation showing a higher value of stiffness as compared to the armchair counterpart. We observe that, the stored elastic energy and Young’s modulus of both the armchair and zigzag configurations decreases with increase in temperature and the variation in stored elastic energy with temperature is shown in figure 6.6.

Table 6.2: Calculated Young's modulus (Y) of pristine h-BN using the engineering stress-strain relation in comparison to the earlier experimental, theoretical and computational analysis. The interatomic potential parameter (IPP) used for the method of calculation has also given.

Reference	**Method (IPP)**	**Year**	**Young's modulus (GPa)**
Present work	MD (Tersoff)	2017	755 (Armchair) 769 (Zigzag)
Kumar et al	MD (Tersoff)	2016	723 (Armchair) 733 (Zigzag)
Han et al	MD (Tersoff)	2014	881
Le M Q	MM	2014	754 (Armchair) 784 (Zigzag)
Zhao et al	MD (Tersoff)	2013	716
Mirnezhad et al	*Ab initio*	2013	829
Mortazavi et al	MD (Tersoff)	2012	825
Andrew et al	Equation of state and DFT	2012	821
Peng et al	DFT	2012	828
Boldrin et al	Atomistic continuum approach	2011	797
Eun-Sok Oh	Continuum Lattice Approach (Tersoff-Brenner)	2011	977
Li Song et al	Experiment	2010	885
Topaskal et al	DFT	2010	768
Sahin et al	DFT	2009	795
Bosak et al	In-elastic X-ray scattering	2006	776
Kudin et al	DFT	2001	807
Obha et al	DFT	2001	807

6.3.4 Young's Modulus of defective h-BN

The theoretical study of defects are very important to analyze various properties of most of the materials, since the experimentally synthesized samples always contain different types of defects which encourages one to look into various types of possible defects in materials and is also close to experimental counterpart. Incorporating defects for the computational analysis of the calculation of mechanical properties helps to understand how the material behaves at different physical situations. Structural defects in materials can be classified as incomplete bonding defects, topological defects and heterogeneous defects. In h-BN, the vacancy and Stone-Wales defects with defect concentration varies from 0.1% to 1% have received much more attention than any other kind of defects and the presence of defects may break the

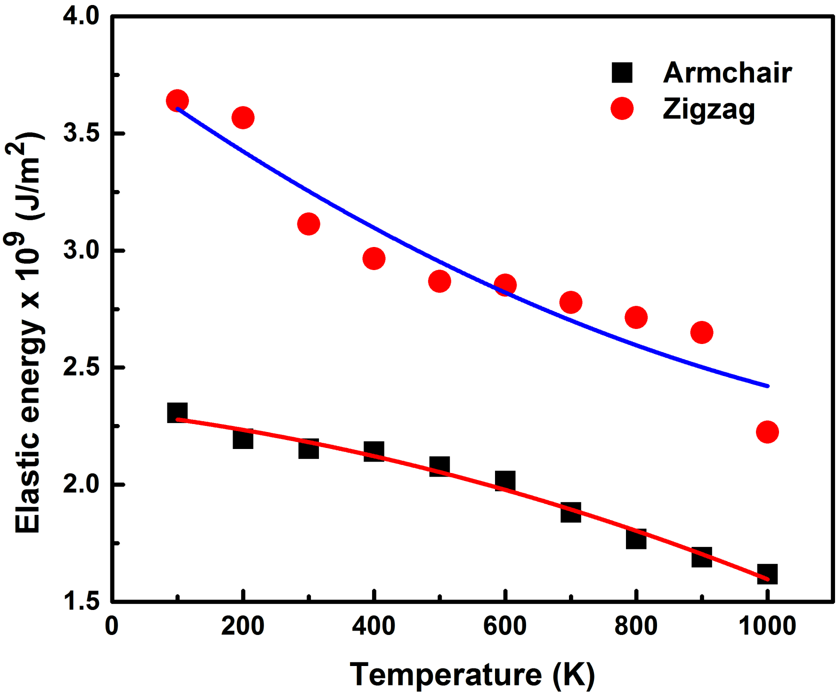

Figure 6.6: Temperature dependence on the elastic energy of pristine h-BN along the armchair and zigzag orientations using the optimized cut-off parameter. The variation in stored elastic energy with increase of temperature has been noticed and the strain rate for the simulation is kept constant at 10^9 s^{-1}.

symmetry of the perfect honeycomb lattice.

Usually vacancies, topological defects, grain boundaries, etc., are the commonly occurring defects in low dimensional materials. Stone-Wales (SW) defect is one of the prominent topological defects observed in h-BN in addition to vacancies. The mono vacancy defects are created by removing one boron or nitrogen atom from the pristine h-BN. Stone-Wales defect leads to the 90° rotation of the bonds between B-N atoms forming a non-hexagonal ring in the lattice without altering the connectivity of the network (Ansari et al. 2014). That is, the rotation of a B-N bond forms a SW defect in h-BN. In the case of a finite system, we can consider the armchair and zigzag termination and here, the boundary itself may be a defect. In vacancy defect, an atom is completely missing from the lattice site and in Stone-Wales, two pairs of hexagons transforms to two pentagons and two heptagons retaining the total number of atoms unlike vacancies.

Usually, the defective h-BN systems exhibit different stress-strain behaviors compared to the pristine case. At first, a significant decrease in the slope has been observed, which indicates a reduced value of Young's modulus in h-BN and the similar situation has already been reported in graphene (Xu et al. 2013). The room temperature variation of engineering stress with engineering strain at different concentration of vacancy and Stone-Wales defects in h-BN with armchair and zigzag configurations have been analyzed. We varied the concentration of defects from 0.1% to 1.0%, which is close to most of the experimental studies. The room temperature variation in the stress-strain curve of h-BN sheet with 0.1% of vacancy and SW defect along the armchair and zigzag direction is shown in figure 6.7. As the concentration of the defects increases, there is a reduction in the fracture stress for both armchair and zigzag configurations.

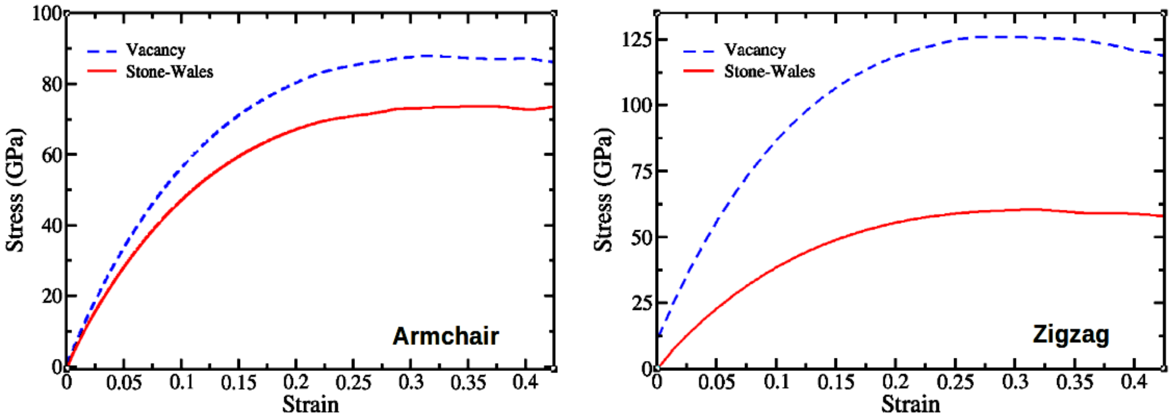

Figure 6.7: The variation in engineering stress corresponds to the applied strain of armchair and zigzag configurations of defective h-BN at 300 K using the optimized cut-off parameter (2.25 Å) of the potential.

The variation in room temperature Young's modulus with vacancy and SW defect concentration of armchair and zigzag configurations is shown in figure 6.8. We noticed that the Young's modulus decreases linearly with increase in defect concentration for both vacancy and Stone-Wales types of defects. We also observed that the material with zigzag configuration possesses a higher fracture stress as compared to the one in armchair configuration in presence of both vacancy and Stone-Wales defects corresponding to a strain value of 0.3.

We noticed that, as compared to SW defect, presence of vacancies leads to a marginal increase in Young's modulus in the armchair and zigzag configurations. The increase in Young's modulus in the zigzag configuration indicate the ability of the material to resist the deformation even with defects, like in the case of pristine h-BN sheet. We also observed that the SW defect retains the total number of atoms in h-BN and preserves the sp^2 B-N bonding by keeping two heptagons and two pentagons corresponding to a single SW defect. But in vacancies, the number of atoms reduces as the defect concentration increases. Here, the missing boron and nitrogen atoms break the perfect bonding in h-BN which results in the formation of dangling bonds, leading to a sharp decrease in the Young's modulus, which is more in armchair direction as compared to zigzag direction. In the case of vacancy defect, as the defect concentration increases, the bond breaking happens and the inter atomic interactions become weaker, resulting in decreasing of the Young's modulus. It has been reported that the interaction between dangling bonds or the chemical instabilities due to the missing atoms in graphene sheet affects its mechanical properties (Jing et al. 2012). Due to the structural similarities and perfect lattice matching of h-BN to graphene, we could expect similar mechanical behavior in h-BN also.

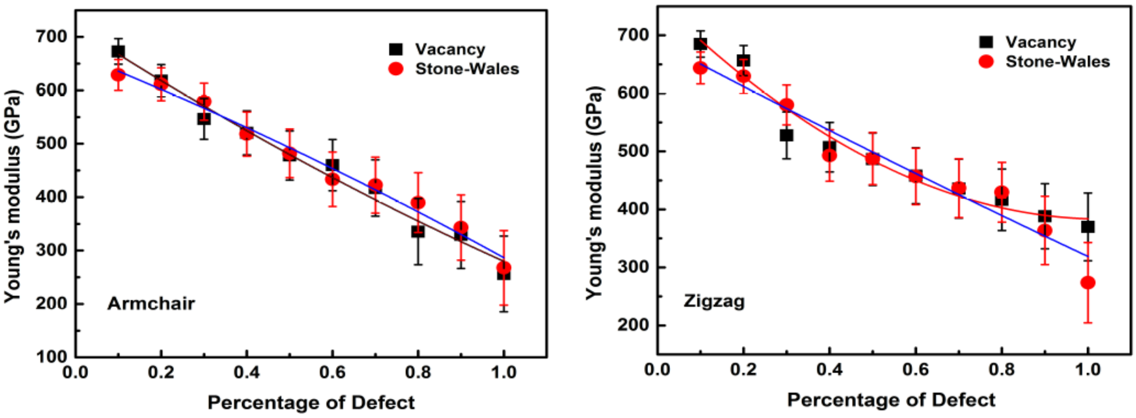

Figure 6.8: The variation of Young's modulus with vacancy and Stone-Wales defect concentration along the armchair and zigzag configurations of h-BN at 300 K using the optimized cut-off parameter. The decrease in Young's modulus shows a linear behavior with increase in defect concentration.

6.3.5 Deformation dynamics

In most of the materials, the fracture mechanism can be temperature dependent. Though graphene and h-BN possesses high mechanical stability, due to their atomically thin nature, they are easily vulnerable to various types of fracture mechanisms and deformations. We observe that, the deformation mechanism in pristine h-BN may involve formation of defects and breakage of bonds as shown in figure 6.9 for the case of armchair orientation, as an example. To understand the transformation from brittle rupture to ductile fracture, we studied snapshots of atomic configurations at different instants of time. Initially, a rectangular simulation cell of h-BN in the MD environment has been relaxed.

After the cell relaxation, uniaxial tension was applied and the additional relaxation has been performed at a temperature of 300 K using NVT ensemble. The snapshots of the deformation mechanisms in the armchair direction at 100 ps and 400 ps are shown in figure 6.9 (a) and (b) respectively. To visualize the atomic structures and deformations, we used Visual Molecular Dynamics (VMD) package (Humphrey et al. 1996). After the proper cell relaxation, the whole simulation is done for 500 picoseconds at 300 K. We also observe that the edges of the h-BN are easily affected by deformation as the material is subjected to deformation for longer time.

6.3.6 Structural integrity analysis

From the earlier sections, we have explained the fracture behavior of pristine and defective h-BN with varying temperature and defect concentration. We have varied the temperature of the system from 100 K to 1000 K to analyze the mechanical properties of pristine and defective h-BN by varying the defect concentration from 0.1 % to 1.0 %. To understand the effect of deformation mechanism in h-BN, we have analyzed the distribution of bond length in the system. The analysis of the radial distribution functions (RDFs) of pristine and defective h-BN using the modified cut-off parameter in the armchair and zigzag orientations also gives more insight into the deformation mechanism. The detailed explanation of RDF can be

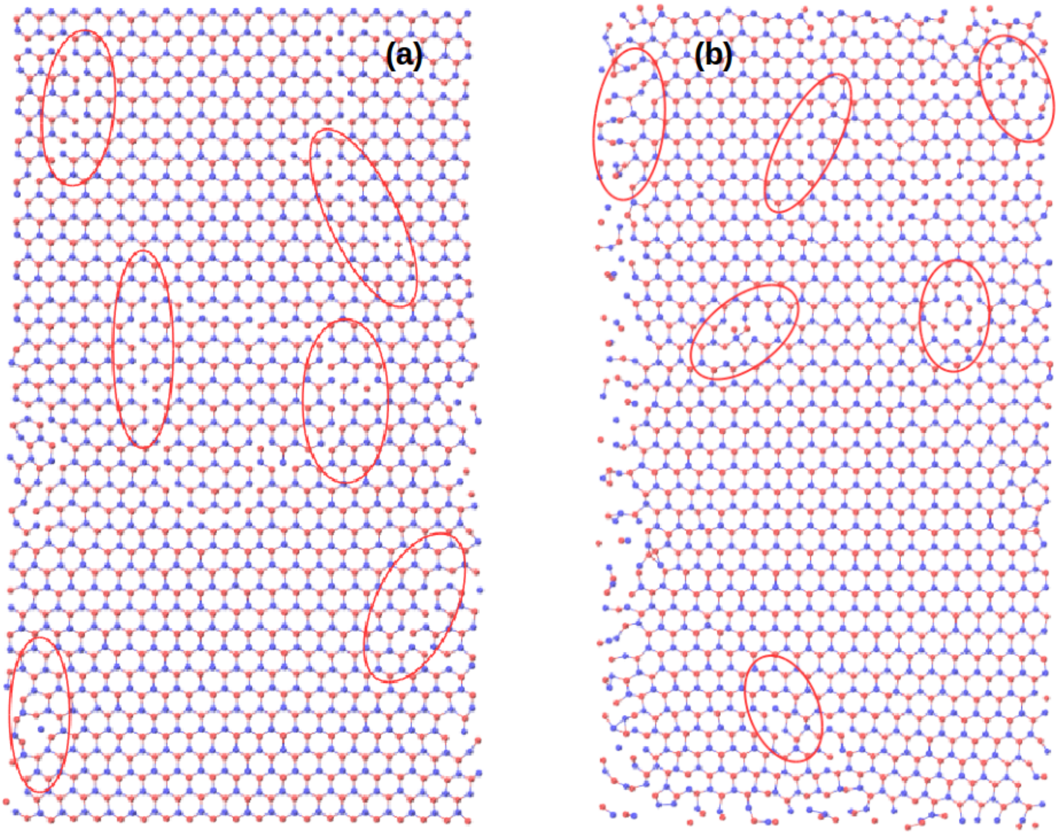

Figure 6.9: Snapshots of the fracturing dynamics of pristine h-BN sheet at 300 K. The snapshot of the deformation during the initial relaxation at 200 ps is shown in (a) and the deformation mechanisms at 400 ps is shown in (b). The oval shape shows the deformed areas in the sheet.

found in section 3.3.2. In general, distribution functions are Dirac delta functions at zero Kelvin temperature.

As the temperature increases, the thermal energy would cause broadening of the delta functions to smooth peaks. Here, the room temperature RDF has been evaluated and observed that the nearest B-N bond length of armchair and zigzag orientations of pristine h-BN in comparison to the defective case as shown in figure 6.10. When the sample is elongated along x direction, it should contract in the y-direction. For pristine h-BN in the armchair termination, the bond length increases to 1.55 Å in the x direction and decreases to 1.41 Å in the y direction both starting from the original value of 1.45 Å. For pristine h-BN in the zigzag termination, the bond length increases to 1.54 Å in the x direction and decreases to 1.44 Å in the y direction both starting from the original value of 1.45 Å. Thus h-BN in zigzag configuration is more resilient to deformation than the one in armchair counterpart.

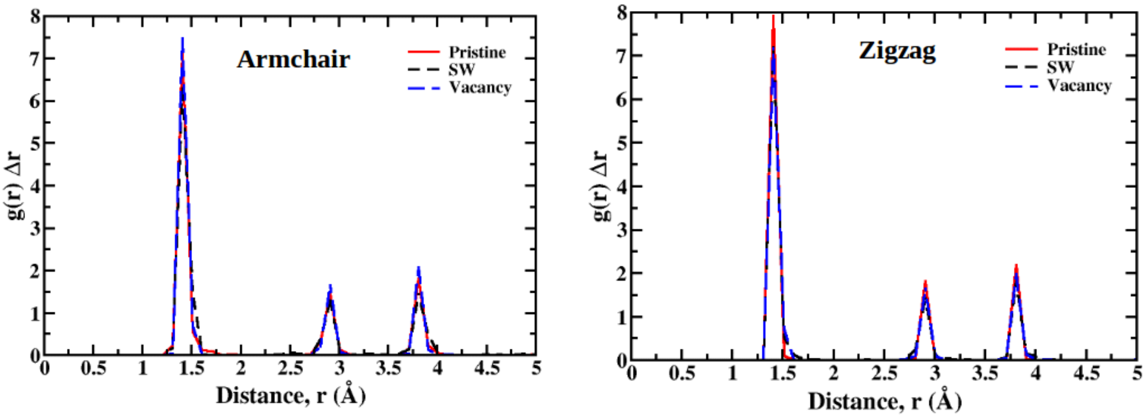

Figure 6.10: The radial distribution functions of pristine and defective h-BN under tensile tests at a temperature of 300 K. The binsize is taken as $\Delta r = 0.005$. The RDFs of pristine h-BN at the equilibrium state is in comparison to the case of Vacancy and SW defect of (a) armchair and (b) zigzag configuration. When the sample is elongated along x direction, it should contract in the y-direction. For pristine h-BN in the armchair termination, the bond length increases to 1.55 Å in the x direction and decreases to 1.41 Å in the y direction both starting from the original value of 1.45 Å. For pristine h-BN in the zigzag termination, the bond length increases to 1.54 Å in the x direction and decreases to 1.44 Å in the y direction both starting from the original value of 1.45 Å. Thus h-BN in zigzag configuration is more resilient to deformation than the one in armchair counterpart.

For h-BN in armchair configuration together with 1% of vacancy, the lattice parameter changes from 1.45 Å to 1.55 Å in the x-direction and 1.50 Å in the y-direction upon deformation. For h-BN in zigzag configuration together with 1% of vacancy, the lattice parameter changes from 1.45 Å to 1.56 Å in the x-direction and 1.44 Å in y-direction. For h-BN in armchair configuration together with 1% of Stone-Wales defects, the lattice parameter changes from 1.45 Å to 1.54 Å in the x-direction and 1.44 Å in the y-direction upon deformation. For h-BN in zigzag configuration together with 1% of Stone-Wales defects, the lattice parameter changes from 1.45 Å to 1.56 Å in the x-direction and 1.44 Å in y-direction. Thus the lattice parameters of h-BN with both armchair and zigzag terminations are relatively insensitive to presence of small concentration of defects, even though the fracture stress and Young's modulus do change.

6.4 Conclusions

We observed that the mechanical properties of h-BN vary substantially with the cut-off distance of the used empirical interatomic potential. As the temperature increases, the observed Young's modulus shows a significant decrease for both the armchair and zigzag terminations, which is attributed to the presence of directional anisotropy in h-BN. The variation of Young's modulus with system size is elucidated for the better understanding of anisotropic behavior in h-BN. We also observed that the computed elastic energy decreases with increase in temperature and the zigzag configuration shows a higher value of stiffness as compared to the armchair counterpart. We observed that the mechanical strength of h-BN is significantly affected by the vacancy and Stone-Wales type defects, etc., and the computed room temperature Young's modulus of pristine h-BN is 755 GPa and 769 GPa respectively for the armchair and zigzag configurations. The decrease in Young's modulus shows a linear behavior with increase in defect concentration. The observed shift in the peak positions in the radial distribution functions of the pristine and defective h-BN shows the changes in the structural features of zigzag and armchair configurations in the presence of applied stress.

Chapter 7

Summary and Future Work

7.1 Summary

Study of two-dimensional (2D) materials has become a vibrant field in condensed matter physics. Two dimensional molecular sheets have received a lot of attention in recent years because of their exceptional properties and applications and are at the forefront of current research. In the present thesis, an attempt has been made to investigate the structural, thermo-mechanical and finite size as well as temperature dependent elastic properties of monolayer hexagonal boron-nitride (h-BN). Classical molecular dynamics simulations were performed using a Tersoff bond order potential tuned for the studies of hybrid Graphene/h-BN layered system.

In chapter 3, we studied the temperature dependence of lattice parameter, radial distribution function (RDF), specific heat at constant volume, linear thermal expansion coefficient (LTEC) and height-height correlation function of the thermally excited ripples on pristine as well as defective h-BN sheet. As temperature increases the amplitude of the peaks in RDF decreases due to thermal broadening. The specific heat shows considerable increase beyond the Dulong-Petit limit at high temperatures, which is interpreted as a signature of strong anharmonicity present in h-BN. The height-height correlation function and bending rigidity, calculated within the frame work of continuum theory of membranes, vary with increase in temperature and defect concentration. The power-law exponent β for the height-height correlation function shows deviation from the harmonic limit of 4 predicted by membrane theory. It decreases from 3.7 to 2.7 as the temperature increases from 200 K to 3000 K. The non-universality of the scaling exponent β is also an indication of the important role played by anharmonicity in h-BN.

In chapter 4, we investigated the system size dependence on the mechanical stability, bending stiffness and elastic properties of hexagonal boron nitride. We observed that the elastic moduli of a finite h-BN sheet is different for the armchair and zigzag directions, thereby demonstrating its anisotropic linear elastic behavior. The values of the independent elastic constants C_{11} and C_{12} are such that Born's criterion for mechanical stability of h-BN is satisfied. We noticed that there is a strong system size dependency for the in-plane stiffness and Poisson's ratio of finite sheets. These properties show a power law convergence to the bulk values when the system size tends to infinity. Using the formula derived from Foppl-von Karman plate theory, variation of bending rigidity with system size is determined from the measured value of thin shell thickness. Due to the the strong in-plane sp^2 bonds and the small mass of boron and nitrogen atoms, 2D h-BN possess high group velocities. As the system size increases, Young's modulus also increases, which leads to an increase in the longitudinal and shear wave velocities.

In chapter 5, the effect of ripples on the temperature dependent elastic constants of monolayer hexagonal boron nitride have been investigated for the first time using strain fluctuation method. Classical molecular dynamics simulations are performed with a tuned Tersoff empirical inter atomic potential and the independent elastic constants C_{11} and C_{12} and thermal expansion coefficient are calculated as a function of temperature. The Young's, bulk and shear moduli, Poisson's ratio, sound velocities, etc., are calculated from the computed values of elastic constants and are found to decrease with increase of temperature. We observed that the out-of-plane intrinsic ripples responsible for strong anharmonic behavior of h-BN leads to large deviation from the isotropic elasticity. Because of the strong thermal rippling in large systems, the h-BN sheet may have a negative thermal expansion coefficient at relatively low temperatures, with a transition to positive thermal expansion at high temperatures and this also soften the elastic constants. This transition is a result of two competing effects: positive thermal expansion due to in-plane modes and negative expansion due to out-of-plane fluctuation. The calculations show that h-BN sheet satisfy Born's criterion for mechanical stability. As the system size become larger, the value of Young's modulus decrease consistently with the variation of elastic constants due to the thermally excited ripples. As the temperature increases, the Young's modulus of h-BN decreases, which leads to the decrease of longitudinal and shear wave velocities.

Chapter 6 explains the influence of empirical potential and effect of temperature on the mechanical properties of pristine and defective hexagonal boron nitride. We observed that the mechanical properties of h-BN vary substantially with the cutoff distance of the used empirical interatomic potential. As the temperature increases, the observed Young's modulus shows a significant decrease for both the armchair and zigzag terminations, which is attributed to the presence of directional anisotropy in h-BN. The variation of Young's modulus with system size is elucidated for the better understanding of anisotropic behavior in h-BN. We also observed that the computed elastic energy decreases with increase in temperature and the zigzag configuration shows a higher value of stiffness as compared to the armchair counterpart. The defect analysis shows that presence of vacancy type defects leads to a higher Young's modulus, in the studied range with different percentage of defect concentration, in comparison with Stone-Wales defect.

Our results indicate that the effect of temperature and defects on the mechanical properties of boron nitride nanosheet should be taken into account for the analysis and development of technologically prominent graphene/h-BN nanodevices for future applications. We also believe that the obtained results can be useful for the strain-based ripple manipulation of h-BN for engineering applications.

7.2 Future prospects

- To elaborate the finite temperature analysis of the structural, thermo-mechanical, finite size elastic properties and the effect of ripples on pristine and defective low dimensional materials such as BC_3, SiC, silicene and MoS_2. and their derivatives like carbon and boron nitride nanotubes (CNTs and BNNTs) using classical molecular dynamics simulation.

- The study of the physical properties of hybrid graphene/h-BN heterostructures and bilayers (graphene on hBN) would help to understand whether or not the h-BN substrate changes fundamentally by the thermal rippling properties of graphene. The most common 2D vertical heterostructures, graphene/hexagonal boron nitride (denoted as G/h-BN), have stimulated extensive interest and have applications in nano electronics, photo-detection and energy harvesting/conversion.
- The study of pristine as well as materials with different types of defects including Stone-Wales, vacancy, tetrahedron, etc., would help to predict their properties realistically for better practical applications.
- To study the Chemistry of materials using reactive force field (ReaxFF) which implicitly describes the chemical bonding without expensive quantum mechanical calculations.
- A more systematic study would be worthwhile to acquire better understanding of temperature dependent elastic constants of pristine and defective 2D structures in arbitrary orientations using stress-fluctuation method.
- The modelling and simulation of different polymers with graphene and h-BN gives information of possible confinement of polymers in these materials and the studies also provide the graphene-polymer and hBN-polymer interfacial mechanical behavior using molecular dynamics. The study of density profiles, structural characteristics and mobility aspects would be promising.

Appendices

Appendix A

LAMMPS Features

LAMMPS is an acronym for Large-scale Atomic/Molecular Massively Parallel Simulator designed to run efficiently on parallel computers. The major features of LAMMPS with specific commands are described here.

A.1 General features

- Runs efficiently on single-processor desktop or laptop machines, but is designed for parallel computers
- Open-source distribution under the terms of the GNU Public License
- Distributed memory message-passing interfaces (MPI)
- Highly portable C++
- Easy to extend with new features and functionality

A.2 Particle and model types

- Atoms
- Polymers and biological systems
- Metallic systems
- Granular materials
- Coarse-grained systems

A.3 Force fields

- **Pairwise potentials:** Lennard-Jones, Morse, Yukawa, etc.
- **Many body potentials:** Tersoff, REBO, AIREBO, LCBOP, ReaxFF, COMB, Stillnger-Weber, EAM, MEAM, etc.

A.4 Integrators

- Velocity-Verlet integrator
- Predictor-corrector algorithm
- Energy minimization via conjugate gradient or Steepest-descent method

A.5 Ensembles, boundary conditions and constrains

- NVE, NVT and NPT ensembles for temperature and pressure control
- Inclusion of thermostats (Nose-Hoover) and barostats (Berendsen) with ensembles
- Periodic and non-periodic (fixed, shrink wrapped, shrink-wrapped with a minimum value) boundary conditions

A.6 Output of the MD simulation

- Text dump files for the information of atom coordinates and temperature info (log file),
- Dump file for velocities and other per-atom (dump) quantities

A.7 LAMMPS non-features

LAMMPS is a fast and parallel engine designed for molecular dynamics (MD) simulations. Till date, LAMMPS itself provides only a modest amount of functionality for setting up simulations and analyzing the output. Many tools are required for the pre and post processing mechanisms which are not included in LAMMPS.

- Run through a GUI
- Build molecular systems

- Assign force-field coefficients automatically
- Visualisation and plotting of data

Appendix B

LAMMPS Input File

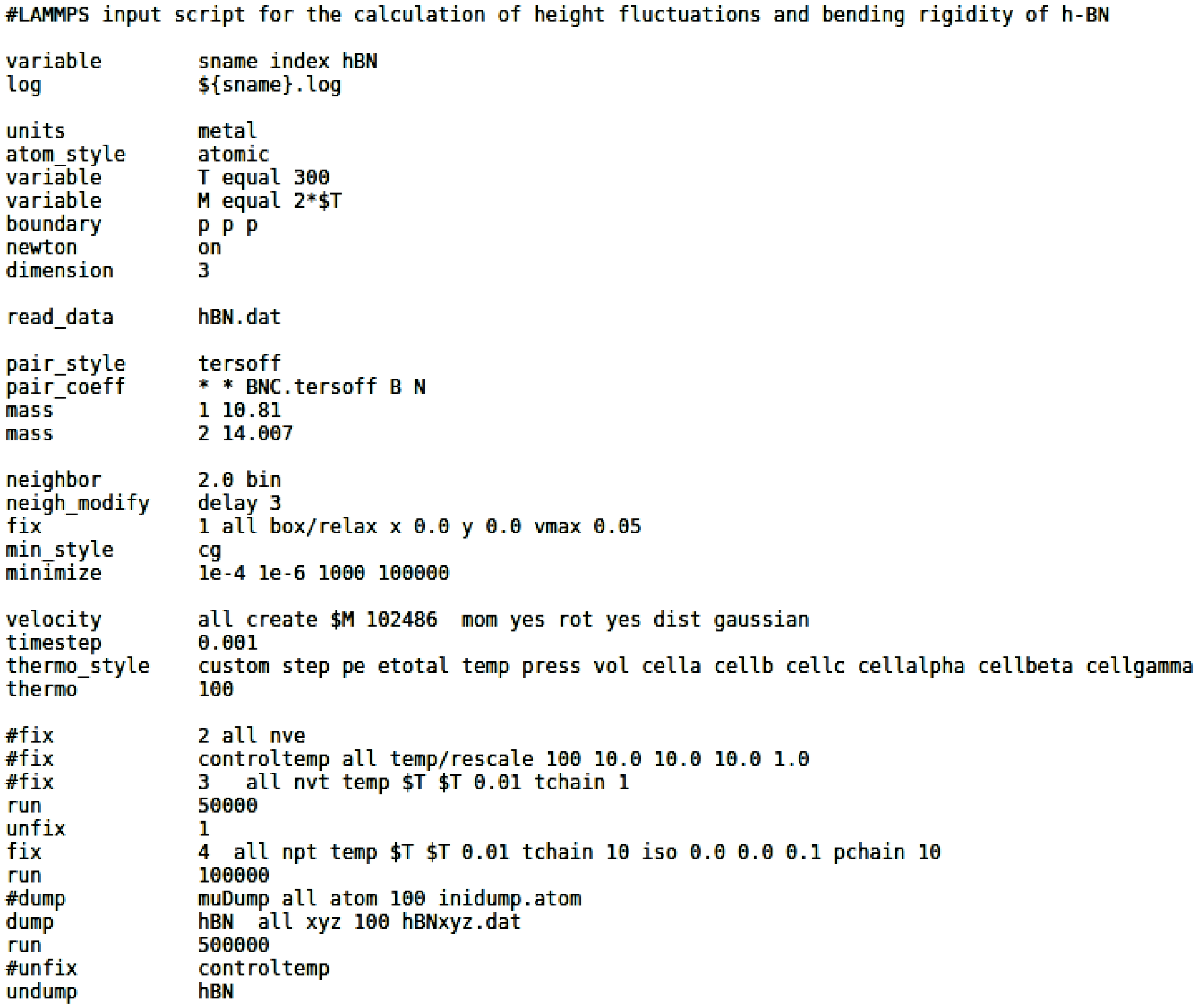

```
#LAMMPS input script for the calculation of height fluctuations and bending rigidity of h-BN

variable        sname index hBN
log             ${sname}.log

units           metal
atom_style      atomic
variable        T equal 300
variable        M equal 2*$T
boundary        p p p
newton          on
dimension       3

read_data       hBN.dat

pair_style      tersoff
pair_coeff      * * BNC.tersoff B N
mass            1 10.81
mass            2 14.007

neighbor        2.0 bin
neigh_modify    delay 3
fix             1 all box/relax x 0.0 y 0.0 vmax 0.05
min_style       cg
minimize        1e-4 1e-6 1000 100000

velocity        all create $M 102486  mom yes rot yes dist gaussian
timestep        0.001
thermo_style    custom step pe etotal temp press vol cella cellb cellc cellalpha cellbeta cellgamma
thermo          100

#fix            2 all nve
#fix            controltemp all temp/rescale 100 10.0 10.0 10.0 1.0
#fix            3   all nvt temp $T $T 0.01 tchain 1
run             50000
unfix           1
fix             4  all npt temp $T $T 0.01 tchain 10 iso 0.0 0.0 0.1 pchain 10
run             100000
#dump           muDump all atom 100 inidump.atom
dump            hBN  all xyz 100 hBNxyz.dat
run             500000
#unfix          controltemp
undump          hBN
```

Appendix C

Theory of Two dimensional Crystalline Membrane

The main aim of this appendix is to understand the physics of two-dimensional crystalline membrane. The structural and thermo-mechanical properties of membranes are of fundamental importance and are relevant for technological applications. Crystalline membranes are two-dimensional membranes whose constituent particles form a crystalline mesh. Crystalline membranes embedding in a three dimensional space allows fluctuations not only within the two internal dimensions of the membrane (in-plane modes) but also in the direction perpendicular to the plane of the membrane (out-of-plane or flexural modes) (Braghin and Hasselmann 2010, Hasselmann and Braghin 2011). In 3D systems, this type of in-plane and out-of-plane displacements takes place only close to the critical temperatures, whereas in 2D systems this behavior happens at any finite temperature. A good example of a truly 2D free standing membrane is graphene where carbon atoms form a membrane with a hexagonal lattice structure.

C.1 Phenomenological Theory of Membranes

Crystal lattice dynamics theories are based on the concept of phonons, i.e., weakly interacting waves of atomic (or ionic) vibrations and corresponding quasiparticles. Harmonic approximation assuming that atomic displacements ($\vec{u}$) from the equilibrium position is much smaller than the interatomic distance (d). For 3D systems, harmonic approximation holds up to the melting temperature while in 2D system, this assumption fails. Therefore, Landau and Peierls (in 1930s) and later Mermin-Wagner, suggested that 2D crystals cannot exist within the framework of harmonic approximation. One can assume that the atomic displacements $\vec{u}$ satisfy the condition

$$\langle \vec{u}_{n,j}^{2} \rangle << d^2, \tag{C.1}$$

where n labels the elementary cell and j is the atom within the elementary cell.

It has been shown that the harmonic approximation cannot be applied at any finite temperature to 2D crystals neither for in-plane nor for out-of-plane modes since the condition in equation (C.1) is violated due to divergent contributions of acoustic long wavelengths modes with $q \to 0$. In this situation, it becomes necessary to consider anharmonic interactions between in-plane and out-of-plane modes. In the limit $q \to 0$, acoustic modes can be described by elasticity (Landau and Lifshitz 1970). Then the corresponding effective Hamiltonian $\mathcal{H}$ reads

$$\mathcal{H} = \frac{1}{2}\int d^2x \left(\kappa(\nabla^2 h)^2 + \mu {u_{\alpha\beta}}^2 + \frac{\lambda}{2} {u_{\alpha\alpha}}^2 \right), \tag{C.2}$$

where h is the out of plane deformation, κ is the bending rigidity, μ and λ are Lame coefficients and the deformation tensor $u_{\alpha\beta}$ is

$$u_{\alpha\beta} = \frac{1}{2}\left(\frac{\partial u_\beta}{\partial x_\alpha} + \frac{\partial u_\alpha}{\partial x_\beta} + \frac{\partial h_\beta}{\partial x_\alpha}\frac{\partial h_\beta}{\partial x_\beta} \right) \tag{C.3}$$

In the deformation tensor, the nonlinear terms $\frac{\partial h_\beta}{\partial x_\alpha}$ are included while $\frac{\partial u_\gamma}{\partial x_\alpha}$ is excluded since out-of-plane fluctuations are stronger than in-plane ones. Neglecting all nonlinear terms in the deformation tensor, $\mathcal{H}$ is split into two independent Hamiltonians in $\vec{q}$ representation and is:

$$\mathcal{H}_0 = \frac{\kappa}{2}\sum_{\vec{q}} q^4 |h_{\vec{q}}|^2 + \frac{1}{2}\sum_{\vec{q}} \left[\mu q^2 |\vec{u}_{\vec{q}}|^2 + (\lambda+\mu)(\vec{q}.\vec{u}_{\vec{q}})^2 \right], \tag{C.4}$$

where the subscript 0 indicates the harmonic approximation and $h_{\vec{q}}$ and $\vec{u}_{\vec{q}}$ are Fourier components of $h(\vec{r})$ and $\vec{u}(\vec{r})$, respectivly.

The correlation functions in harmonic approximation,

$$G_o(\vec{q}) = \langle |h_{\vec{q}}|^2 \rangle_0 = \frac{T}{\kappa q^4} \tag{C.5}$$

$$D_0^{\alpha\beta}(\vec{q}) = \langle u^*_{\alpha\vec{q}}\, u_{\beta\vec{q}} \rangle_0 = \frac{q_\alpha\, q_\beta}{q^2} \frac{T}{(\lambda+2\mu)q^2} + \left[\delta_{\alpha\beta} - \frac{q_\alpha q_\beta}{q^2}\right] \frac{1}{\mu q^4}, \tag{C.6}$$

where $\langle\rangle_0$ means average with the Hamiltonian $\mathcal{H}_0$ in equation (C.4).

For a surface $z = h(x,y)$, the components of the normal are:

$$n_x = -\frac{\partial h}{\partial x} \frac{1}{\sqrt{1+|\nabla h|^2}} \tag{C.7}$$

$$n_y = -\frac{\partial h}{\partial y} \frac{1}{\sqrt{1+|\nabla h|^2}} \tag{C.8}$$

$$n_z = \frac{1}{\sqrt{1+|\nabla h|^2}} \tag{C.9}$$

Where ∇h is a 2D gradient and if $|\nabla h| << 1$, the normal-normal correlation function is related to $\langle |h_{\vec{q}}|^2 \rangle$ as

$$\langle \vec{n}_{\vec{q}}\, \vec{n}_{-\vec{q}} \rangle = q^2 \langle |h_{\vec{q}}|^2 \rangle \tag{C.10}$$

On substituting equation (C.5) into (C.10), we find

$$\langle \vec{n}_{\vec{q}}\, \vec{n}_{-\vec{q}} \rangle = \frac{T}{\kappa q^2} \tag{C.11}$$

A membrane is globally flat if the correlation function $\langle \vec{n}_0 \vec{n}_{\vec{r}} \rangle = \sum_q \langle |\vec{n}_{\vec{q}}| \rangle e^{i\vec{q}\vec{R}}$ leads to a constant as $R \to \infty$ (normals at large distances have, on average, the same direction). Equation (C.11) leads to a logarithmic divergence. Moreover, the mean square in-plane and out-of-plane displacements calculated from equations (C.5) and (C.6) are diverged as $L \to \infty$ (L is the sample size). Therefore it is concluded that the statistical mechanics of 2D systems cannot be based on the harmonic approximation. While taking into account, the coupling between $\vec{u}$ and h due to the non-linear terms in the equation (C.3) (deformation tensor) drastically changes.

We can introduce the renormalized bending rigidity $\kappa_R(q)$ by writing

$$G(\vec{q}) = \frac{T}{\kappa_R(q)q^4} \tag{C.12}$$

Then the first order anharmonic correction to κ is

$$\delta\kappa = \kappa_R(q) - \kappa = \frac{3TY}{8\pi\kappa q^2}, \tag{C.13}$$

where, $Y = [4\mu(\lambda+\mu)/\lambda+2\mu]$ is the 2D Young's modulus. At

$$q = q^* = \sqrt{\frac{3TY}{8\pi\kappa^2}} \tag{C.14}$$

the correction $\delta\kappa = \kappa$, and the coupling between in-plane and out-of-plane distortions cannot be considered in the context of perturbation.

In the presence of strongly interacting long-wavelength fluctuations, scaling considerations are useful (Ma 2000). Let us assume the behaviour of the renormalized bending rigidity $\kappa_R(q)$ at small q is determined by some exponent η, $\kappa_R(q) \propto q^{-\eta}$, yielding

$$G(q) = \frac{A}{q^4 - \eta q_0^\eta}, \langle|\vec{n}_{\vec{q}}|^2\rangle = \frac{A}{q^2 - \eta q_0^\eta}, \tag{C.15}$$

where the parameter $q_0 = (Y/\kappa)^{1/2}$ of the order of d^{-1} is introduced to make A dimensionless. One can also assume a renormalization of the effective Lame coefficients $\lambda_R(q)$, $\mu_R(q) \propto q^{\eta_u}$ which means

$$\langle u^*_{\alpha\vec{q}}\, u_{\beta\vec{q}}\rangle \propto \frac{1}{q^{2+\eta_u}} \tag{C.16}$$

Finally, it has been assumed that anharmonicities changes the equation $\langle h^2_{nj}\rangle \propto \frac{T}{E_{at}}\sum_q \frac{1}{q^4} \propto \frac{T}{E_{at}}L^2$ (where E_{at} is of the order of cohesive energy) in to

$$\langle h^2\rangle \propto L^{2\zeta} \tag{C.17}$$

The values of η, η_u and ζ are similar to critical exponents in the theory of critical phenomena. They are not independent.

$$\zeta = 1 - \eta/2, \eta_u = 2 - 2\eta \tag{C.18}$$

The exponent η_u is positive if $0 < \eta < 1$. This means that the interaction between out-of- plane and in-plane phonons makes the former one harder and the latter one softer. For a complete description of membrane theory, readers are highly recommended to read chapter 9 of the standard textbook (Katsnelson 2012) and also the articles (Katsnelson and Fasolino 2012, Los et al. 2009).

Bibliography

Abell, G. (1985). “Empirical chemical pseudopotential theory of molecular and metallic bonding”. *Phys. Rev. B*, 31(10):6184.

Albe, K., Möller, W., and Heinig, K.-H. (1997). “Computer simulation and boron nitride”. *Radiat Eff. Defects Solids*, 141(1-4):85–97.

Alem, N., Erni, R., Kisielowski, C., Rossell, M. D., Gannett, W., and Zettl, A. (2009). “Atomically thin hexagonal boron nitride probed by ultrahigh-resolution transmission electron microscopy”. *Phys. Rev. B*, 80(15):155425.

Allen, M. P. and Tildesley, D. J. (1989). *“Computer simulation of liquids”*. Oxford university press.

Andrew, R. C., Mapasha, R. E., Ukpong, A. M., and Chetty, N. (2012). “Mechanical properties of graphene and boronitrene”. *Phys. Rev. B.*, 85(12):125428.

Anees, P., Valsakumar, M., Chandra, S., and Panigrahi, B. (2014). “Ab initio study on stacking sequences, free energy, dynamical stability and potential energy surfaces of graphite structures”. *Modell. Simul. Mater. Sci. Eng.*, 22(3):035016.

Anees, P., Valsakumar, M., and Panigrahi, B. (2015). “Temperature dependent phonon frequency shift and structural stability of free-standing graphene: a spectral energy density analysis”. *2D Mater.*, 2(3):035014.

Anees, P., Valsakumar, M., and Panigrahi, B. (2016). “Effect of strong phonon–phonon coupling on the temperature dependent structural stability and frequency shift of 2d hexagonal boron nitride”. *Phys. Chem. Chem. Phys*, 18(4):2672–2681.

Ansari, N., Nazari, F., and Illas, F. (2014). “Line defects and induced doping effects in graphene, hexagonal boron nitride and hybrid bnc”. *Phys. Chem. Chem. Phys.*, 16(39):21473–21485.

Barnard, A. S., Snook, I. K., and Russo, S. P. (2007). “Bonding and structure in b_x n_y nanotubes (x,y= 1, 2)”. *J. Mater. Chem.*, 17(28):2892–2898.

Baskes, M. (1987). “Application of the embedded-atom method to covalent materials: a semiempirical potential for silicon”. *Phys. Rev. Lett.*, 59(23):2666.

Baskes, M., Nelson, J., and Wright, A. (1989). “Semiempirical modified embedded-atom potentials for silicon and germanium”. *Phys. Rev. B*, 40(9):6085.

Bazant, M. Z., Kaxiras, E., and Justo, J. (1997). “Environment-dependent interatomic potential for bulk silicon”. *Phys. Rev. B*, 56(14):8542.

Belenkii, G., Salaev, E. Y., Suleimanov, R., Abdullaev, N., and Shteinshraiber, V. Y. (1985). “The nature of negative linear expansion in layer crystals c, bn, gas, gase and inse”. *Solid State Commun.*, 53(11):967–971.

Boldrin, L., Scarpa, F., Chowdhury, R., and Adhikari, S. (2011). “Effective mechanical properties of hexagonal boron nitride nanosheets”. *Nanotechnology*, 22(50):505702.

Born, M. and Huang, K. (1966). *“Dynamical theory of cristal lattices”*. Clarendon Press, Oxford, 2nd edition.

Bosak, A., Serrano, J., Krisch, M., Watanabe, K., Taniguchi, T., and Kanda, H. (2006). “Elasticity of hexagonal boron nitride: Inelastic x-ray scattering measurements”. *Phys. rev. B*, 73(4):041402.

Braghin, F. and Hasselmann, N. (2010). “Thermal fluctuations of free-standing graphene”. *Phys. Rev. B*, 82(3):035407.

Brenner, D. W. (1990). “Empirical potential for hydrocarbons for use in simulating the chemical vapor deposition of diamond films”. *Phys. Rev. B*, 42(15):9458.

Brenner, D. W., Shenderova, O. A., Harrison, J. A., Stuart, S. J., Ni, B., and Sinnott, S. B. (2002). “A second-generation reactive empirical bond order (rebo) potential energy expression for hydrocarbons”. *J. Phys: Cond. Matter*, 14(4):783.

Cadelano, E. and Colombo, L. (2012). “Effect of hydrogen coverage on the young’s modulus of graphene”. *Phys. Rev. B*, 85(24):245434.

Cai, J. and Wang, J.-S. (2001). “Reconstruction of si (001) and adsorption of si adatoms and ad-dimers on the surface: Many-body potential calculations”. *Phys. Rev. B*, 64(3):035402.

Cai, W., Li, J., and Yip, S. (2012). “Molecular dynamics-1.09”. *Comprehensive Nuclear Materials, JMK, Rudy, editor. Elsevier: Oxford*, 1:249–265.

Cao, G. (2014). “Atomistic studies of mechanical properties of graphene”. *Polymers*, 6(9):2404–2432.

Chen, S. (2012). “Buckling and topological defects in graphene and carbon nanotubes”.

Costamagna, S., Neek-Amal, M., Los, J., and Peeters, F. (2012). “Thermal rippling behavior of graphane”. *Phys. Rev. B*, 86(4):041408.

da Silva, A., Cândido, L., Rabelo, J. T., Hai, G.-Q., and Peeters, F. (2014). “Anharmonic effects on thermodynamic properties of a graphene monolayer”. *EPL (Europhysics Letters)*, 107(5):56004.

Dean, C. R., Young, A. F., Meric, I., Lee, C., Wang, L., Sorgenfrei, S., Watanabe, K., Taniguchi, T., Kim, P., Shepard, K., et al. (2010). “Boron nitride substrates for high-quality graphene electronics”. *Nat. Nanotechnol.*, 5(10):722–726.

Dilrukshi, K., Dewapriya, M., and Puswewala, U. (2015). “Size dependency and potential field influence on deriving mechanical properties of carbon nanotubes using molecular dynamics”. *Theoretical and Applied Mechanics Letters*, 5(4):167–172.

Ding, N., Chen, X., and Wu, C.-M. L. (2016). “Mechanical properties and failure behaviors of the interface of hybrid graphene/hexagonal boron nitride sheets”. *Sci. Rep.*, 6.

Ding, Y. and Wang, Y. (2013). “Density functional theory study of the silicene-like si$_x$ and xsi$_3$ (x= b, c, n, al, p) honeycomb lattices: The various buckled structures and versatile electronic properties”. *J. Phys. Chem. C*, 117(35):18266–18278.

Eichler, J. and Lesniak, C. (2008). “Boron nitride (bn) and bn composites for high-temperature applications”. *J. Eur. Ceram. Soc.*, 28(5):1105–1109.

Ercolessi, F. (1997). “A molecular dynamics primer”. *Spring college in computational physics, ICTP, Trieste*, 19.

Fasolino, A., Los, J., and Katsnelson, M. I. (2007). “Intrinsic ripples in graphene”. *Nat. Mater.*, 6(11):858–861.

Fay, P. J. and Ray, J. R. (1992). “Monte carlo simulations in the isoenthalpic-isotension-isobaric ensemble”. *Phys. Rev. A*, 46(8):4645.

Finnis, M. and Sinclair, J. (1984). “A simple empirical n-body potential for transition metals”. *Philo. Mag. A*, 50(1):45–55.

Frenkel, D. and Smit, B. (2001). *"Understanding molecular simulation: from algorithms to applications"*, volume 1. Academic press, The Edinburgh Building, Cambridge CB2 8RU, UK., 2nd edition.

Furthmüller, J., Hafner, J., and Kresse, G. (1994). "Structural and electronic properties of clean and hydrogenated diamond (100) surfaces". *EPL (Europhysics Letters)*, 28(9):659.

Gao, E. and Xu, Z. (2015). "Thin-shell thickness of two-dimensional materials". *J. Appl. Mech.*, 82(12):121012.

Gao, G., Van Workum, K., Schall, J. D., and Harrison, J. A. (2006). "Elastic constants of diamond from molecular dynamics simulations". *J. Phys. Condens. Matter*, 18(32):S1737.

Gao, W. and Huang, R. (2014). "Thermomechanics of monolayer graphene: Rippling, thermal expansion and elasticity". *J. Mech. Phys. Solids*, 66:42–58.

Geim, A. K. and Novoselov, K. S. (2007). "The rise of graphene". *Nat. mater.*, 6(3):183–191.

Golberg, D., Bando, Y., Huang, Y., Xu, Z., Wei, X., Bourgeois, L., Wang, M.-S., Zeng, H., Lin, J., and Zhi, C. (2010). "Recent advances in boron nitride nanotubes and nanosheets". *Isr. J. Chem.*, 50(4):405–416.

Green, J., Bolland, T., and Bolland, J. (1976). "Theoretical elastic behavior for hexagonal boron nitride". *J. Chem. Phys.*, 64(2):656–662.

Greenwood, N. (1984). *"Chemistry of the elements"*. Perganion, New York.

Grotendorst, J., Attig, N., Blügel, S., and Marx, D. (2009). "Multiscale simulation methods in molecular sciences". *Lecture Notes, NIC Series*, 42.

Gusev, A. A., Zehnder, M. M., and Suter, U. W. (1996). "Fluctuation formula for elastic constants". *Phys. Rev. B.*, 54(1):1.

Hamdi, I. and Meskini, N. (2010). "Ab initio study of the structural, elastic, vibrational and thermodynamic properties of the hexagonal boron nitride: Performance of lda and gga". *Physica B: Condens. Matter*, 405(13):2785–2794.

Han, T., Luo, Y., and Wang, C. (2013). "Effects of temperature and strain rate on the mechanical properties of hexagonal boron nitride nanosheets". *J Phys D: Appl Phys.*, 47(2):025303.

Hasselmann, N. and Braghin, F. (2011). “Nonlocal effective-average-action approach to crystalline phantom membranes”. *Phys. Rev. E*, 83(3):031137.

Hiki, Y. (1981). “Higher order elastic constants of solids”. *Ann. Rev. Mater. Sci.,*, 11(1):51–73.

Hod, O. (2012). “Graphite and hexagonal boron-nitride have the same interlayer distance. why?”. *J. Chem. Theory Comput.*, 8(4):1360–1369.

Hoover, W. G. (1985). “Canonical dynamics: equilibrium phase-space distributions”. *Phy. Rev. A*, 31(3):1695.

Humphrey, W., Dalke, A., and Schulten, K. (1996). “Vmd: visual molecular dynamics”. *Journal of molecular graphics*, 14(1):33–38.

Jain, N., Bansal, T., Durcan, C. A., Xu, Y., and Yu, B. (2013). “Monolayer graphene/hexagonal boron nitride heterostructure”. *Carbon*, 54:396–402.

Jin, C., Lin, F., Suenaga, K., and Iijima, S. (2009). “Fabrication of a freestanding boron nitride single layer and its defect assignments”. *Phys. Rev. Lett.*, 102(19):195505.

Jing, N., Xue, Q., Ling, C., Shan, M., Zhang, T., Zhou, X., and Jiao, Z. (2012). “Effect of defects on young’s modulus of graphene sheets: a molecular dynamics simulation”. *Rsc Adv.*, 2(24):9124–9129.

John, S. T. and Klug, D. D. (1991). “Mechanical instability of α-quartz: A molecular dynamics study”. *Phys. Rev. Lett.*, 67(25):3559.

Jones, J. E. (1924). “On the determination of molecular fields. ii. from the equation of state of a gas”. In *Proc. R. Soc. A*, volume 106, pages 463–477. The Royal Society.

Justo, J. F., Bazant, M. Z., Kaxiras, E., Bulatov, V., and Yip, S. (1998). “Interatomic potential for silicon defects and disordered phases”. *Phys. Rev. B*, 58(5):2539.

Kaloni, T. P. and Mukherjee, S. (2011). “Comparative study of electronic properties of graphite and hexagonal boron nitride (h-bn) using pseudopotential plane wave method”. *Mod. Phys. Lett. B.*, 25(22):1855–1866.

Kara, A., Enriquez, H., Seitsonen, A. P., Voon, L. L. Y., Vizzini, S., Aufray, B., and Oughaddou, H. (2012). “A review on silicene-new candidate for electronics”. *Surf. Sci. Rep.*, 67(1):1–18.

Karssemeijer, L. and Fasolino, A. (2011). “Phonons of graphene and graphitic materials derived from the empirical potential lcbopii”. *Surf. Sci.*, 605(17):1611–1615.

Katsnelson, M. (2005). Encyclopedia of condensed matter physics, edited by gf bassani, gl liedl, and p. wyder.

Katsnelson, M. and Geim, A. (2008). "Electron scattering on microscopic corrugations in graphene". *Phil. Trans. R. Soc. A*, 366(1863):195–204.

Katsnelson, M. I. (2012). *"Graphene: carbon in two dimensions"*. Cambridge University Press.

Katsnelson, M. I. and Fasolino, A. (2012). "Graphene as a prototype crystalline membrane". *Acc. Chem. Res.*, 46(1):97–105.

Keller, J. M. and Wallace, D. C. (1962). "Anharmonic contributions to specific heat". *Phys. Rev.*, 126(4):1275.

Kinaci, A., Haskins, J. B., Sevik, C., and Çağın, T. (2012). "Thermal conductivity of bn-c nanostructures". *Phy. Rev. B*, 86(11):115410.

Kinsler, L. E., Frey, A. R., Coppens, A. B., and Sanders, J. V. (1999). *"Fundamentals of acoustics"*.

Kouvetakis, J., Kaner, R. B., Sattler, M. L., and Bartlett, N. (1986). "A novel graphite-like material of composition bc_3, and nitrogen–carbon graphites". *Chem. Commun.*, (24):1758–1759.

Krishnan, N. A. and Ghosh, D. (2014). "Chirality dependent elastic properties of single-walled boron nitride nanotubes under uniaxial and torsional loading". *J. Appl. Phys.*, 115(6):064303.

Kudin, K. N., Scuseria, G. E., and Yakobson, B. I. (2001). "C_2f, bn, and c nanoshell elasticity from ab initio computations". *Phys. Rev. B*, 64(23):235406.

Kumar, R., Rajasekaran, G., and Parashar, A. (2016). "Optimised cut-off function for tersoff-like potentials for a bn nanosheet: a molecular dynamics study". *Nanotechnology*, 27(8):085706.

Lajevardipour, A., Neek-Amal, M., and Peeters, F. (2012). "Thermomechanical properties of graphene: valence force field model approach". *J. Phys. Condens. Matter*, 24(17):175303.

Landau, L. and Lifshitz, E. (1958). Statistical physics, part 1, 3^{rd} edition. *"Course of Theoretical Physics"*, 5:230.

Landau, L. and Lifshitz, E. (1970). "Theory of elasticity": 2^{nd} end.

Landau, P. D. and Binder, K. (2005). *"A Guide to Monte Carlo Simulations in Statistical Physics"*. Cambridge University Press, The Edinburgh Building, Cambridge CB2 8RU, UK.

Lau, K. C. and Pandey, R. (2008). "Thermodynamic stability of novel boron sheet configurations". *J. Phys. Chem. B*, 112(33):10217–10220.

Le, M.-Q. (2015). "Prediction of young's modulus of hexagonal monolayer sheets based on molecular mechanics". *International Journal of Mechanics and Materials in Design*, 11(1):15–24.

Le, M.-Q. and Nguyen, D.-T. (2014). "Atomistic simulations of pristine and defective hexagonal bn and sic sheets under uniaxial tension". *Mater. Sci. Engg. A.*, 615:481–488.

Le Doussal, P. and Radzihovsky, L. (1992). "Self-consistent theory of polymerized membranes". *Phys. Rev. Lett.*, 69(8):1209.

Lee, J. G. (2011). *"Computational Materials Science : An Introduction"*. CRC Press, Taylor & Francis, Boca Raton, United States.

Lee, S. (2015). "Effect of intrinsic ripples on elasticity of the graphene monolayer". *Nanoscale Res. Lett.*, 10(1):422.

Lehtinen, O., Dumur, E., Kotakoski, J., Krasheninnikov, A., Nordlund, K., and Keinonen, J. (2011). "Production of defects in hexagonal boron nitride monolayer under ion irradiation". *Nucl. Instr. Meth. Phys. Res.*, 269(11):1327–1331.

Lipp, A., Schwetz, K. A., and Hunold, K. (1989). "Hexagonal boron nitride: fabrication, properties and applications". *J. Eur. Ceram. Soc.*, 5(1):3–9.

Liu, H., Gao, J., and Zhao, J. (2013a). "From boron cluster to two-dimensional boron sheet on cu (111) surface: Growth mechanism and hole formation". *Sci. Rep.*, 3.

Liu, H., Neal, A. T., Zhu, Z., Tomanek, D., and Ye, P. D. (2014). "Phosphorene: a new 2d material with high carrier mobility". *arXiv preprint arXiv:1401.4133*.

Liu, X., Metcalf, T. H., Robinson, J. T., Houston, B. H., and Scarpa, F. (2012). "Shear modulus of monolayer graphene prepared by chemical vapor deposition". *Nano lett.*, 12(2):1013–1017.

Liu, Z., Gong, Y., Zhou, W., Ma, L., Yu, J., Idrobo, J. C., Jung, J., MacDonald, A. H., Vajtai, R., Lou, J., et al. (2013b). "Ultrathin high-temperature oxidation-resistant coatings of hexagonal boron nitride". *Nat. Commun.*, 4.

López-Polín, G., Jaafar, M., Guinea, F., Roldán, R., Gómez-Navarro, C., and Gómez-Herrero, J. (2015). "Strain dependent elastic modulus of graphene". *arXiv preprint arXiv:1504.05521*.

Los, J., Katsnelson, M. I., Yazyev, O., Zakharchenko, K., and Fasolino, A. (2009). "Scaling properties of flexible membranes from atomistic simulations: application to graphene". *Phys. Rev. B*, 80(12):121405.

Lovett, D. (1999). *"Tensor properties of crystals"*. CRC Press.

Lutsko, J. (1989). "Generalized expressions for the calculation of elastic constants by computer simulation". *J. App. Phys.*, 65(8):2991–2997.

Ma, S.-K. (2000). *"Modern theory of critical phenomena"*. Number 46. Da Capo Press.

Matsunaga, K., Fisher, C., and Matsubara, H. (2000). "Tersoff potential parameters for simulating cubic boron carbonitrides". *Jpn. J. Appl. Phys.*, 39(1A):L48.

Mendelev, M., Han, S., Srolovitz, D., Ackland, G., Sun, D., and Asta, M. (2003). "Development of new interatomic potentials appropriate for crystalline and liquid iron". *Philos. Mag.*, 83(35):3977–3994.

Mermin, N. D. (1968). "Crystalline order in two dimensions". *Phys. Rev.*, 176(1):250.

Mermin, N. D. and Wagner, H. (1966). "Absence of ferromagnetism or antiferromagnetism in one-or two-dimensional isotropic heisenberg models". *Phys. Rev. Lett.*, 17(22):1133.

Milowska, K. Z., Woin´ska, M., and Wierzbowska, M. (2013). "Contrasting elastic properties of heavily b-and n-doped graphene with random impurity distributions including aggregates". *J. Phys. Chem. C*, 117(39):20229–20235.

Mirnezhad, M., Ansari, R., and Rouhi, H. (2013). "Mechanical properties of multilayer boron nitride with different stacking orders". *Superlattices Microstruct.*, 53:223–231.

Mortazavi, B. and Rémond, Y. (2012). "Investigation of tensile response and thermal conductivity of boron-nitride nanosheets using molecular dynamics simulations". *Physica E: Low Dimens. Syst. Nanostruct.*, 44(9):1846–1852.

Mouhat, F. and Coudert, F.-X. (2014). "Necessary and sufficient elastic stability conditions in various crystal systems". *Phys. Rev. B*, 90(22):224104.

Mounet, N. and Marzari, N. (2005). "First-principles determination of the structural, vibrational and thermodynamic properties of diamond, graphite, and derivatives". *Phys. Rev. B*, 71(20):205214.

Nelson, D. and Peliti, L. (1987). “Fluctuations in membranes with crystalline and hexatic order”. *J. physique*, 48(7):1085–1092.

Nelson, D., Piran, T., and Weinberg, S. (2004). *Statistical mechanics of membranes and surfaces*. World Scientific.

Novoselov, K. S., Jiang, D., Schedin, F., Booth, T. J., Khotkevich, V. V., Morozov, S. V., and Geim, A. K. (2005). “Two-dimensional atomic crystals”. *Proc. Natl. Acad. Sci. U.S.A.*, 102(30).

Oh, E.-S. (2010). “Elastic properties of boron-nitride nanotubes through the continuum lattice approach”. *Mater. Lett.*, 64(7):859–862.

Ohba, N., Miwa, K., Nagasako, N., and Fukumoto, A. (2001). “First-principles study on structural, dielectric, and dynamical properties for three bn polytypes”. *Phys. Rev. B.*, 63(11):115207.

Okada, S. (2009). “Atomic configurations and energetics of vacancies in hexagonal boron nitride: First-principles total-energy calculations”. *Phys. Rev. B*, 80(16):161404.

Oleinik, I. and Pettifor, D. (1999). “Analytic bond-order potentials beyond tersoff-brenner. ii. application to the hydrocarbons”. *Phys. Rev. B*, 59(13):8500.

Pacile, D., Meyer, J., Girit, Ç., and Zettl, A. (2008). “The two-dimensional phase of boron nitride: few-atomic-layer sheets and suspended membranes”. *App. Phys. Lett.*, 92(13):133107.

Parrinello, M. and Rahman, A. (1980). “Crystal structure and pair potentials: A molecular-dynamics study”. *Phys. Rev. Lett.*, 45(14):1196.

Parrinello, M. and Rahman, A. (1982). “Strain fluctuations and elastic constants”. *J. Chem. Phys.*, 76(5):2662–2666.

Paszkowicz, W., Pelka, J., Knapp, M., Szyszko, T., and Podsiadlo, S. (2002). “Lattice parameters and anisotropic thermal expansion of hexagonal boron nitride in the 10–297.5 k temperature range”. *Applied Physics A*, 75(3):431–435.

Peng, Q., Ji, W., and De, S. (2012a). “Mechanical properties of the hexagonal boron nitride monolayer: Ab initio study”. *Comput. Mater. Sci.*, 56:11–17.

Peng, Q., Zamiri, A. R., Ji, W., and De, S. (2012b). “Elastic properties of hybrid graphene/boron nitride monolayer”. *Acta Mech.*, 223(12):2591–2596.

Pettifor, D. (1989). “New many-body potential for the bond order”. *Phys. Rev. Lett.*, 63(22):2480.

Pettifor, D. and Oleinik, I. (1999). “Analytic bond-order potentials beyond tersoff-brenner. i. theory”. *Phys. Rev. B*, 59(13):8487.

Plimpton, S. (1995). “Fast parallel algorithms for short-range molecular dynamics”. *J. Comput. Phys.*, 117(1):1–19.

Plimpton, S., Crozier, P., and Thompson, A. (2007). “Lammps-large-scale atomic/molecular massively parallel simulator”, http://lammps.sandia.gov/. *Sandia National Laboratories*, 18.

Popov, I. A. and Boldyrev, A. I. (2012). “Deciphering chemical bonding in a bc_3 honeycomb epitaxial sheet”. *J. Phys. Chem. C*, 116(4):3147–3152.

Pozzo, M., Alfe, D., Lacovig, P., Hofmann, P., Lizzit, S., and Baraldi, A. (2011). “Thermal expansion of supported and freestanding graphene: lattice constant versus interatomic distance”. *Phys. Rev. Lett.*, 106(13):135501.

Qi-lin, X., Zhen-huan, L., and Xiao-geng, T. (2015). “The defect-induced fracture behaviors of hexagonal boron-nitride monolayer nanosheets under uniaxial tension”. *J Phys D: Appl Phys.*, 48(37):375502.

Radisavljevic, B., Radenovic, A., Brivio, J., Giacometti, i. V., and Kis, A. (2011). “Single-layer mos2 transistors”. *Nat. Nanotechnol.*, 6(3):147–150.

Rahman, A. (1964). “Correlations in the motion of atoms in liquid argon”. *Phys. Rev.*, 136(2A):A405.

Rapoport, D. C. (1995). *“The Art of Molecular Dynamics Simulations”*. Cambridge University Press, The Edinburgh Building, Cambridge CB2 2RU, UK, 2nd edition.

Ray, J. R. (1982). “Fluctuations and thermodynamic properties of anisotropic solids”. *J. App. Phys.*, 53(9):6441–6443.

Ray, J. R. (1988). “Elastic constants and statistical ensembles in molecular dynamics”. *Computer Physics Reports*, 8(3):109–151.

Ray, J. R., Moody, M. C., and Rahman, A. (1985). “Molecular dynamics calculation of elastic constants for a crystalline system in equilibrium”. *Phys. Rev. B.*, 32(2):733.

Ray, J. R. and Rahman, A. (1984). “Statistical ensembles and molecular dynamics studies of anisotropic solids”. *J. Chem. Phys.*, 80(9):4423–4428.

Ray, J. R. and Rahman, A. (1985). "Statistical ensembles and molecular dynamics studies of anisotropic solids. ii". *J. Chem. Phys.*, 82(9):4243–4247.

Roldán, R., Fasolino, A., Zakharchenko, K. V., and Katsnelson, M. I. (2011). "Suppression of anharmonicities in crystalline membranes by external strain". *Phys. Rev. B*, 83(17):174104.

Rubio, A., Corkill, J. L., and Cohen, M. L. (1994). "Theory of graphitic boron nitride nanotubes". *Phys. Rev. B*, 49(7):5081.

Şahin, H., Cahangirov, S., Topsakal, M., Bekaroglu, E., Akturk, E., Senger, R. T., and Ciraci, S. (2009). "Monolayer honeycomb structures of group-iv elements and iii-v binary compounds: First-principles calculations". *Phys. Rev. B.*, 80(15):155453.

Sevik, C. (2014). "Assessment on lattice thermal properties of two-dimensional honeycomb structures: Graphene, h-bn, h-mos$_2$, and h-mose$_2$". *Phys. Rev. B*, 89(3):035422.

Sevik, C., Kinaci, A., Haskins, J. B., and Çağın, T. (2011). "Characterization of thermal transport in low-dimensional boron nitride nanostructures". *Phys. Rev. B*, 84(8):085409.

Sevik, C., Kinaci, A., Haskins, J. B., and Çağın, T. (2012). "Influence of disorder on thermal transport properties of boron nitride nanostructures". *Phys. Rev. B*, 86(7):075403.

Singh, S. K., Neek-Amal, M., Costamagna, S., and Peeters, F. (2013). "Thermomechanical properties of a single hexagonal boron nitride sheet". *Phys. Rev. B*, 87(18):184106.

Slotman, G. and Fasolino, A. (2012). "Structure, stability and defects of single layer hexagonal bn in comparison to graphene". . *Phys.: Condens. Matter*, 25(4):045009.

Solozhenko, V., Will, G., and Elf, F. (1995). "Isothermal compression of hexagonal graphite-like boron nitride up to 12 gpa". *Solid State Commun.*, 96(1):1–3.

Song, L., Ci, L., Lu, H., Sorokin, P. B., Jin, C., Ni, J., Kvashnin, A. G., Kvashnin, D. G., Lou, J., Yakobson, B. I., and Pulickel, A. M. (2010). "Large scale growth and characterization of atomic hexagonal boron nitride layers". *Nano lett.*, 10(8):3209–3215.

Sprik, M., Impey, R. W., and Klein, M. L. (1984). "Second-order elastic constants for the lennard-jones solid". *Phys. rev. B.*, 29(8):4368.

Stillinger, F. H. and Weber, T. A. (1985). “Computer simulation of local order in condensed phases of silicon”. *Phys. Rev. B*, 31(8):5262.

Stone, A. J. and Wales, D. J. (1986). “Theoretical studies of icosahedral c 60 and some related species”. *Chem. Phys. Lett.*, 128(5):501–503.

Swope, W. C., Andersen, H. C., Berens, P. H., and Wilson, K. R. (1982). “A computer simulation method for the calculation of equilibrium constants for the formation of physical clusters of molecules: Application to small water clusters”. *J. Chem. Phys.*, 76(1):637–649.

Takeda, K. and Shiraishi, K. (1994). “Theoretical possibility of stage corrugation in si and ge analogs of graphite”. *Phys. Rev. B*, 50(20):14916.

Tang, Q. and Zhou, Z. (2013). “Graphene-analogous low-dimensional materials”. *Progress in Materials Science*, 58(8):1244–1315.

Tersoff, J. (1986). “New empirical model for the structural properties of silicon”. *Phys. Rev. Lett.*, 56(6):632.

Tersoff, J. (1988a). “Empirical interatomic potential for carbon, with applications to amorphous carbon”. *Phys. Rev. Lett.*, 61(25):2879.

Tersoff, J. (1988b). “New empirical approach for the structure and energy of covalent systems”. *Phys. Rev. B*, 37(12):6991.

Tersoff, J. (1989). “Modeling solid-state chemistry: Interatomic potentials for multicomponent systems”. *Phys. Rev. B*, 39(8):5566.

Thomas, S., Ajith, K., Chandra, S., and Valsakumar, M. (2015). “Temperature dependent structural properties and bending rigidity of pristine and defective hexagonal boron nitride”. *J. Phys.: Condens. Matter*, 27(31):315302.

Thomas, S., Ajith, K., and Valsakumar, M. (2016). “Directional anisotropy, finite size effect and elastic properties of hexagonal boron nitride”. *J. Phys. Condens. Matter*, 28(29):295302.

Topsakal, M. and Ciraci, S. (2010). “Elastic and plastic deformation of graphene, silicene, and boron nitride honeycomb nanoribbons under uniaxial tension: A first-principles density-functional theory study”. *Phys. Rev. B.*, 81(2):024107.

Tuckerman, M. (2010). *“Statistical mechanics: theory and molecular simulation”*. Oxford University Press.

Verlet, L. (1967). “Computer ”experiments” on classical fluids. i. thermodynamical properties of lennard-jones molecules”. *Phys. Rev.*, 159(1):98.

Verma, V., Jindal, V., and Dharamvir, K. (2007). “Elastic moduli of a boron nitride nanotube”. *Nanotechnology*, 18(43):435711.

Vogt, P., De Padova, P., Quaresima, C., Avila, J., Frantzeskakis, E., Asensio, M. C., Resta, A., Ealet, B., and Le Lay, G. (2012). “Silicene: compelling experimental evidence for graphenelike two-dimensional silicon”. *Phys. Rev. Lett.*, 108(15):155501.

Weiner, J. (2002). “Statistical mechanics of elasticity”, dover publications. *Mineola, NY*.

Wu, J., Wang, B., Wei, Y., Yang, R., and Dresselhaus, M. (2013). “Mechanics and mechanically tunable band gap in single-layer hexagonal boron-nitride”. *Materials Research Letters*, 1(4):200–206.

Xiao, Y., Yan, X., Cao, J., Ding, J., Mao, Y., and Xiang, J. (2004). “Specific heat and quantized thermal conductance of single-walled boron nitride nanotubes”. *Phys. Rev. B*, 69(20):205415.

Xiong, Q.-l. and Tian, X. G. (2015). “Torsional properties of hexagonal boron nitride nanotubes, carbon nanotubes and their hybrid structures: A molecular dynamics study”. *AIP Adv.*, 5(10):107215.

Xu, L., Wei, N., and Zheng, Y. (2013). “Mechanical properties of highly defective graphene: from brittle rupture to ductile fracture”. *Nanotechnology*, 24(50):505703.

Xu, Y.-N. and Ching, W. (1993). “Electronic, optical, and structural properties of some wurtzite crystals”. *Phys. Rev. B*, 48(7):4335.

Xu, Z. and Buehler, M. J. (2010). “Geometry controls conformation of graphene sheets: membranes, ribbons, and scrolls”. *ACS Nano*, 4(7):3869–3876.

Xue, J., Sanchez-Yamagishi, J., Bulmash, D., Jacquod, P., Deshpande, A., Watanabe, K., Taniguchi, T., Jarillo-Herrero, P., and LeRoy, B. J. (2011). “Scanning tunnelling microscopy and spectroscopy of ultra-flat graphene on hexagonal boron nitride”. *Nat. Mater.*, 10(4):282–285.

Yang, J., Shahid, M., Wan, C., Jing, F., and Pan, W. (2017). “Anisotropy in elasticity, sound velocities and minimum thermal conductivity of zirconia from first-principles calculations”. *J. Eur. Ceram. Soc.*, 37(2):689–695.

Yates, B., Overy, M., and Pirgon, O. (1975). “The anisotropic thermal expansion of boron nitride: I. experimental results and their analysis”. *Philos. Mag.*, 32(4):847–857.

Yoshimoto, K., Papakonstantopoulos, G. J., Lutsko, J. F., and de Pablo, J. J. (2005). “Statistical calculation of elastic moduli for atomistic models”. *Phys. Rev. B.*, 71(18):184108.

Yuan, J. and Liew, K. (2014). “Structure stability and high-temperature distortion resistance of trilayer complexes formed from graphenes and boron nitride nanosheets”. *Phys. Chem. Chem. Phys.*, 16(1):88–94.

Zakharchenko, K., Katsnelson, M., and Fasolino, A. (2009). “Finite temperature lattice properties of graphene beyond the quasiharmonic approximation”. *Phys. Rev. Lett.*, 102(4):046808.

Zakharchenko, K., Los, J., Katsnelson, M. I., and Fasolino, A. (2010a). “Atomistic simulations of structural and thermodynamic properties of bilayer graphene”. *Phys. Rev. B*, 81(23):235439.

Zakharchenko, K., Roldán, R., Fasolino, A., and Katsnelson, M. (2010b). “Self-consistent screening approximation for flexible membranes: Application to graphene”. *Phys. Rev. B*, 82(12):125435.

Zeng, H., Zhi, C., Zhang, Z., Wei, X., Wang, X., Guo, W., Bando, Y., and Golberg, D. (2010). “White graphenes: boron nitride nanoribbons via boron nitride nanotube unwrapping”. *Nano lett.*, 10(12):5049–5055.

Zhao, S. and Xue, J. (2013). “Mechanical properties of hybrid graphene and hexagonal boron nitride sheets as revealed by molecular dynamic simulations”. *J. Phys. D: Appl. Phys.*, 46(13):135303.

Zhou, J. and Huang, R. (2008). “Internal lattice relaxation of single-layer graphene under in-plane deformation”. *J. Mech. Phys. Solids*, 56(4):1609–1623.

Zobelli, A., Ewels, C., Gloter, A., and Seifert, G. (2007). “Vacancy migration in hexagonal boron nitride”. *Phys. Rev. B*, 75(9):094104.

LIST OF PUBLICATIONS

1. Peer Reviewed International Journals:

1. **Siby Thomas**, K M Ajith and M C Valsakumar. (2017). "Effect of ripples on the finite temperature elastic properties of hexagonal boron nitride using strain-fluctuation method". *Superlattices Microstruct.* http://dx.doi.org/10.1016/j.spmi.2017.06.051.
2. **Siby Thomas**, K M Ajith and M C Valsakumar. (2017). "Empirical potential influence and effect of temperature on the mechanical properties of pristine and defective hexagonal boron nitride". *Mater. Res. Express*, **4**, 065005; doi:https://doi.org/10.1088/20531591/aa72bf.
3. **Siby Thomas**, K M Ajith and M C Valsakumar. (2016). "Directional anisotropy, finite size effect and elastic properties of hexagonal boron nitride ". *J. Phys.: Condens. Matter,* **28**, 295302. doi:10.1088/0953-8984/28/29/295302.
4. **Siby Thomas**, K M Ajith, Sharat Chandra and M C Valsakumar. (2015). "Temperature dependent structural properties and bending rigidity of pristine and defective hexagonal boron nitride". *J. Phys.: Condens. Matter,* **27**, 315302. doi:10.1088/0953-8984/27/31/315302.

2. Peer Reviewed International Journal proceedings:

1. **Siby Thomas**, M S Mrudul, K M Ajith and M C Valsakumar. (2016). "Young's modulus of defective graphene sheet from intrinsic thermal vibrations ". *J. Phys.: Conf. Ser.*, **759**, 012048.
2. **Siby Thomas**, K M Ajith and M C Valsakumar. (2016). "Structural Analysis of Graphene and h-BN: A Molecular Dynamics Approach ". *AIP Conf. Proc.* **1728**, 020608 (2016). http:/dx.doi.org/10.1063/1.4946659.
3. **Siby Thomas** and K M Ajith. (2014). "Molecular Dynamics Simulation of the Thermo-mechanical Properties of Monolayer Graphene Sheet". *Procedia Mater. Sci.,* **5C**, pp. 489-498. doi:10.1016/j.mspro.2014.07.292.

3. International Conferences Presentations:

1. **Siby Thomas**, K M Ajith and M C Valsakumar. "Anisotropic elastic properties of graphene using Classical Molecular Dynamics". *NanoteC16 - The British Carbon Group's Conference on Carbon Nanoscience and Nanotechnology* at Trinity College, Dublin, Ireland during August 31 - September 3, 2016.
2. **Siby Thomas**, M S Mrudul, K M Ajith and M C Valsakumar. "Young's modulus of defective graphene sheet from intrinsic thermal vibrations". *XXVII IUPAP Conference on Computational Physics: CCP2015* at Indian Institute of Technology Guwahati, Assam, India during December 2-5, 2015.
3. **Siby Thomas**, K M Ajith and M C Valsakumar. "Structural Analysis of Graphene and *h*-BN: A Molecular Dynamics Approach". *International Conference on Condensed Matter and Applied Physics* at Govt. Engineering College, Bikaner, Rajasthan, India during October 30-31, 2015.
4. **Siby Thomas**, K M Ajith, Sharat Chandra and M C Valsakumar. "High temperature studies of pristine and defective h-BN sheet using Molecular Dynamics". *International Symposium on Molecular Simulations* at Hyderabad Central University, Gachibowli, Telangana State, India on August 24, 2014.
5. **Siby Thomas** and K M Ajith. "Molecular Dynamics Simulation of the Thermomechanical Properties of Monolayer Graphene Sheet". *International Conference on Advances in Manufacturing and Materials Engineering (ICAMME-2014)* at National Institute of Technology Karnataka (NITK), Surathkal, India during March 27-29, 2014.
6. **Siby Thomas** and K M Ajith. "Molecular Dynamics Simulation of the Structural and Thermodynamic Properties of Monolayer Graphene Sheet". *International Conference on Advanced Functional Materials 2014 (ICAFM-2014)* at CSIR-National Institute for Interdisciplinary Science ad Technology (NIIST), Thiruvananthapuram, India during February 19-21, 2014.

CURRICULUM VITAE

SIBY THOMAS

Permanent Address :

Pathilakkandam, Pattena,
PO: Nileshwar, Kasaragod Dist,
Kerala, India - 671314

Mobile:(+91)-9035790469
E-mail: siby.ph11f09@nitk.ac.in,
sibythomas1989@gmail.com.

Academic Qualifications :

Master of Science Score : 78.72%
Mahatma Gandhi University,
Kottayam, Kerala, India

Bachelor of Science Score : 78.6%
Kannur University,
Kerala, India

Research Publications :

Articles in International Journals : 4
Articles in International Proceedings : 3
Papers presented in International Conferences : 6
Workshops and Schools attended : 10